Verification of strong wind gusts in COSMO-2

Master's Thesis

Faculty of Science
University of Bern

presented by

Hélène Barras

2016

Supervisor:

Prof. Dr. Olivia Romppainen-Martius

Institute of Geography of the University of Bern and Oeschger Centre for Climate Change Research, University of Bern

Advisor:

Simona Trefalt

Institute of Geography of the University of Bern and Oeschger Centre for Climate Change Research, University of Bern
Federal Office of Meteorology and Climatology, MeteoSwiss, Locarno-Monti

Abstract

Wind gusts impact many sectors such as wind energy, insurance, transportation and weather forecasting. Whereas mean wind speeds are regularly verified in models, strong wind gusts (wind gusts >20 ms^{-1}) are not often analysed. The aim of this study is to verify how well the COSMO-2 model simulates wind gusts and strong wind gusts in different weather situations in Switzerland. SwissMetNet ground weather station measurements for the period 18.02.2008–31.12.2014 are used as the reference dataset. The 2.2 km model resolution requires the use of a single-observation neighbourhood-model verification, where not only the grid-point containing the station, but a neighbourhood of grid-points are involved. Out of the neighbourhoods, four different data sets are generated. With the aid of the strong wind gust measurements, lightning data, ERA-Interim front data and MeteoSwiss' foehn index, a new adapted weather events classification is produced for each station location. These events allow the calculation of skill scores and accuracy measures for each weather situation and at each station. To capture differences in accuracy, the results are displayed on maps, as well as correlation-similarity and error-decomposition diagrams. The accuracy and the skill, as well as the difference in number of hours with strong wind gusts between the measurements and the model data sets vary strongly between stations. The highest skill in simulating strong wind gusts is found for winter storms, followed by foehn and mixed situations. The lowest skill is found for front and convective situations. The biases are mostly positive for all wind gusts and negative for strong wind gusts. For convective, foehn, front, mixed and all situations, approximately half the stations have biases in all wind gusts that significantly contribute to the total error. For winter storms there are less stations. For the maximum gusts most stations have significant biases. The error in correlation generally contributes more to the pattern error than the error in variance. The smallest pattern errors in all wind gusts are found for front and all situations, followed by mixed, winter storms, foehn and the greatest pattern errors occur in convective situations. This project has shown a way of verifying wind gusts and strong wind gusts for different weather situations in a high-resolution model.

Contents

Chapter 1

Introduction

Wind gusts play an important role in numerous activity sectors. For example, to assess the possible wind energy resources at a potential wind park site, the turbulence in the local environment needs precise modelling (Landberg et al., 2003). Turbulence that is too strong is detrimental to wind rotors (Storm et al., 2009) and wind turbines need to be slowed down in case of wind speeds that are too high. The importance of wind gusts in the train transportation sector can be seen by the use of wind nowcasting along train tracks (e.g. Hoppmann et al., 2002). Due to lighter bodied designs and increasing speeds of trains, crosswinds are more influential than they were before. Furthermore, strong wind gusts cause damage to infrastructures and constructions (Heneka and Ruck, 2008). These damages have increased because of the greater exposure of constructions (Barredo, 2010). According to several studies, greenhouse-gas warming is likely to further increase economical losses related to winter storms in Europe (e.g. Della-Marta et al., 2009; Schwierz et al., 2010).

Through dynamical downscaling and subsequent parametrisation of turbulence, wind gusts can be estimated at local scales (e.g. Goyette et al., 2003). This was done, for example, in the near-convection resolving numerical weather model COSMO-2 (Consortium for Small Scale Modeling) by MeteoSwiss, which simulates, among other variables, wind gusts at an hourly resolution and a spacial resolution of 2.2 km. Users can best benefit from the models' full potential when the quality and performance of the model are known. The performance is commonly quantified through a verification, which may also expose possible ways of improvement. In this study, the wind gusts of the COSMO-2 model analysis will be verified.

Traditionally, model verifications compare station measurements with their corresponding grid-point values in the model (also called Single-Observation Single-Forecast Verification, in short SOSF-Verification; Ebert, 2008). However, for instance because of the "double-penalty" effect (Jolliffe and Stephenson, 2012; Gilleland et al., 2009; Ebert, 2008), SOSF-Verifications are unable to show the benefits of a high spatial resolution (Gofa et al., 2015). Fortunately, along with the

increase in resolution, verification methods have been adapted (more about the progress and challenges of forecast verification in Ebert et al., 2013). An overview of verification methods is given in Gilleland et al. (2009). For the present study, the method of interest is the single-observation neighbourhood-forecast verification (SONF-Verification Ebert, 2008), which compares single observations with a neighbourhood of grid-point values. Each measurement is matched with a value from the neighbourhood of grid-points, out of which verification measures can be calculated. There are several ways of composing vectors of grid-point values for the ensuing comparison: The grid-point values can for example be inverse-distance averaged (IWD), or the vector can be composed of the maximum value of all grid-points (MAX). In this study, these two versions are complemented by the values of the grid-points with the smallest horizontal distance (HOR) and the values of the grid-point with the smallest optimal distance (OPT; following Kaufmann, 2008), which favours grid-points with small vertical distances to the stations.

Several studies have verified wind speed simulations (e.g. Pinson and Hagedorn, 2012; Friederichs et al., 2009; Garcia-Diez et al., 2015; Friederichs and Thorarinsdottir, 2012), however not many have verified strong wind gusts for different weather situations simultaneously. For the model COSMO-2, Schubiger et al. (2012) observed an underestimation of the wind gusts >20 ms^{-1} at the ground-level. Stucki et al. (2016) compared wind gust parametrisations of different models for recent and historical winter storms in Switzerland. The bias in the COSMO-2 simulation of peak gusts was found to be negative and larger in mountain regions than on the Swiss Plateau. They also reported that valleys can have both positive and negative biases. Furthermore, they established that the model is able to reproduce the observed evolution of gustiness but has difficulties in capturing the magnitude and timing of peak gusts. Lastly, the turbulent part of the wind gust parametrisation was found to be under-represented (Stucki et al., 2016). Aside from winter storms, other weather phenomena such as for example foehn, fronts and convective processes can produce strong wind gusts. With a resolution of 2.2 km, the COSMO-2 model can easily resolve large-scale weather processes, but convective processes pose a greater challenge. Since each weather phenomenon produces strong wind gusts differently, the model is likely to have varying success in simulating them.

1.1 Objectives and research questions

In this study the wind gusts and strong wind gusts (>20 ms^{-1}) of the COSMO-2 model analysis will be verified for different weather situations at ground-level in Switzerland. The four mentioned versions of neighbourhood data sets will be compared to the measurements from SwissMetNet ground weather stations. The following research questions will be addressed:

- How well does the COSMO-2 model analysis represent wind gusts and strong wind gusts (wind gusts >20ms^{-1}) in different weather situations and in different regions of Switzerland?
- Which version of the four neighbourhood data sets is best suited to represent strong wind gust in different weather situations?

Chapter 2

Data

This verification is done on the hourly COSMO-2 model analysis wind gust speeds (section 2.2) over Switzerland. They are compared for different weather situations to wind measurements from 108 SwissMetNet ground weather stations (chapter 2.1). The weather situations are classified using the measured wind speeds, lightning data (chapter 2.3), foehn index data (chapter 2.4) and ERA-Interim front data (chapter 2.5).

2.1 SwissMetNet ground weather stations

The SwissMetNet station network is composed of more than 100 modern, automatised and standardised ground weather stations, of which 133 provide the wind measurements that are necessary for the analysis. 25 of these 133 stations were left out because they did not measure wind between at 10±3 metres above ground (table A.1). The network assembles earlier station networks (ANETZ, Klima and ENET) and since 2009, new stations have continuously been added (MeteoSwiss, 2016c). Fig. 2.1 shows which stations have measurements for less than the full research period.

For most stations, the wind measurements are either done by a combined wind sensor 14512 by Lambrecht (anem_lamb_14512_SMN) or by an Ultrasonic Anemometer 2D tool produced by Thies (anem_thies_2D MeteoSwiss, 2016b; Widmer, 2016, table A.1). The Lambrecht wind sensor measures wind speed at an accuracy of ±2 % and a 0.1 ms^{-1} resolution. The wind direction has an accuracy of ±1 % and a resolution of 0.1 degrees. The measuring range is between 0 and 35 ms^{-1} (Lambrecht, 2016). The Thies anemometer measures wind speed and direction with the same accuracy and resolution as the Lambrecht wind sensor, however the measuring range goes up to 75 ms^{-1} (Thies Clima, 2016). Most stations measure wind speed every 10 minutes at 10 m above ground (data provided by Widmer, 2016; Fisler, 2016), but for representativeness reasons, some use different measurement heights (Fig. A.4). If for instance the wind encounters obstacles close to the stations, the different height minimizes their influence by accounting for the zero-plane displacement. It is difficult to gauge how this adaptation influences the results of the

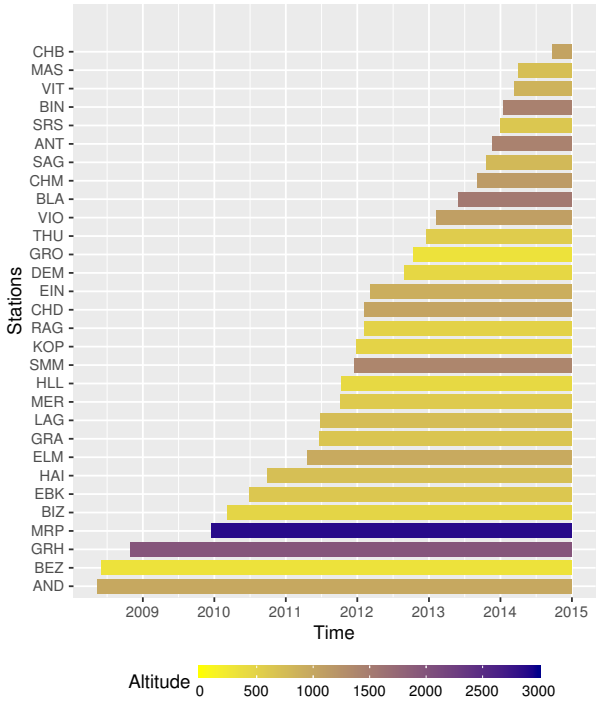

Figure 2.1: Temporal data availability of all SwissMetNet stations that do not have measurements for the entire research period (18.02.2008-31.12.2014). The colors indicate the altitudes of the individual stations. Periods with missing data are not shown.

verification. To hinder a great influence of very different measurement heights on the results, the stations with measurement heights smaller than 7 and greater than 13 m were therefore left out. The wind measurements are at a later stage routinely checked for quality and main instrumental errors are removed (MeteoSwiss, 2016a).

Aside from measurement heights and altitudes, 4 station criteria rating the representativeness of the location were provided by Fisler (2016) for 72 stations, of which 56 are within the list of 108 stations. These criteria are the wind class according to Davenport (Davenport; Fig. A.1 and table A.2), the CIMO Siting Classification (CIMO, Fig. A.2 and table A.3) and the effective roughness length (ERL, Fig. A.3) (see Appendix chapter A.2).

2.2 COSMO-2 model analysis

The Consortium for Small-Scale Modeling (COSMO)-Model is a non-hydrostatic, limited-area, numeric weather prediction model that is based on primitive, thermo-hydrodynamical equations describing compressible flow in a moist atmosphere. The model values are calculated for a rotated

coordinate system with grid-cells that have defined altitudes. The basic version of the model was developed by the German Weather Service (DWD) and since then, several meteorological services have complemented their own model versions (Doms et al., 2011). The COSMO-2 model was further developed by MeteoSwiss and its analysis of the strong wind gusts at ten meters above ground (called `VMAX_10M`) is being verified here. A model analysis uses observations on an irregular grid to represent the atmospheric state and correct the model forecast (Dee et al., 2011). The model has a spatial resolution of 2.2 km and a temporal resolution of one hour. It covers central Europe and data was provided for the period between 18.02.2008 and 31.12.2014.

2.2.1 Wind gust parametrisation

In COSMO-2, the wind gusts are parametrised following Panofsky and Dutton (1984) as shown in Eq. 2.1. The wind gusts are calculated by adding a product of the tuning parameter α (=3), the drag coefficient for momentum C_D and the mean wind speeds at approximately 10 meters V'_m to the mean wind speeds at 30 meters V_m (Schubiger et al., 2012).

$$V_{turb} = V_m + \alpha * 2.4 * \sqrt{C_D} * V'_m \tag{2.1}$$

2.3 Lightning data

By measuring with several electromagnetic sensors, lightning strikes can be geographically located. The measured parameters comprise the impact points (coordinates), the exact time (in seconds), the current intensity, the current polarity as well as the number of subsequent strikes (EUCLID, 2016b). For Switzerland the data was provided to MeteoSwiss by the European Cooperation for Lightning Detection (EUCLID) service operator Meteorage (EUCLID, 2016a). Lightning occurs typically in convective weather situations, which is why it was used to determine the convective hours for each station (see chapter 3.2.1).

2.4 Foehnindex data

Dürr (2008) developed an index that automatically detects South foehn in Switzerland. It is calculated with the mean wind speeds, the gust wind speeds, the wind directions, the relative humidities and the potential temperatures from several ground weather stations in the Alps. For each station, thresholds must be exceeded and conditions met such that the past 10 minutes can either be considered without foehn (0), with foehn (mixed situation (in german *Foehnmischluft*) and foehn with lower wind speeds; 1) or with foehn where strong gusts are clearly expected (2). The foehn index data was provided by MeteoSwiss, except for the foehn index data of station EVI, which was provide by (Dürr, 2016). Additionally to the foehn index data, foehn wind direction

sectors that indicate the possible wind direction of foehn wind were also provided. With these wind direction sectors, foehn events can be validated.

2.5 Front data

Schemm et al. (2015) developed two automated methods to detect extra-tropical fronts in the lower troposphere. One method relies on the gradient of equivalent potential temperatures and the other is based on the wind shift (for more details read Schemm et al., 2015). Using these methods, the fronts from 1979 to 2014 have been detected on the 850 hPa level in the ERA-Interim reanalysis dataset (more about this dataset in Dee et al., 2011). This data set has a 1° x 1° grid spacing and 6-hourly temporal resolution.

Chapter 3

Methods

The methods, that are used for this analysis have been divided into six main sections. After a first data processing and quality check (chapter 3.1), weather situations and weather events are determined for each station individually (chapter 3.2). The high resolution of the model and the relatively large distance between stations suggests applying a single-observation neighbourhood-forecast (here model) verification (chapter 3.3). By using this method, more than one grid-point per station are taken into account and the double-penalty effects are avoided. This method involves defining neighbourhoods (nbs) and calculating new nb model data sets as well as normalized accuracy measures (chapter 3.5) for each station and weather situation. Preceding the accuracy measures, simple scores provide another way of describing the model performance (chapter 3.4). In the last step, spatial patterns of resulting values are further investigated (chapter 3.6).

3.1 Data quality control

Wind measurements are unique, because they provide a true record of the speed and direction of the wind at the time and location where they were measured. However, instruments sometimes fail due to external influences such as the instruments being frozen up. Such periods of data are usually already replaced with a filling element indicating missing data, such as "NA" or "-999". However, to be sure no instrumental error is still present within the data, a few steps have been taken to check the data quality. The first step is to simply plot the wind speed time series. On such graphs, missing data periods become visible and outliers or strange patterns can emerge. The second step is to produce histograms of the wind speeds of each station. If no wind speed occurs unusually often, the data is expected to be error-free. The last step is to calculate box plots of the wind speeds at each station, through which the range and distribution of the data is summarized. Since the data does not have any overly strange patterns, outliers or unusually frequent wind speeds, no corrective measures needed to be taken.

3.2 Weather Situations

Although several wind and weather classifications already exist for Switzerland and Europe (see Schuepp et al., 1994; Weber and Furger, 2001; Weusthoff, 2011) a new hourly classification that is tailored for strong wind gusts in Switzerland has been constructed for each station. The hours of the research period are attributed to the main weather situations that are expected to deliver strong wind gusts. There are six weather classes, composed of five weather situations: *fronts*, *foehn*, *convective* situations, *winter storms* and *mixed* situations. The sixth class is called *all* situations; it joins all other classes into one class. Except for the *winter storm* situations, all situations were defined independently of the available strong wind gust data. *Mixed* situations are the hours during which several weather situations occurred simultaneously. A weather event is defined as a continuous sequence of hours with the same weather situation. If possible, weather events involving strong wind gusts are extended such that they last at least 7 hours. This minimum period approximates the time interval within which the model is being allowed to temporally misplace a strong wind gust. Each station has its own weather classification (also called weather events time vector) which is independent of any other stations classification (except for *foehn*; will be explained in chapters 3.2.2 and 3.2.5). By identifying all weather events for each station individually, the stations end up having a varying number of events of different lengths. The individuality is because of the substantial movement of weather phenomena across time and space, which renders a single temporal weather classification for all stations simultaneously problematic. Moreover, depending on their location, the stations are exposed to different weather phenomena with different frequencies. Lastly, having individual weather events time vectors for each station also simplifies finding regional patterns within the results. To avoid simultaneous weather situations and too short events, the vectors are post-processed (see chapter 3.2.5). The weather events will also be the base for the binary verification involving simple scores (see chapter 3.4).

3.2.1 Convective situations

A definition that separates *convective* from non-convective events with lightning data has been developed at the Karlsruhe Institute for Technology. By this definition, the weather is convective for a location, if within 20 minutes at least 5 lightning strikes have been measured within a 10 x 10 km area at a proximity of 30, 40 or 50 km to a station. The numbers in this definition were chosen based on a sensitivity study (Mohr, 2015). For this study, the definition was applied to a 50 km radius. The reason being that a strong convective wind gust should not, if possible, be missed due to a restricted lightning scan radius around a station. However, to find the hours that are clearly convective, the convective hours need at least 20 convective strikes.

3.2.2 Foehn situations

Since *foehn* produces strong wind gusts mostly in valleys, not all stations in Switzerland are expected to have this weather situation within their weather events time vector. However, some stations that are in the vicinity of the stations with Foehnindex data (from now on called "foehn stations") shown in Figure 3.1 do not have their own Foehnindex data. For these stations, the periods with foehn are copied from neighbouring foehn stations. The neighbouring foehn stations are chosen based on the distance and location within the valley. Which station is associated with which other foehn station is written on the top left of Figure 3.1. Figure 3.1 shows more stations, than the stations used in the verification, because the foehn index is independent of heights of the measurement instruments. Therefore, to define *foehn* events, all available stations have been taken into account. To define foehn hours, the 10 minutes foehn indices equal to 2 were extracted. The foehn indices equal to 1 were left out, because they are expected to only indicate foehn situations with low wind speeds. A repeated analysis which included these showed no clear difference. If within an hour, at least one 10 minute period has a foehn index of 2, this hour is considered to have *foehn*. Choosing a higher number of 10 minute periods within the hour instead of only one does not alter the result enough to instigate a more detailed study that would justify the choice of another threshold.

3.2.3 Front situations

Following the main wind direction, fronts generally cross Switzerland from west to east. At ground-level, a front is displaced by around 100 km relative to the location at 850 hPa (Markowski and Richardson, 2010). Since the ERA-Interim front data show the fronts at 850 hPa, the related strong wind gusts at ground-level are expected to be geographically displaced accordingly. This is why, additionally to the grid-cells in Switzerland, a few grid-cells west of Switzerland have been chosen to indicate front hours. Twelve grid-cells were chosen for the North- and Alpsstations and three cells for the South-Stations (see areas delimited by the dashed blue line on Fig. 3.2). If fronts are found on any of these grid-cells, any strong wind gust measured by the corresponding stations during this or the subsequent five hours will be classified as frontal wind gusts.

3.2.4 Winter storm situations

In Europe, winter storms are extreme weather phenomena that are associated with intense cyclones. Their winds can be very strong and since they cross large areas, their gusts are expected to be measured by many stations. Once the events from weather situations mentioned previously are defined, the remaining unclassified hours are likely to be winter storms, if within the same hour, numerous stations simultaneously measure strong wind gusts. After defining *convective*, *foehn* and *front* events, they are superimposed to form one vector containing events from three different weather situations. Since the events are identified independently from each other, they

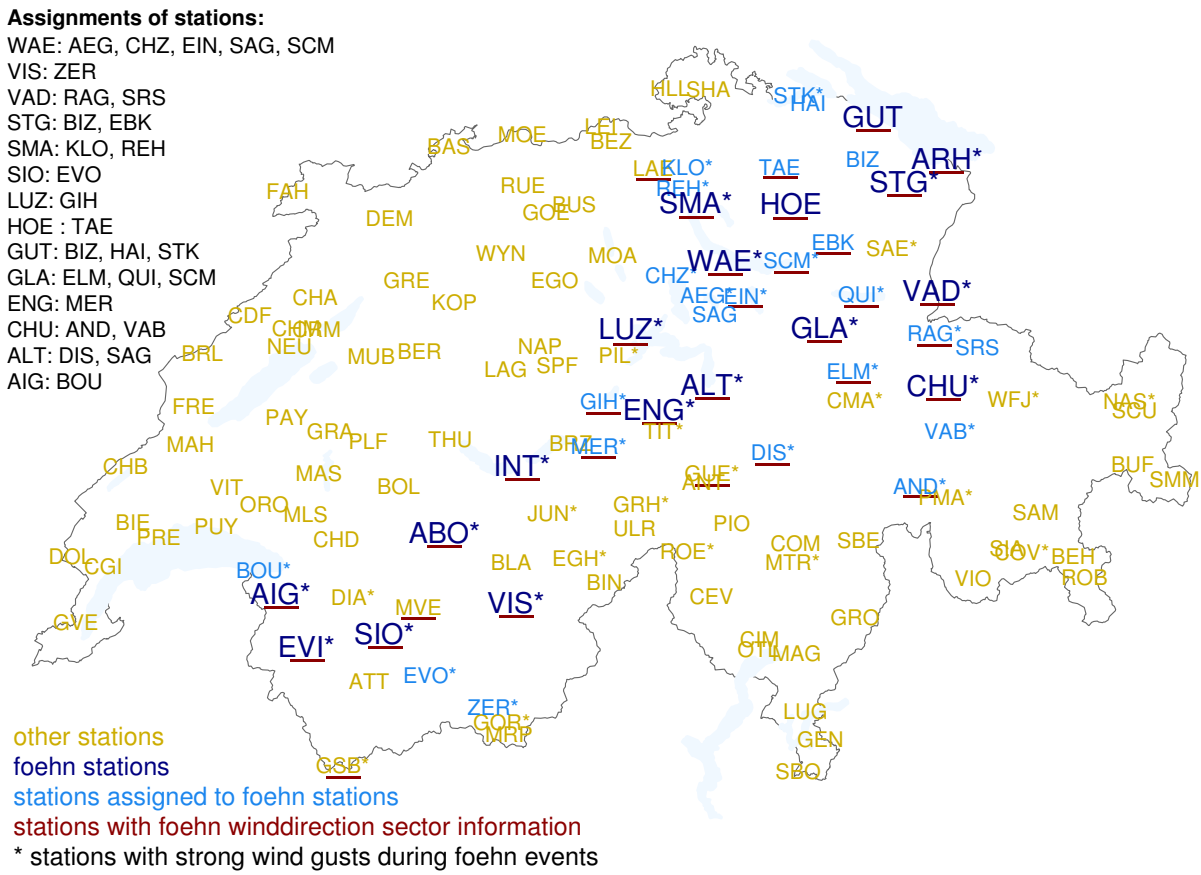

Figure 3.1: Map showing Switzerland and the SwissMetNet Stations. The stations with Foehnindex data are in navy, stations that are additionally given Foehnindex data are in blue, the red lines indicate stations that have information on the wind direction sector that is usual in foehn situations and the asterisks indicate which stations have events with strong wind gusts during foehn weather situations.

sometimes overlap. Before defining winter storm events, this vector goes through the first two post-processing steps (see chapter 3.2.5). This is done to bypass classifying strong wind gust hours as winter storm events while the potential winter storm event is actually found within short gaps between existing weather events. Winter storms are investigated between October and April when a minimum of 13 stations measure a strong wind gust within the same hour. Additionally, the cases where the median wind direction of all stations is less than 180 degrees are left out. As the wind storm hours now only contain the actual strong wind gust hours, the events are extended by 5 hours in both directions.

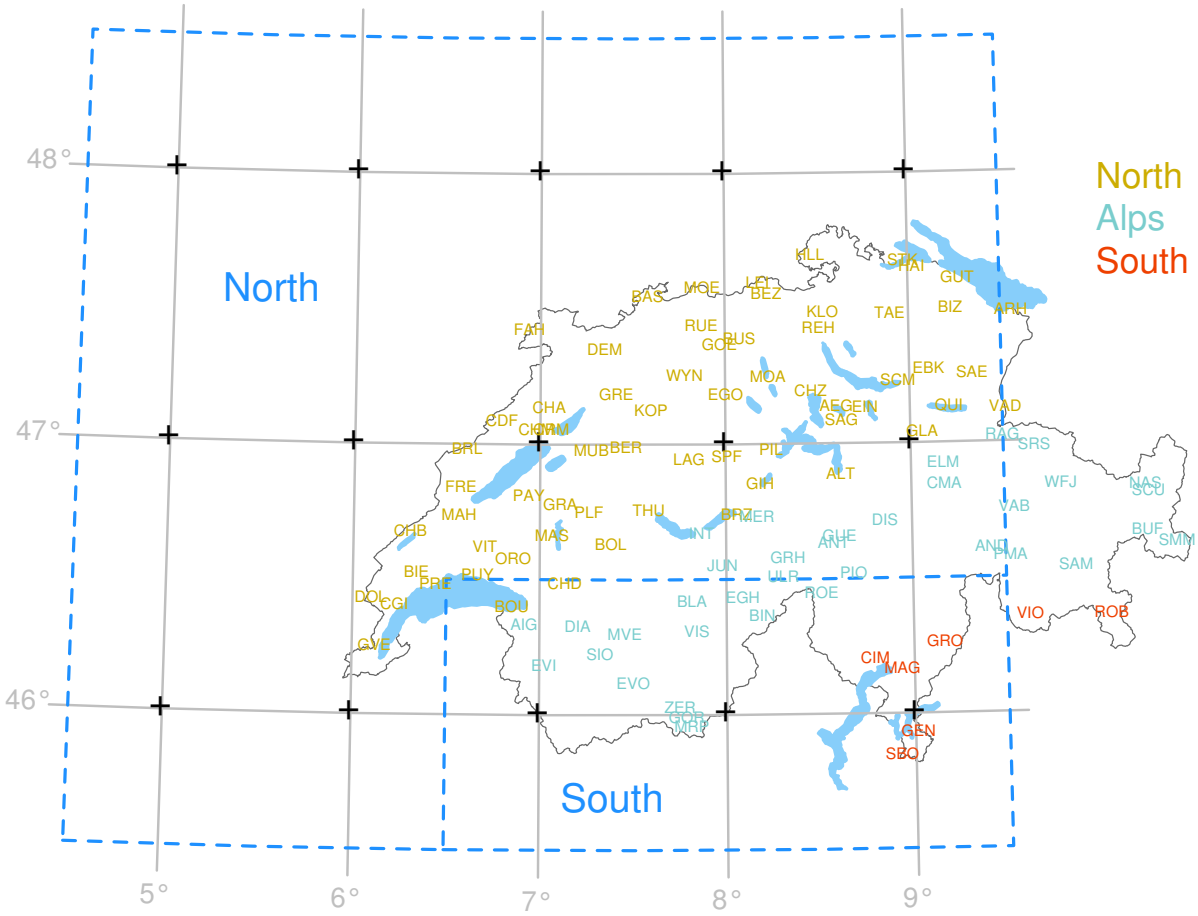

Figure 3.2: Map showing Switzerland, the SwissMetNet Stations and the ERA-Interim grid. The stations are coloured according to their region. The North and South grid-areas of the ERA-Interim data set used to determine front hours are shown in blue.

3.2.5 Post-Processing of the hourly weather situations time vectors

By separately defining the hours with the different weather situations (see rows "Foehn","Convection" and "Front" in Fig. 3.3) and then superimposing them into one time vector per station (see row "Initial vector") some hours have multiple weather situations at the same time (blue cells). In the first post-processing step, the hours with more than one weather situation within the same hour (from now on called hybrid events) are either converted to one of the five weather situations (1 = foehn, 2 = convection, 3 = front, 4 = winter storms, 5 = mixed situations) (see row "After 1st step" in Fig. 3.3). The hybrid events that involve foehn are treated differently if that station has information on foehn wind direction sectors: If the wind direction of the mean wind is within the foehn wind direction sector, then the hybrid event is converted to foehn (see in the example hours 6 and 18). If it is not, the hour is attributed to either the other weather situation (see hour 7) or to mixed situations (see hour 17). For all stations that have foehn index data but no foehn wind

direction sectors, mixed situations involving strong wind gusts and foehn are assigned to "mixed situations". Table 3.1 shows which hybrid event is converted into which weather situation.

Table 3.1: Assignment of hybrid events to weather situations. The numbers are explained below the table.

hybrid events (old numbers)	**weather situations (new numbers)**
101,103,105,107,109,111,113,115	foehn (1)
3,102	convection (2)
5,104	front (3)
9,12,13,108,112	winter storm (4)
6,7,10,11,14,15,106,110,114	mixed (5)

old numbers: (1 = foehn (F), 2 = convection (C) ,) 3 = F+C, (4 = front (T),) 5 = T+F, 6 = T+C, 7 = T+C+F, (8 = winter storm (S) ,) 9 = S+F, 10 = S+C, 11 = S+C+F, 12 = S+T, 13 = S+T+F, 14 = S+T+C, 15 = S+T+C+F.
All numbers +100 = mean wind direction is within foehn wind direction sector.

With the second step, up to 3 hours long gaps between same weather situations are filled to form one long weather event. Gaps are periods that have not been assigned to any weather situation (see row "After 2nd step", hour 3). Thirdly, each weather event is extended to any unclassified strong wind gust if it occurs within 3 hours of this event, since this strong wind gust is likely to be part of the same event (see row "After 3rd step"). Cases, where two weather situations are in the vicinity of the strong wind gust are attributed to "mixed situations". Lastly, weather events that are not "mixed situations", that do not have strong wind gusts and that last only one hour are either replaced by neighbouring situations or, if the event is surrounded by "no weather situation" (0), converted to "no weather situation" (see row "After 4th step"). Through this 4th step, two events that in reality could be one are united and one hour long events are left out. The "mixed situations"-events do not receive this treatment, because the point of mixed situations is to avoid assigning strong wind gusts to either weather situations, if it is not clear to which situation it belongs. Even after these four steps, many strong wind gusts still remain unclassified. These are often measured during foehn at stations of high altitudes. This is why another post-processing step has been added: At any of the stations in the Alps above 1850m and at the Stations Pilatus (PIL) and Säntis (SAE), unclassified strong wind gusts are attributed to foehn if the following is true: It is done if some stations indicate foehn, but no other weather situation except possibly convective weather is detected at any other station in Switzerland during the same hour. Convective situations are allowed because any yet unclassified strong wind gust at a higher altitude is very unlikely to be associated with them.

Hours	20	21	22	23	24	1	2	3	4	5	6	7	8	9	10	11	12	13	14	15	16	17	18	19	20	21	22	23	24	1	2	3
Foehn	1	1	1	1	0	1	1	0	1	1	1	1	0	0	0	0	0	0	0	0	0	1	1	0	0	0	0	0	0	0	0	0
Convection	0	0	0	0	2	0	0	0	0	0	0	0	0	0	2	2	0	0	0	0	0	2	2	0	0	0	0	2	2	0	0	0
Front	0	0	0	0	0	0	0	0	0	0	4	4	4	4	4	4	4	4	4	4	4	4	0	0	0	0	0	0	0	0	0	0
Initial vector (sum)	1	1	1	1	2	1	1	0	1	1	5	5	4	4	6	6	4	4	4	4	4	7	3	0	0	0	0	2	2	0	0	0
Wind sector foehn*											y	n										n	y									
After 1st step	1	1	1	1	2	1	1	0	1	1	**1**	**3**	**3**	**3**	**5**	**5**	**3**	**3**	**3**	**3**	**3**	**5**	1	0	0	0	0	2	2	0	0	0
After 2nd step	1	1	1	1	2	1	1	**1**	1	1	1	3	3	3	5	5	3	3	3	3	3	5	1	0	0	0	0	2	2	0	0	0
Presence of SWG*	0	1	0	0	0	0	1	1	0	0	1	0	0	0	0	1	1	1	1	0	0	0	0	0	0	0	0	0	0	0	1	0
After 3rd step	1	1	1	1	2	1	1	1	1	1	1	3	3	3	5	5	3	3	3	3	3	5	1	0	0	0	0	2	2	**2**	**2**	0
After 4th step	1	1	1	1	**1**	1	1	1	1	1	1	3	3	3	5	5	3	3	3	3	3	5	**5**	0	0	0	0	2	2	2	2	0

Figure 3.3: Example of how the weather situations vectors are post-processed. Changes are written in bold. "Wind sector foehn" indicates whether the mean wind direction of mixed events involving foehn are within the foehn wind direction sector (y) or not (n). "Presence of SWG" tells if this hour has a strong wind gust (measured wind gust $>20ms^{-1}$) (1) or not (0). See section 3.2.5 for more explanations.

3.3 Single-Observation Neighbourhood-Forecast verification

A single-observation neighbourhood-forecast (SONF; here model) verification consists of evaluating a model by comparing several surrounding model-grid point values to a single observation for each measurement location. This method is, on the one hand, useful in cases where observations are coarsely distributed. On the other hand, it is fitted for medium to high resolution models because it accounts for the closeness of a simulated phenomenon. When doing a traditional verification (single-observation single-forecast) of a high-resolution model, the double-penalty effect can affect the results. The double-penalty effect describes when a model is penalized twice, once for missing and a second time for giving a false alarm on the same event. Rather than reprimanding the model twice for not simulating a phenomenon at the exact right location and time, the SONF method allows the model to simulate it with a slight lag or delay. A neighbourhood (nb) can either be squared or circular (Jolliffe and Stephenson, 2012). In this study, the nb is chosen following Kaufmann (2008): The nb includes all grid-points that are within a horizontal distance of 1.415 times the grid resolution, which in this case means within 3.14 km. Using this radius, each station is surrounded by 4 to 7 grid-points as shown in Figure 3.4. The varying number of grid-points depends on the location of the station within the COSMO-2 grid-cell. Having several grid-points around a station poses two challenges: Firstly, the altitudes of all grid-points of the model are expected to represent the average altitude of the topography covered by their grid-cells. As shown in Fig. 3.5, these altitudes can approach but also clearly deviate from the altitudes of the corresponding station. The average vertical distance between all grid-points within the nb and the altitude of a station was calculated in two steps: After calculating the vertical distance between each grid-point and the station, the distances were averaged with the equation

$$trimean = \frac{Q1 + 2 * Q2 + Q3}{4} \tag{3.1}$$

where Q1, Q2 and Q3 are the first, second and third quartile. The trimean was chosen instead of the average, because with the average the large distances would be too influential. The trimean values vary between -842 m and +713 m with most values between 0 and 200 m. The larger vert dist are clearly at stations on mountain tops; the two big dark red points are the stations PIL (Pilatus) and SAE (Säntis). The second challenge is to define new simulation time series using the values of the nb grid-points. Accordingly, four data sets have been defined below. Two of them use the optimal distance, which accounts for the vertical distance and gives it more weight as shown in eq. 3.2. d_{opt} is the optimal distance, d_{hor} is the horizontal distance, d_{vert} is the vertical distance and f_{ve} is the vertical emphasis factor (Kaufmann, 2008).

$$d_{opt} = d_{hor} + f_{ve} * |d_{vert}| \qquad \text{with} \quad f_{ve} = 500 \tag{3.2}$$

The data sets used for the SONF verification are:

- Values of the grid-point with the smallest horizontal distance (HOR): These values should represent the grid-cell in which the station is located and are the values that would be used in a traditional verification.
- Values of the grid-point with the smallest optimal distance (OPT): Even though the horizontal distance might be larger, this grid-point is expected to simulate more similarly wind speeds because of the similar altitude. If the vertical distance between the station and the closest horizontal grid-point is small, OPT will be identical to HOR.
- The highest value of all grid-points within the neighbourhood (MAX): This data set will indicate how much the maximum values within the neighbourhood resemble the measurements.
- The inverse-optimal-distance-weighted average of all grid-points within the neighbourhood (IDW): This data set represents the average of all grid-point values. By using the optimal distance, the grid-points with large vertical distances are given less weight.

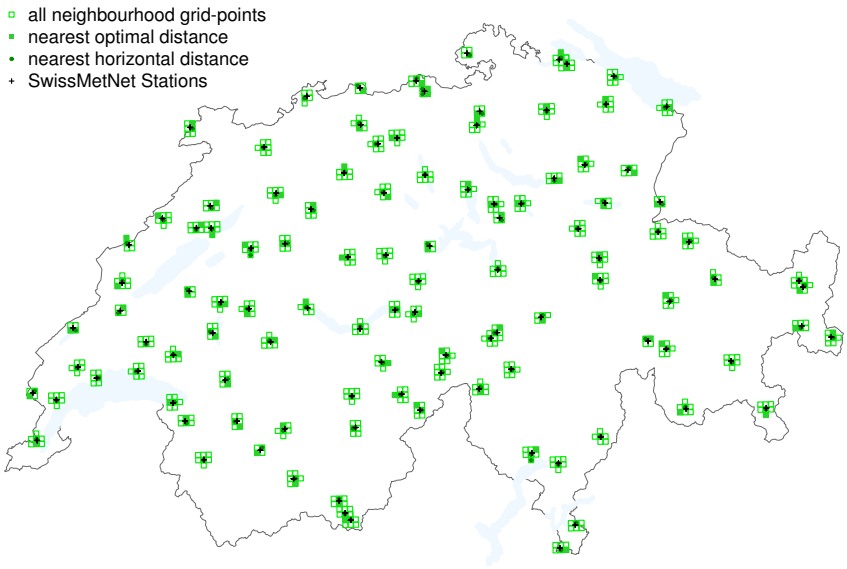

Figure 3.4: Map of Switzerland with COSMO-2 grid-cells within 3.14 km of each SwissMetNet Station, the grid-cells with the smallest horizontal and smallest optimal distances to the corresponding station are indicated as explained in the legend.

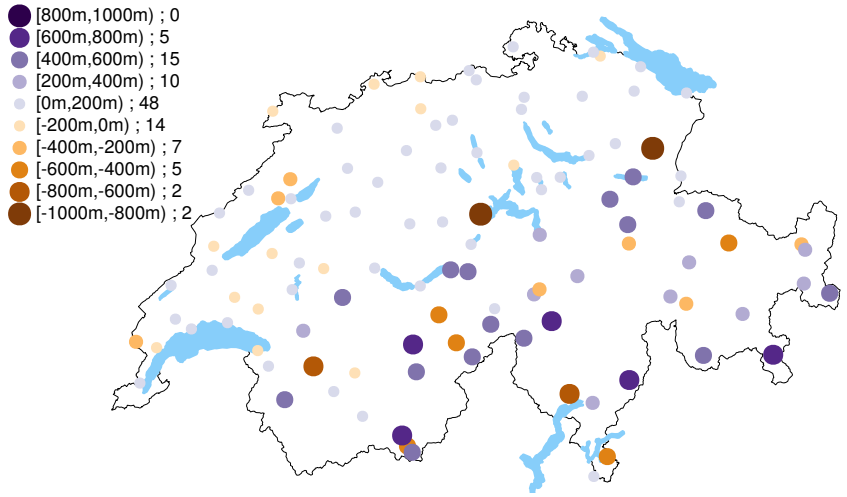

Figure 3.5: Trimean of the vertical distances between the altitudes of the COSMO-2 grid-points within 3.14 km of each station and the altitudes of the stations, divided into 10 classes. Positive (negative) values indicate cases where the grid-points are on average higher (lower) than the station. The legend shows the distance ranges of each class and the number of stations that are within each class.

3.4 Skill measures

For binary events, the number of events and non-events of observations and models are commonly displayed in a 2x2 contingency table (see Table 3.2). Using this table as a base, many summary statistics (also called performance measures) are calculated (Ferro and Stephenson, 2011; Mason, 2003). The reader is referred to the website http://www.cawcr.gov.au/projects/verification/#Methods_for_dichotomous_forecasts to get a quick overview of these measures. In this study, events and nonevents are divided by the existence respectively lack of existence of at least one strong wind gust (wind gust $>20\text{ms}^{-1}$) within the weather event.

Table 3.2: Contingency table for binary (yes-no) events (adapted from Ferro and Stephenson, 2011)

	Events observed	Nonevents observed	Total
Events modelled	a (hits)	b (false alarms)	a+b
Nonevents modelled	c (misses)	d (correct non-events)	c+d
Total	a+c	b+d	n

The measures that were chosen are the Hit Rate (also called the Probability of Detection; eq. 3.3), the False Alarm Ratio (eq. 3.4) and the Critical Success Index (also called Threat Score; eq. 3.5; Wilks, 2011). a, b and c are the values from the contingency table. These equations have two main advantages: Firstly, they are independent on the number of correct non-events (d) and secondly they together give all the necessary information about the relation of number of hits compared to the number of false alarms and misses.

$$HR = \frac{a}{a+c} \tag{3.3}$$

$$FAR = \frac{b}{a+b} \tag{3.4}$$

$$CSI = \frac{a}{a+b+c} \tag{3.5}$$

3.5 Accuracy measures

Model accuracy is usually measured with the unconditional bias, the root-mean-square error (RMSE) and the Pearson correlation coefficient (Koh et al., 2012). In order to quantify model accuracy for a scalar field, these accuracy measures are commonly normalised by the variance of the observations (σ_O^2). However, the observations and model cannot be exchanged because these normalised measures are not symmetric. Another consequence is, for instance, that the over- and under-prediction of atmospheric variability is not penalised equally. Koh et al. (2012) suggests to normalise the accuracy measures with the sum of the variances of the observations O and the model F ($\sigma_O^2 + \sigma_F^2$). With this method, the normalised measures become symmetric and the accuracy more transparent. Following Koh et al. (2012), the accuracy (or model performance) is described by decomposing the total error into the pattern error (chapter 3.5.1) and the bias error (chapter 3.5.3). To simplify the comparison of model performances, two new plots that resemble the Taylor diagram were supplemented. The following paragraphs will present these new plots and discuss the characteristics, qualities and limitations of these new measures in detail.

3.5.1 Measures of pattern error

The natural generalization of the correlation coefficient

The natural generalization of the correlation coefficient (ρ ; eq. 3.6) is a measure of difference in phase. It was defined by Dietzius (1916) and has been evaluated to be the least noisy correlation diagnostic by Aparna et al. (2005). ρ can range between -1 to 1 with 1 being the best possible value. A ρ of 1 (-1) indicates that the model and observations are completely in (out of) phase.

$$\rho = \frac{1}{\sigma_O * \sigma_F} * \overline{(F - \overline{F}) \cdot (O - \overline{O})} \qquad , -1 \leq \rho \leq 1 \tag{3.6}$$

The variance similarity

As the name suggests, the variance similarity (η ; eq. 3.7) quantifies how much the variances of the model and observation are similar, which is done by comparing the standard deviations. η ranges between 0 and 1 with 1 meaning that the model and observation have an equal standard deviation. An η of 0 indicates that the the model and observations fluctuate with infinitely different amplitudes.

$$\eta = \frac{\sigma_O * \sigma_F}{0.5 * (\sigma_O^2 + \sigma_F^2)} \qquad , 0 \leq \eta \leq 1 \tag{3.7}$$

This measure has the additional advantage that it increases monotonically with increasing similarity (Koh et al., 2012).

The normalized error variance

The normalized error variance (α ; eq. 3.8) is a measure that calibrates the pattern error (which combines both the error in phase and amplitude) made by the model against a random forecast made from knowing the climatological mean. α ranges between 0 and 2 with 0 being the best value. A value of 0 means that the phases and amplitudes of the model and observation match perfectly. A value of 1 indicates that the model has equal chance of predicting an anomaly in one direction or the opposite, i.e. the model is as well as the random forecast and the covariance of the model and observation is equal to 0. If α is 2, the observation and forecast have an equal variance but are exactly out-of-phase (Koh et al., 2012).

$$\alpha = \frac{\sigma_D^2}{\sigma_O^2 + \sigma_F^2} \qquad \text{with} \quad D = F - O \tag{3.8}$$

ρ, η and α can be visualized on the correlation-similarity diagram, which is similar to the Taylor diagram (see next chapter).

3.5.2 Correlation-Similarity Diagram

The Correlation-Similarity Diagram (CorrSim; Fig. 3.6) is a polar plot that summarizes all information about similarity in variance and correlation. The radial distance indicates the size of the error in phase (natural generalisation of the correlation coefficient ρ, eq. 3.6) and the angle from the y-axis ϕ (eq. 3.9) denotes the error in amplitude (variance similarity η, eq. 3.7). In case ρ is positive (negative), the point will be in the lower (upper) half of the plot.

$$\phi = \arccos(\eta) \tag{3.9}$$

The η values are also shown surrounding the plot in black font. The bigger the angle towards the right (left) side of the central y-axis, the greater (smaller) is the variance of the model compared to the variance of the measurements. The other y axis shown on the left of the plot scales the normalized error variance α. Additionally, circular contours corresponding to ρ/η are drawn. $|\rho/\eta|$ smaller (bigger) than 1 means that the amplitude error contributes less (more) to the total error than the phase error (Koh et al., 2012).
As an example, points A and B represent the results for two different data sets: A and B are both within the lower half of the plot, which means that for both simulation data sets the correlations with the reference data set are positive. Data set A (B) has a greater (smaller) variance than the reference data set, since the point is on the right (left) side of the y-axis. Compared to data set A, data set B is more similar in amplitude like the reference data set (because ϕ_B is smaller than ϕ_A). However, data set A is more similar in phase, since ρ_A is bigger than ρ_B. Since point A is on the ρ/η=1 circle, the contribution from the phase error is as high as the contribution from the amplitude error. Point B is within the ρ/η=1 circle so the contribution from the phase error

is more important than the contribution from the amplitude error. In the context of this study, a bigger amplitude error would be worse than a bigger phase error. The reason is that a lag or lead in timing a strong wind gust incident is not as bad as missing or giving a false alarm on the presence of strong wind gusts during an event.

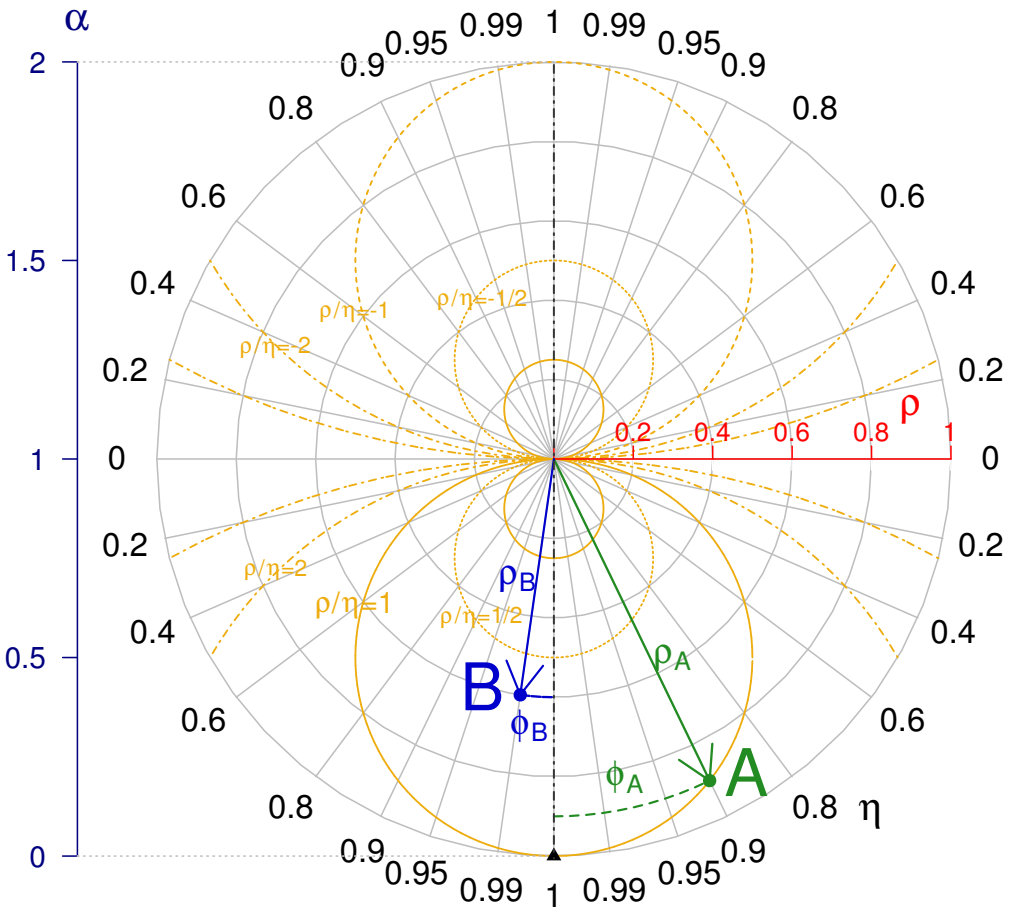

Figure 3.6: Correlation-Similarity Diagram (following Koh et al., 2012) with example points A and B (see explanations in chapter 3.5.2).

To improve comparisons of point clouds on the same diagram, two kinds of medians are drawn. The difference lies in how the point clouds are treated: The first kind of median ignores the polar coordinate system and shows the actual centre of the point cloud (see for example Fig. 4.12). This median represent neither the medians of η nor ρ, it shows the centre of α and emphasises how the points are distributed horizontally and vertically. Since this median would give a false impression of the centres of ρ and η, a second kind of median is provided: The second kind shows the true centres of ρ and η. η does not indicate by itself which variance is larger, it only tells the magnitude of the difference between variances. To know if η should be drawn on the left or the right side of the diagram, the standard deviations of the measurements and the simulations have to be compared. Furthermore, the size of η increases both from the left and from the right side of the y axis, it is not possible to draw only one point to represent the median of η. Therefore, the medians of all ρ and all η values within each quarter of the diagram are calculated separately. In the results, only the medians of the bottom two quarters are shown (see for example Fig. 4.14).

3.5.3 Measures of bias error

Normalising the RMSE and the bias, which are related as shown in eq. 3.10, results in a new equation (eq. 3.11; fully written out in eq. 3.12) with three new variables, the normalised RMSE δ, the normalised pattern error σ and the normalised bias μ.

$$RMSE^2 = var(D) + bias^2 \qquad \text{with} \quad D = F - O \tag{3.10}$$

$$\delta^2 = \sigma^2(1 + |\mu|^2) \tag{3.11}$$

$$\left(\frac{RMSE}{\sqrt{\sigma_O^2 + \sigma_F^2}}\right)^2 = \left(\frac{\sigma_D}{\sqrt{\sigma_O^2 + \sigma_F^2}}\right)^2 \left(1 + \left(\left|\frac{\overline{D}}{\sigma_D}\right|\right)^2\right) \tag{3.12}$$

μ also measures statistical significance because the magnitude of μ is the paired t-statistic multiplied by the square root of the number of degrees of freedom in the data. The larger μ, the more significant is the bias error. If μ is within the range -0.5 to 0.5, the contribution of the bias to the total error is negligible, because the error variance is at least twice as big as the bias itself (Koh et al., 2012). The size of δ gives information on the contribution of the RMSE to the error, compared to the variances of the data sets: If δ is very large, the variances of the model and observation are very small compared to the RMSE. If δ is smaller than 1, either or both variances are big compared to the RMSE. Finally, σ measures the normalized pattern error and can range between 0 and$\sqrt{2}$. The upper limit comes from the relation with α: σ is defined to be the square root of α and thus cannot exceed$\sqrt{2}$. σ^2 in eq. 3.11 could be replaced with α or with $(1 - \rho * \eta)$. The smaller σ, the better is the performance of the model.
For an easy comparison, the values of δ, σ, and μ are plotted in an error decomposition diagram (see section 3.5.4).

3.5.4 Error-Decomposition Diagram

Like the correlation similarity diagram, the error decomposition diagram (ErrDec; Fig. 3.7) is a polar plot that shows three variables, however it summarises the results on the bias error. The radius has the length of the normalised RMSE δ, the angle γ from the y axis is a measure for the normalised bias μ (eq. 3.13) and the left y axis shows the scale of the normalised pattern error σ (Koh et al., 2012).

$$\gamma = \tan^{-1} \mu \tag{3.13}$$

For an interpretation example, points A and B are added in Fig. 3.7: What initially stands out are the differing sign in μ, the greater radius (δ) for point A compared to point B and the almost equal angles from the y axis. Since A has a μ of -2, it means that the average bias is negative and twice as big as its standard deviation. The δ of A is 1.6, which means that the RMSE is bigger than both or one of the variances of the model and observation. In a similar fashion as for the Correlation Similarity Diagram, the median μ and δ are displayed to represent the average of all points of a point cloud. In this case, there is only one point, because the scale of μ is continuous and not congruent like the scales of η (see for example Fig. 4.11).

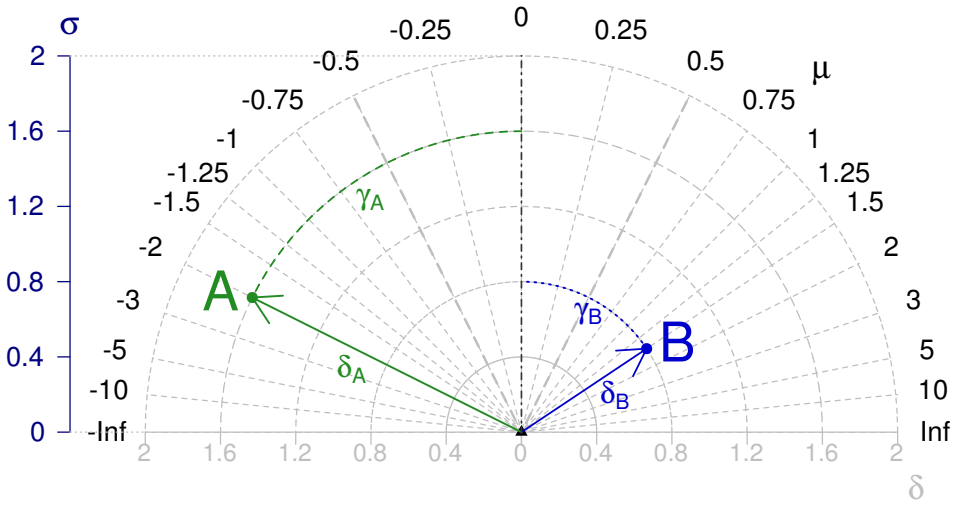

Figure 3.7: Error-Decomposition Diagram (following Koh et al., 2012) with example points A and B (see explanations in chapter 3.5.4).

3.6 Determination of patterns in space

Once the verification is done, two methods are used to investigate spatial patterns. The first is to display the results on maps and visually inspect the patterns. The second method is to measure the strength of the relationship between the results of the verification (for example the simple scores or the accuracy measures) and stations criteria by calculating rank correlation coefficients. The criteria are the ones mentioned in chapter 2.1 and A.2; the the altitudes, CIMO, Davenport and ERL. They are complemented with the (average) vertical distance (vert dist) between the altitudes of stations and the altitudes of the grid-points. For IDW and MAX, the vert dist used is the average of the distances of all grid-points within the neighbourhood as explained in chapter 3.3. For OPT (HOR) vert dist are the actual vertical distances between the grid-points that have the smallest optimal (horizontal) distances to the stations (see figures 3.8 and 3.9).

In this study, the rank correlation was chosen to be calculated using Spearman's rank correlation coefficient (also called Spearman's rho; Wilks, 2011). Spearman's rho has the advantage of being able to recognise strong relationships, regardless of their linearity. By using the ranks instead of the actual values, the result is resistant to outliers and independent of the unit of the correlated variables. It assumes that the relationship between the two variables is monotonic and can have values between -1 (negative association of ranks) and +1 (positive association of ranks). The closer Spearman's rho is to zero, the weaker is the associations between the ranks. Along with the rank correlation, a statistical significance test can indicate if the strength of the relationship happened by chance or not. If the p-value is below 0.05 (0.01), it means that the probability of getting this rank correlation, when actually there is no association between the two variables, is less than 5 % (1 %). If it is the case, the rank correlation is considered to be significant (Jolliffe and Stephenson, 2012). Whenever rank correlations are mentioned in the results and unless the opposite is clearly indicated, the relations are significant with a significance level of 0.05 (*) or 0.01 (**).

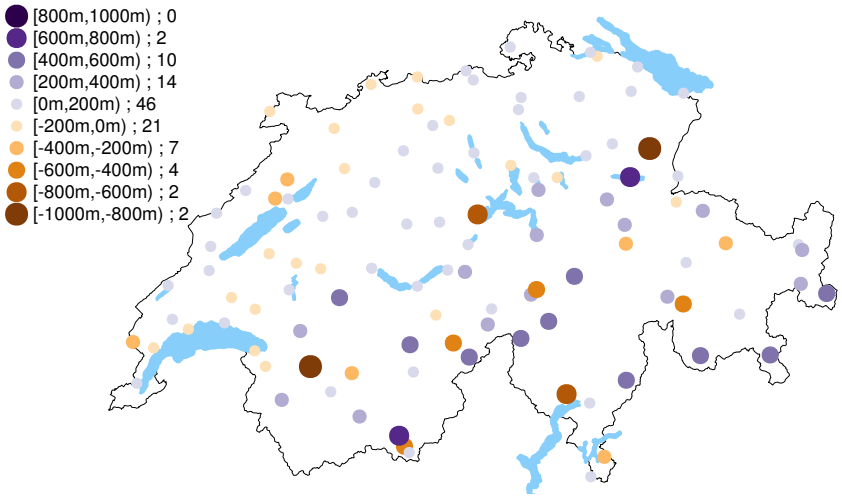

Figure 3.8: Vertical distances between the altitudes of the COSMO-2 grid-points that have the smallest horizontal distance to the stations and the altitudes of the stations, divided into 10 classes. Positive (negative) values indicate cases where the grid-points are on average higher (lower) than the station. The legend shows the distance ranges of each class and the number of stations that are within each class.

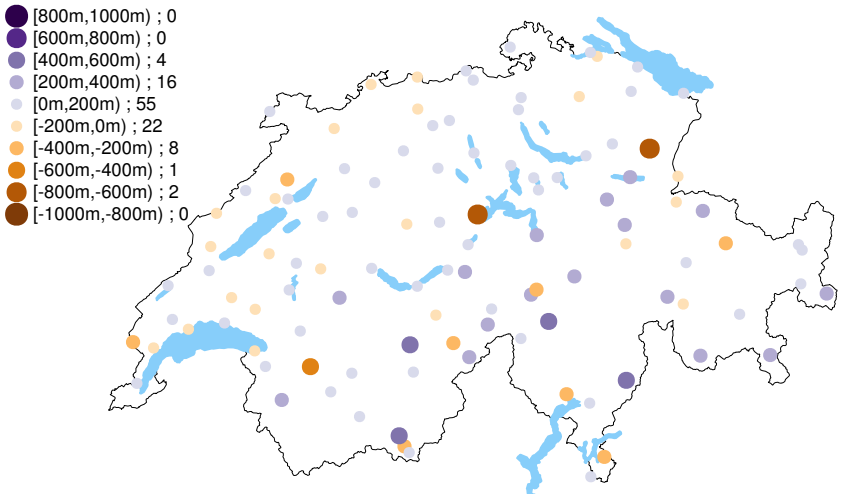

Figure 3.9: Same as figure 3.8, but between between the altitudes of the COSMO-2 grid-points that have the smallest optimal distance (see eq. 3.2) to the stations and the altitudes of the stations.

Chapter 4

Results

4.1 Presence of strong wind gusts in Switzerland

Before showing the results of the verification, this chapter shall given a short overview of the presence of strong wind gusts (SWG) in Switzerland. The highest SWGs ever simulated and measured during the research period are shown in Fig. 4.1. As expected, the lower wind speeds occur in low altitudes and higher wind speeds appear in alpine areas, particularly on mountain tops. At several stations, the measured wind speed maxima are lower than the simulated ones (see for example the stations that have measured maxima between 20 and 26 ms^{-1}). Almost all COSMO-2 grid-points of Switzerland (except the white areas) and each SwissMetNet station have measured or simulated at least one wind gust $>20ms^{-1}$.

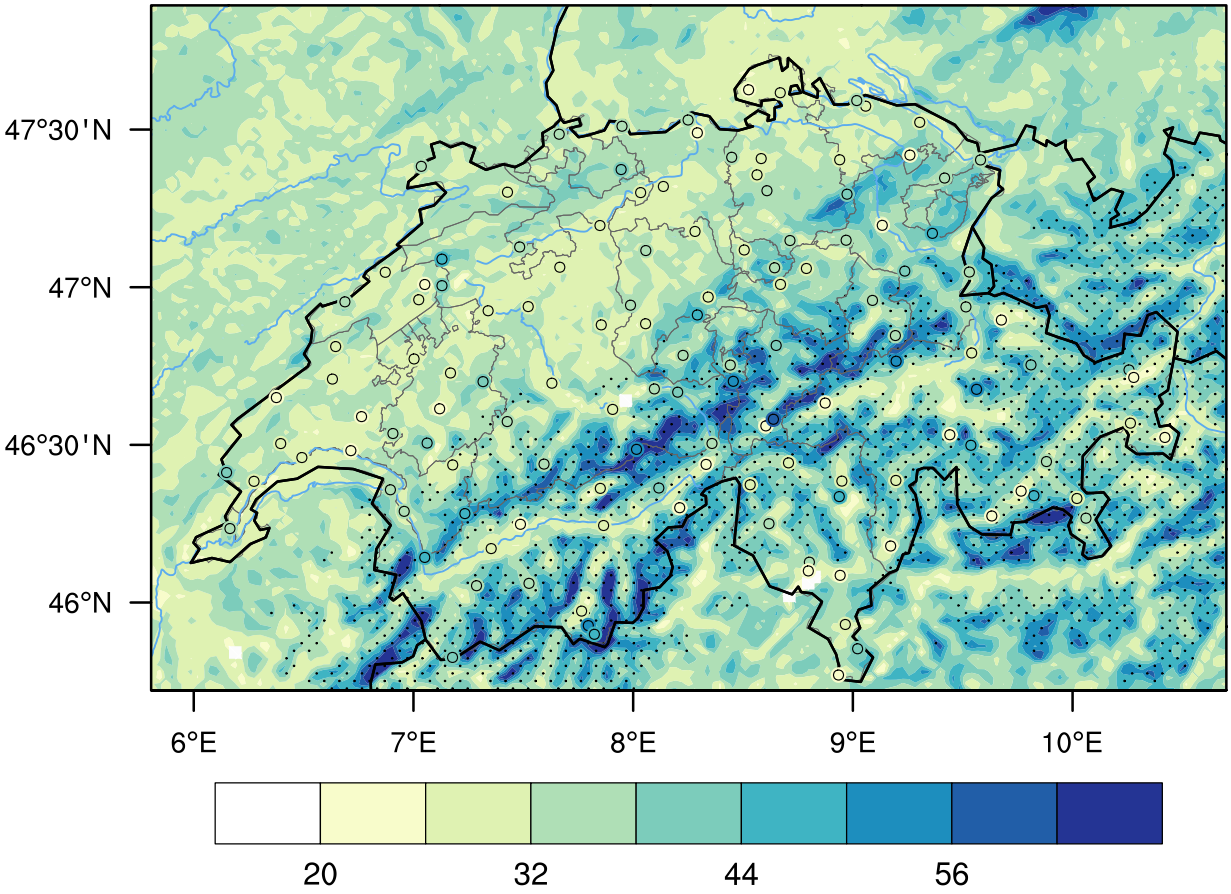

Figure 4.1: Map of Switzerland with maximum speeds of strong wind gusts in COSMO-2 (coloured contours) and at each SwissMetNet Station (points) in ms^{-1} for the period 18.02.2008-31.12.2014. The stippling shows areas with altitudes above 1500m asl, the thin grey lines show the borders of cantons and the blue lines show the main rivers.

4.1.1 Number of hours

The number hours with measured SWGs at each station is shown in Fig. 4.2. The stations with the least hours are MAS (in the canton of Fribourg) and SMM (the easternmost station) and the highest number of hours is at station DIA (6734 hours). The average (median) is 582 (98) hours and the IQR ranges between 31 and 318 hours. In northern Switzerland, the number of hours mostly ranges between 11 and 1000 hours. In the Alps, the numbers vary strongly, depending if the stations are sheltered in valley bottoms or exposed in higher altitudes.

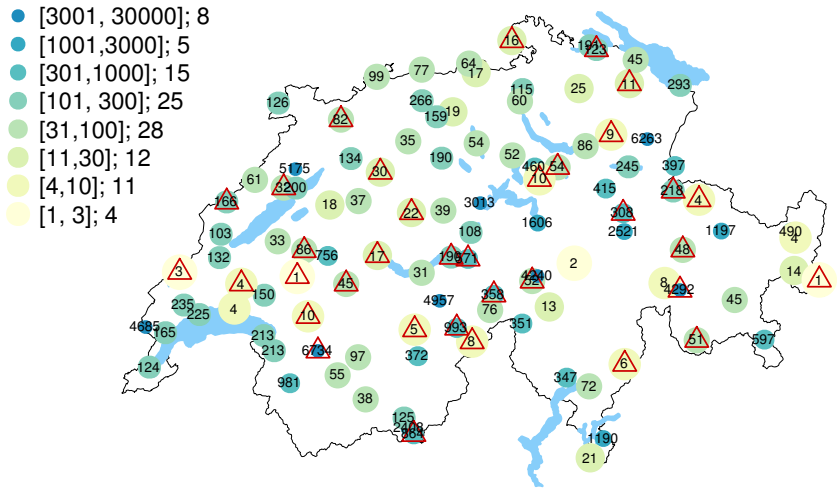

Figure 4.2: Map of Switzerland with number of hours (as numbers and in point classes) with strong wind gusts between 18.02.2008-31.12.2014 measured at each SwissMetNet Station. Aside from the range of each point class, the legend shows the number of stations per class. The red triangles show which stations have data for less than 95 % of the entire research period.

As a first comparison, the number of hours with SWGs of the four data sets MAX, IDW, HOR and OPT (see chapter 3.3) are compared to the number of hours in the measurements (see Fig. 4.3, 4.4, A.5 and A.6). In the model data set, the number of hours were counted within the same available data periods as in the measurements. In data set MAX, the station locations have in the mean (median) 749 (294) more hours with SWGs. This median of 294 more hours is more than twice the median number of hours in the measurements. 26 (4) station locations have more than 1000 more (less) hours. The larger positive differences are predominantly at stations in the Alps. The equivalent figures for data sets IDW, HOR and OPT look very similar; The same stations have larger and smaller differences in number of hours. However, IDW, HOR and OPT have less stations with large positive differences. The average differences between the number of hours are closer to zero than with MAX; the values are -121 (IDW; median is +21), 61 (OPT; median is +42) and -47 hours (HOR; median is +42). With IDW, the largest positive (negative) difference is +3434 (-4692) hours, with HOR it is +3852 (-3979) hours and with OPT it is +4478 (-4824) hours.

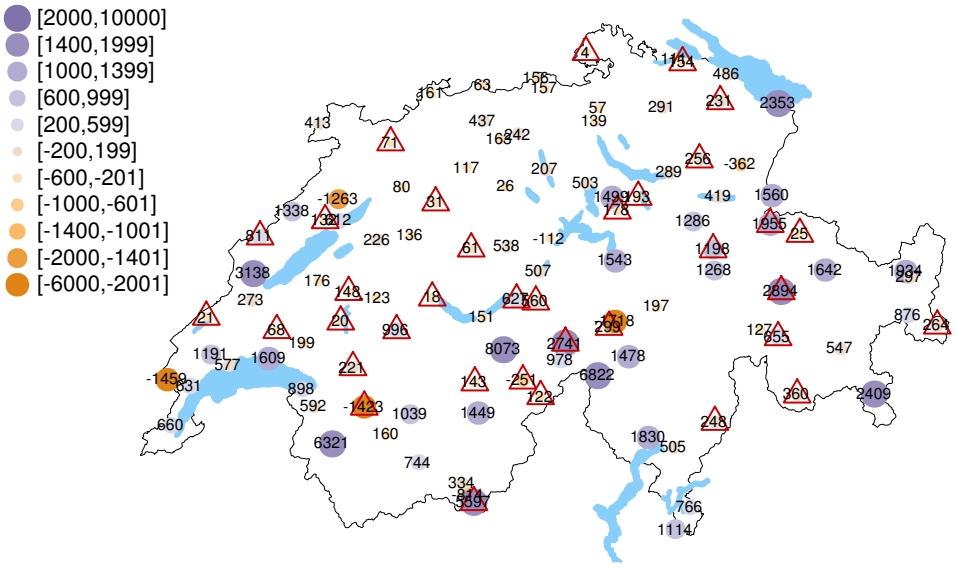

Figure 4.3: Map of Switzerland with difference between data sets MAX and measurements for the number of hours with strong wind gusts between 18.02.2008-31.12.2014 at each SwissMetNet Station (see absolute Nr of hours in measurements in Fig. 4.2). The red triangles show which stations have data for less than 95 % of the entire research period.

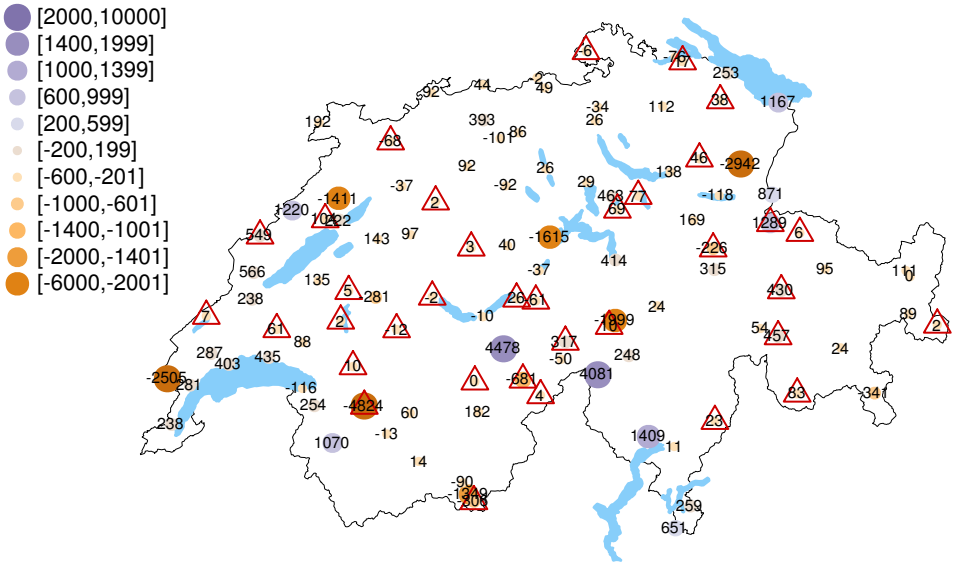

Figure 4.4: Same as Fig. 4.3 but for data set OPT.

4.2 Weather event classification

The different methods mentioned in chapter 3.2, including the post-processing, have successfully assigned 63% of all SWG hours to weather situations. Before post-processing, about 35% of the classified SWG hours were hybrid hours. The steps used in the post-processing of the initial weather situations vectors have reduced the number of SWG hours with no weather situation by about 30%. Still, mostly the stations at high altitudes still have a larger number of SWG hours with no weather situation. Fig. 4.5 shows the (relative) number of hours with SWGs per station and to which weather situation they are assigned to before (see b) and c)) and after post-processing (d)). The top plot (a)) shows the order of the stations in b), c) and d). The stations were first separated by region (as shown in Fig. 3.2), then by altitude (see legend of 4.5 a)) and lastly they were sorted in decreasing order by the stations latitude. The first thing that stands out when looking at panel b) are the larger number of hours in the regions with high altitudes and the very low number of hours in the Alps at stations between 700 and 1850 m. On panels c) and d) the large percentage of hours with the weather situation *winter storm* are striking. The fraction of hours with no weather situation visibly decreases after post processing (panel d) compared to before (panel c). Except for a few stations that are in the southern parts, the stations of region "North<1100m" have approximately 80 to 90% of SWGs with weather situations. Within this region, two stations have more than 500 hours with SWGs: ALT (Altdorf; in Fig. 4.5 Nr. 40) and PLF (Plaffeien; canton of Fribourg; Nr. 45). In Altdorf, about 90% of the SWGs happen during *foehn* events. In Plaffeien, the *winter storms* predominate. Stations with a high number of SWG hours often have a lot of hybrid F+S hours (*foehn* and *winter storm*; blue bars above the dark brown bars); in most cases these are then converted to *foehn*. After post-processing, some stations in "Alps >1850m" have hours with *foehn* situations (because of post-processing step 5); these SWGs are not really foehn wind gusts but they occur at the same time as other *foehn* events at lower stations. With a few exceptions, the percentages of hours with *convection* and *front* are smaller than the percentages of hours with *winter storm* or no situation. Stations in the regions "North >1100m", "Alps >1850m" and both South regions have about twice as large fractions with *front* hours than stations in other regions. All the hours with weather situations have been distributed into weather events, as shown in the Fig. 4.6, 4.7, A.9, A.10 and A.11.

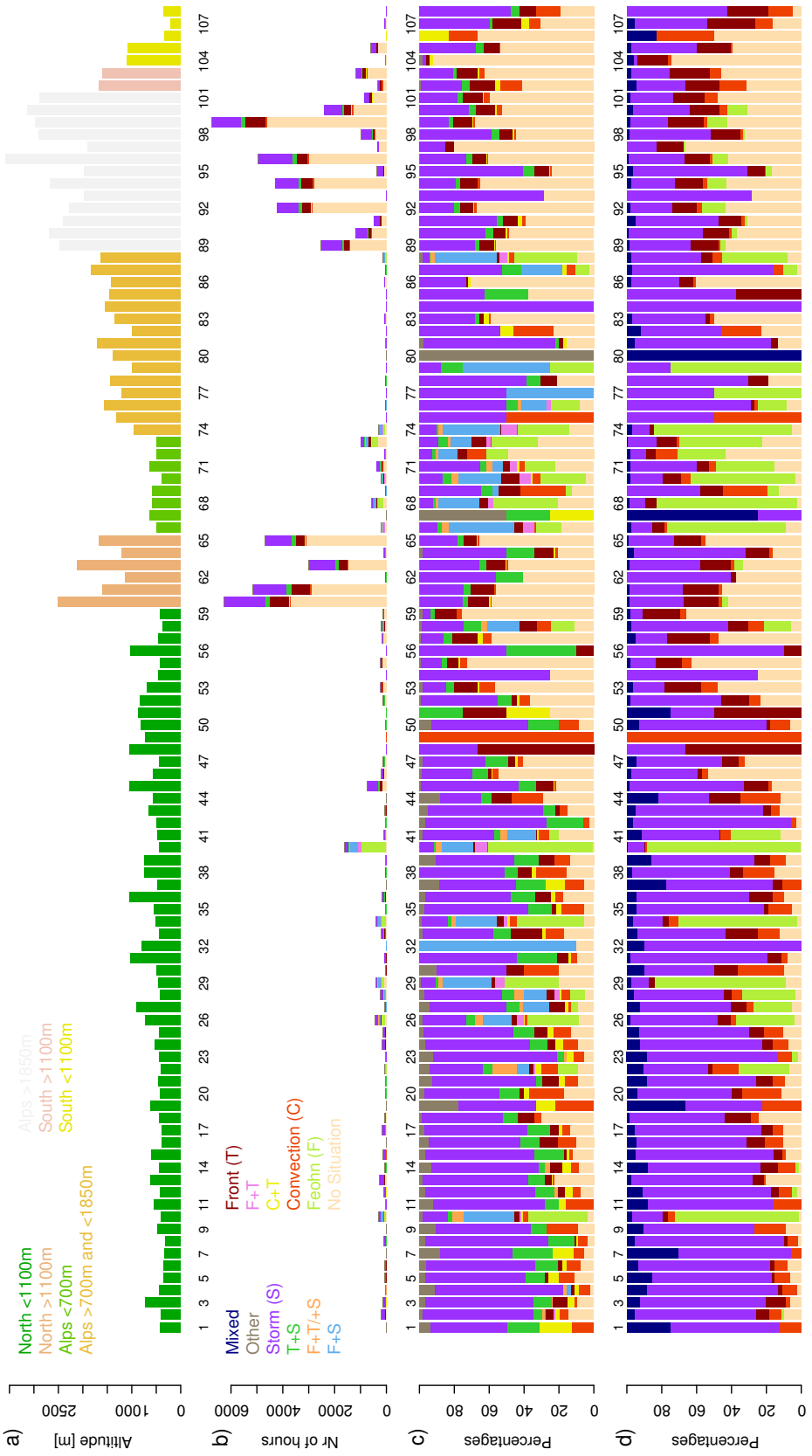

Figure 4.5: ***a)*** *Attitude of SwissMetNet stations order by region and latitude (see Fig. A.7 to see which station is which number);* ***b)*** *Cumulative number of hours with strong wind gusts measured between 18.02.2008-31.12.2014 at all stations, divided into weather situations before post-processing, ordered like a). "Other" includes "F+C","C+S" ,"F+T+C" and "C+T+S". Hours with "F+C+S" and "F+T+C+S" do not occur at all;* ***c)*** *b) as cumulative percentages ;* ***d)*** *same as c) but after post-processing. c) and d) have the same legend as b).*

For the weather situation *foehn*, station ALT (Altdorf) has the highest number of SWG events (see fig. 4.6). Even though stations GUT (Güttingen) is a foehn stations, it has no *foehn* SWG events. Additionally, the stations EBK (Ebnat-Kappel), TAE (Aadorf/Tänikon), BIZ (Bischofszell), HAI (Salen-Reutenen), SRS (Schiers) and SAG (Sattel_Aegeri) have no *foehn* SWG events either, even though foehn index data was assigned to the stations (see chapter 3.2.2). Despite not having any foehn wind direction sector, the stations AEG (Oberägeri), SCM (Schmerikon) and Qui (Quinten) have 32, 16 and 26 *foehn* SWG events. These are all cases where clearly no other weather situation competed for these SWG hours. The legend indicates that 9 (15) stations out of 36 have less than 6 (12) events.

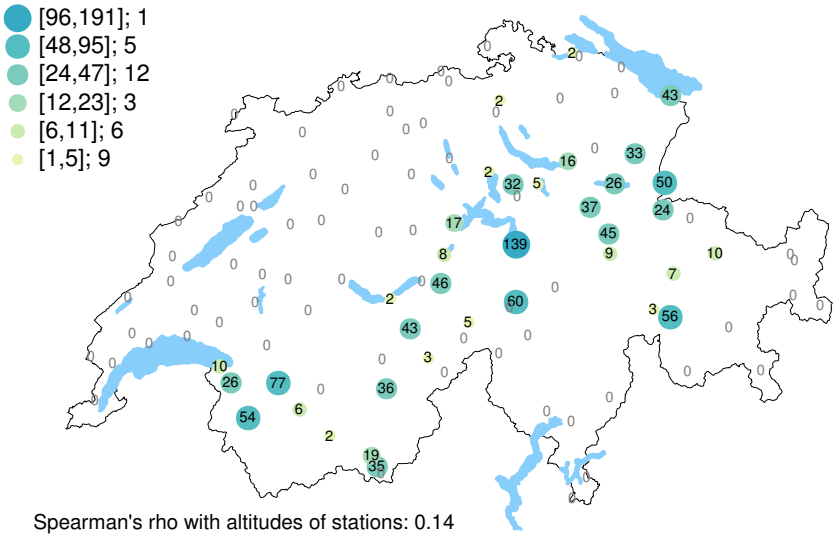

Figure 4.6: Number of strong wind gust events in foehn situations at each SwissMetNet Station. Aside from the range of each point class, the legend shows the number of stations per class.

In *convective* situations, 84 stations have at least one SWG event, out of which 59 stations have less than 12 SWG events (Fig. 4.7). These 59 stations are found in every region. The Spearman's rho value indicates a weak but significant rank correlation (significance level = 0.05) with the altitudes of the stations. Most stations that have no *convective* SWG events are within alpine areas. The highest number of SWG events is found at station SAE (Säntis; 48 SWG events). This station is located on the mountain Säntis, which has a tall telecommunication antenna that attracts lightning strikes. The antenna artificially increased the number of lightning strikes to a much higher number than the surrounding (see red square in north eastern Switzerland on Fig. A.8). Though to a lesser extend, it is also the case for stations PIL (Pilatus) and DOL (La Dôle) and CHA (Chasseral). In regions with fewer lightning strikes, some stations have nonetheless a lot of *convective* events (for example stations JUN (Jungfraujoch)or DIA (Les Diablerets)).
Compared to the previous two weather situations, the *front* class has much more stations with a high number of events (Fig. A.9). 12 stations have more than 47 events, compared to 6 for *feohn*

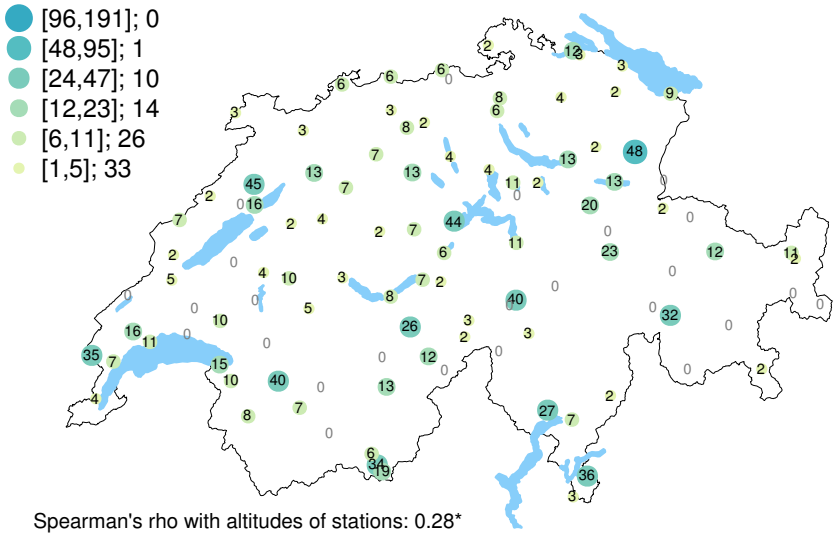

Figure 4.7: Number of strong wind gust events in convective situations at each SwissMetNet Station. Aside from the range of each point class, the legend shows the number of stations per class.

and 1 for *convective* situations. These 12 stations are located at high altitudes or are particularly exposed to wind (for example CHA, PLF, LAE and HOE). The patterns in Fig. A.9 shows that SWGs during *front* situations very rarely reach stations at very low altitudes. The relation to the altitude is also represented in the significant Spearman's rho value of 0.52**. For *winter storms*, the number of event reflects the high fraction of SWG hours at most stations as shown in Fig. 4.5 (A.10). 18 stations have less than 6 events, 70 stations have between 12 and 47 events; and 12 stations have more than 47 events. Differently than *fronts*, no station has more than 95 *winter storm* events. *Mixed* events occur at 78 stations, most of which are not in the Alps (A.11). 41 of these stations have less than 6 *mixed* events. In the region around the lake of Zurich, most stations have between 3 and 10 events and in the region around Bern, many stations have 2 or 3 events. While the highest number of *mixed* events is at station SAE, most high altitude stations have 20 or more *mixed* events.

4.3 Skill measures

In following chapter the skill in simulating SWGs during events where SWGs were measured is assessed. For extreme events, skill scores such as for example the extreme dependency index (EDI) would be efficient at assessing the skill. However, the EDI requires the number of correct non-events (d in the contingency table). Attempts have been made to calculate the numbers for each station and each weather situation but the results were not convincing enough to calculate the EDI (see appendix chapter A.5 for more details). Consequently, simple scores using only the number of hits (a), false alarms (b) and misses (c) were calculated. These simple scores are the Hit Rate (also called the probability of detection), the False Alarm Ratio and the Critical Success Index (see Methods chapter 3.4).

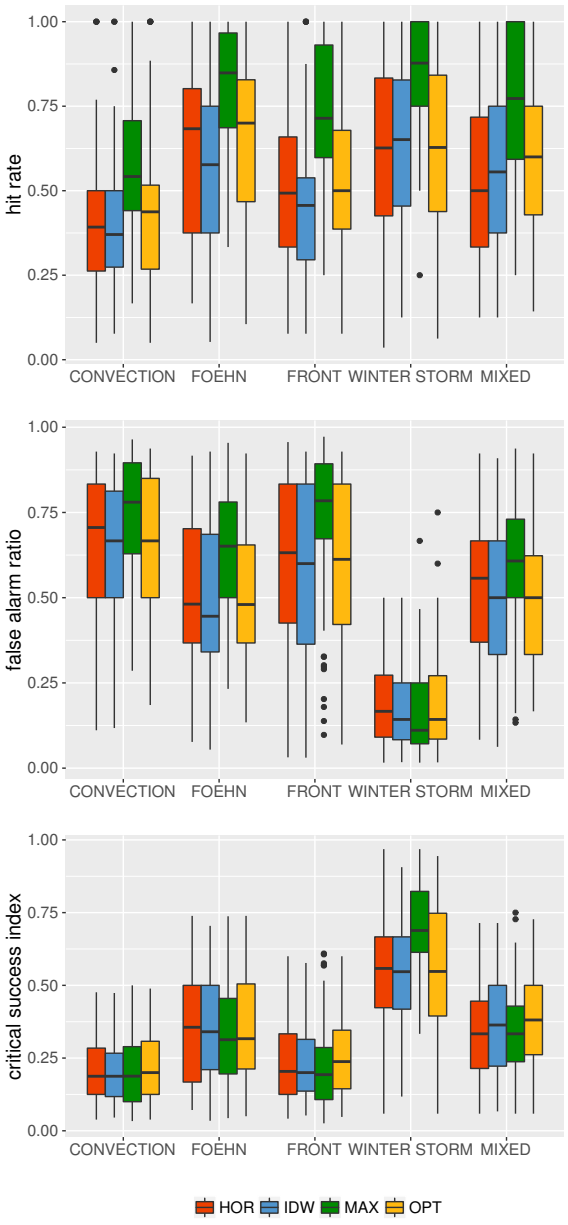

Figure 4.8: Box plots of hit rates, false alarm ratios and critical success indices (also called threat score) for each weather situation and each data set.

The hit rates (HR) are the highest with data set MAX (Fig. 4.8; top panel). After MAX, the highest median HR are reached by OPT, except in *winter storm* situations where IDW has a higher median than OPT. Generally, the box plots of OPT, HOR and IDW are more similar than MAX. IDW has the lowest HR in *convective*, *foehn* and particularly in *front* situations. The HR are lowest in *convective* and highest in *foehn* (for OPT and HOR; Fig. 4.9) and *winter storm* (for IDW and MAX) situations. In *front* situations, the differences between data sets are particularly large; the interquartile range (IQR) of MAX does not overlap with the IQR of IDW. MAX has also the highest false alarm ratios (FAR; Fig. 4.8 ; middle panel). Even though the ranges and medians are very similar, the lowest FAR are with IDW or

OPT. In **winter storm** situations, the FAR are much lower than in other weather situations. This characteristic is not surprising, since the method used to determine *winter storm* events is based on the occurrence of SWGs in the measurements. As the *winter storm* events are defined using the presence of SWGs, the number of events with no measured SWG (b+d) is very small and the model will automatically get a smaller FAR. The number of false alarms (b) is thus not necessarily low thanks to the high skill, but because the number of events with no measured SWGs is very low in the first place. The *mixed* situations have slightly lower FAR than *convective* and *front* situations. These lower rates can be explained by the necessary proximity of at least two different weather situations; the probability that SWGs are detected during hours, where (*mixed*) events with different weather situations happen, is higher than for the single situations. Even so, the median values of the FAR of *foehn* situations are lower for HOR, OPT and IDW. Excluding *winter storms*, these box plots indicate that even though MAX has the highest HR, it also has the highest FAR. As such, out of all four data sets, OPT has the best combination of relatively high HR and low FAR. For *winter storms*, the FAR is as low for MAX as it is for OPT, but the higher HR of MAX increases the skill for detecting SWGs.

The bottom panel of Fig. 4.8 shows the box plots of the critical success index (CSI). These results refine and slightly summarise the information given by the HR and FAR: The CSI is the highest in *winter storm* situations, followed by *foehn* and *mixed* situations and the worst happen in *front* and *convective* situations. As anticipated, the high FAR in MAX is penalised more than the lower HR for OPT: For *convective*, *front* and *mixed* situations, the CSI is the highest with OPT. In *foehn* situations, HOR has the highest CSI, which is unexpected since the combination of HR and FAR are more favourable for OPT. The difference between the different data sets is however not very large in general. Tendentiously, MAX has the higher number of false alarms and HOR, IDW and OPT have a higher number of misses.

In *convective*, *front* and *storm* situations, the CSI (FAR) rank correlates positively (negatively) with the altitudes and negatively (positively) with the vertical distances. The rank correlations of FAR are particularly strong in *front* situations: With the altitudes, FAR correlates between -0.53** and -0.61** and with the vertical dist by between 0.53** and 0.73**. In *winter storm* situations, the rank correlation between FAR (CSI) and the altitudes (vert dist) is weaker than between FAR (CSI) and the vert dist (altitudes). The FAR of *mixed* situations rank correlate by 0.4** to 0.5** with the vert dist. In *front* (*mixed*) situations, the HR of OPT (MAX and IDW) rank correlate by 0.53** (0.55** and 0.56**) with CIMO. In *foehn* situations, the HR of MAX and HOR and the CSI of OPT strongly anti rank correlate with CIMO, Davenport and ERL. The values range between -0.56** and -0.79**. The FAR of *foehn* do not rank correlate significantly with any stations criteria.

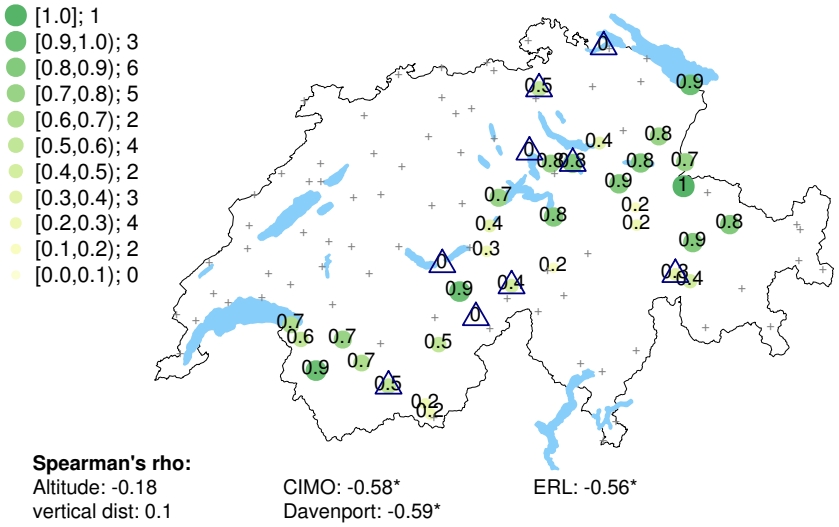

Figure 4.9: Map of Switzerland with Hit Rates of HOR in foehn situations for each SwissMetNet Station as numbers and divided into classes as shown in the legend. The legend shows the ranges of each class and the number of stations that are within each class. The grey crosses show stations that have no strong wind gust events and the triangles indicate the stations that have less than 6 strong wind gust events within this weather situation class. Under the map Spearman's rank correlation coefficients are shown, calculated between the shown data set (excluding the stations that have less than 6 strong wind gust events) and the stations criteria described in chapter 3.6. If a correlation coefficient has one (two) asterisks, the correlation coefficient has a p-value <0.05 (0.01).

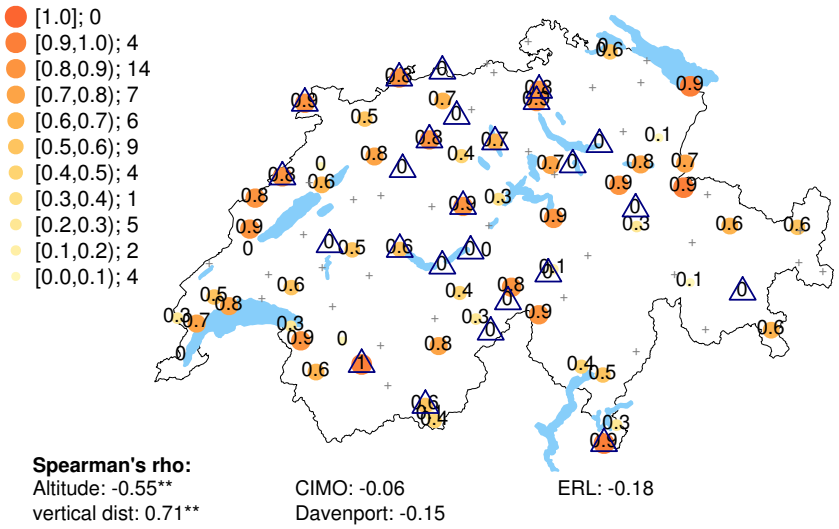

Figure 4.10: Same as Fig. 4.9 but showing the false alarm ratios in front situations.

4.4 Accuracy measures

For each data set, all accuracy measures were calculated once for all weather situations simultaneously and once for each weather situation separately. The measures were calculated in two ways: The first includes all wind gust values of each hour that is within any event of the weather situation, even the values that are below 20 ms^{-1}. This way will be referred as the "all gusts method". The second way was to calculate the measures for only the maximum values of the events where SWGs were measured, called "maximum gusts method". With the later method, it follows that all values of the measurements are at least 20 ms^{-1}. The former method could be seen as a reference accuracy, to which the values of the maximum gusts method can be compared to. To investigate spatial patterns, the results were rank correlated with the stations criteria as mentioned in chapter 3.6. The most important results from the accuracy calculations are summarised in chapter 4.5.

4.4.1 Comparison of data sets and weather situations

All gusts

In general, the data sets IDW, HOR and OPT represent wind gusts very similarly (see for example Fig. 4.11 and 4.12; the same figures for the other weather situations can be viewed in the appendix chapter A.6.1). The difference between data sets is always smaller than the difference between weather situations. The values of the different stations can vary a lot, but the size of the ranges where most values are, stays mostly constant for all weather classes. In all different weather classes and with all stations, the error in correlation is more important the the error in variance. With a few exceptions, which happen mostly in *foehn* situations, the variance similarities (η) are larger than 0.8. The ranges of the (natural generalisation of the) correlation coefficient ρ differ for the different weather situations: The correlations (ρ) tend to be the highest in *front* and *all* situations (values mostly between 0.5 and 0.8) and the lowest in *convective* situations (values mostly between 0.1 and 0.6). In *winter storm (foehn)* situations, the ρ mostly range between 0.4 (0.2) and 0.7 and in *mixed* situations between 0.4 and 0.8. In *foehn* situations with HOR, IDW and MAX, one station (NAS; Naluns/Schlivera) has a negative correlation coefficient. With OPT, HOR and IDW, the median normalised biases are around 0.5 for all but *winter storm* situations. With OPT, HOR and IDW, around half the stations have biases that significantly contribute to the total error. In *winter storm* situations, the median normalised biases are between 0 and 0.1. With MAX, the normalised biases (μ) are consistently more positive than the normalised biases of the other data sets. The median normalised biases vary between 0.8 and 1.1. Except in *winter storm* situations (59%), at least 80% of all stations have biases in MAX that are significant. In MAX, these significant biases are positive in all weather classes and for all stations but three (DOL (La Dôle) in *winter storm* situations; EGH (Eggishorn) and GUE (Gütsch ob Andermatt) in *foehn* situations). With IDW, HOR and OPT, the significant biases in *winter*

storm situations are negative for about a third of the stations (roughly 15 to 20 stations). In the other situations, less than 10 stations have significantly negative biases. Except for *winter storm* situations and with a smaller difference in *mixed* situations, the median of the normalised RMSE (δ) is always about 0.15 larger with MAX than with OPT, HOR or IDW. With OPT, HOR and IDW, the median normalised RMSE δ is the lowest in *all* and *front* situations (0.7), higher in *winter storm* and *mixed* situations (0.75) and the highest in *foehn* and *convective* situations (0.8). The difference between the *winter storm* situations and the other situations is visible in the differences in variance too: For most stations in all weather classes except *mixed* and *winter storm* situations, the OPT, HOR and IDW have larger variances in wind gust speeds than the measurements. In *winter storm* and *mixed* situations, more stations have a smaller variance in the model simulations than the measurements. With MAX, the variances are even larger than with OPT, HOR and IDW. In *winter storm* situations, the balance between stations that have larger and smaller variances in MAX than in the measurement is about equal.

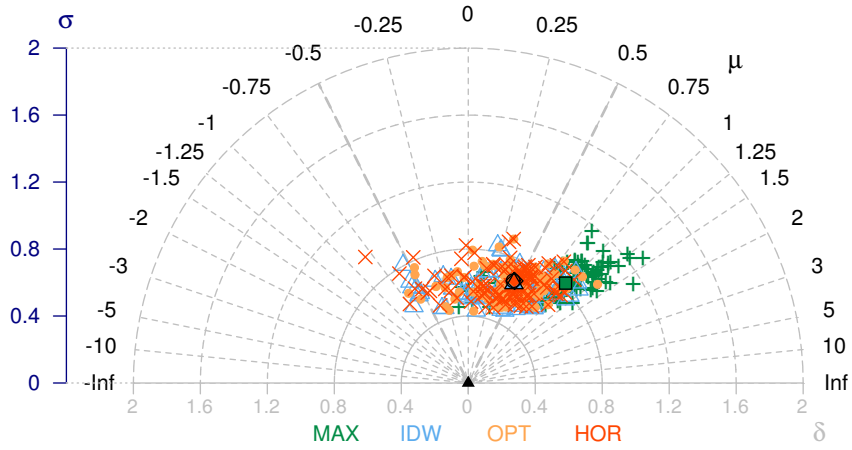

Figure 4.11: Error decomposition diagram showing the normalised RMSE δ, normalised bias μ and the normalized pattern error σ of all wind gust speeds of all events of all weather situations between all COSMO-2 data sets and the measurements (model minus measurements). Each point shows the results of one station and each colour represents a different data set. The points with the black edges are the medians of the equally coloured point clouds. For more explanations about the diagram and median, please read chapter 3.5.4.

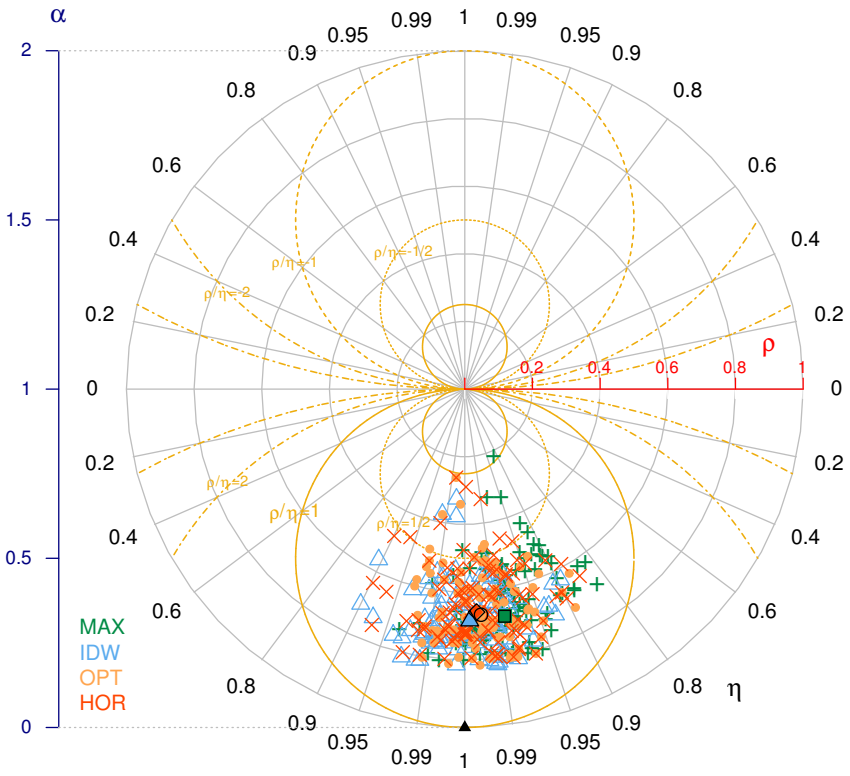

Figure 4.12: Correlation similarity diagram showing the natural generalisation of the correlation coefficient ρ, the variance similarity η and the normalised error variance α of all wind gust speeds of all events of all weather situations between all COSMO-2 data sets and the measurements. Each point shows the result of one station and each colour represents a different data set. The points with the black edges are the medians of the equally coloured point clouds. For more explanations about the diagram and median, please read chapter 3.5.2.

Maximum gusts

Compared to all gusts, the results produced with the maximum gusts method differ manifoldly: First, the accuracy measures vary much more between stations and reach higher and lower values than with all gusts (see for example Fig. 4.13 and 4.14; see Appendix chapter A.6.2 for the corresponding figures showing the other weather classes). Second, the majority of normalised biases (μ) are not as positive as before, but much more negative. Third, the median μ differ strongly between weather situations: For data set MAX, the median μ are negative in *convective* and *mixed* situations (-0.4 and -0.3), (almost) neutral in *front* and *all* situations (-0.1 and 0) and positive in *storm* and *foehn* situations (0.15 and 0.5). With data sets OPT, HOR and IDW, all the median μ are negative. In *foehn* situations, the medians are -0.3 (HOR) and -0.5 (OPT, IDW), in *all* situations they range between -0.6 and -0.75, in *storm* situations they are at -0.75 and in *convective*, *front* and *mixed* situations, they are between -0.75 and -1. Even though the normalised biases are more negative, the variances of the simulated maximum wind gusts are still almost always larger than the variances of the measurements. In these cases, the medians of the correlation coefficient (ρ) range between 0.4 and 0.5 (Fig. 4.14; bottom right quarter). In *convective* situations they range more between 0.3 and 0.4. The median variance similarity (η) also does not vary much; the values are always between 0.8 and 0.9 and for *winter storms* between 0.9 and 0.95. At stations, where the variance of the simulation is smaller than the variance of the measurements (Fig. 4.14; bottom left quarter), the median ρ are much larger (ranging between 0.5 and 0.7; in *convective* situations between 0.2 and 0.5). The third difference is that some stations have fewer values that contribute to the results of the accuracy measures: For these stations, the differences in variance are sometimes more important than the differences in correlation (points in the Correlation Similarity Diagram are outside the $\rho/\eta = 1$ circle), and often they have negative correlations. In most cases, stations with a large number of SWG events have large correlation coefficients (ρ). Lastly, the median normalised RMSE (δ) are larger than with all gusts: With MAX they range between 0.8 and 1 (highest in *all*, *convective* and *foehn* situations; lowest in *winter storm* situations) and with OPT, HOR and IDW they range between 1 and 1.3 (highest in *convective* and *front* situations; lowest in *all* and *foehn* situations).

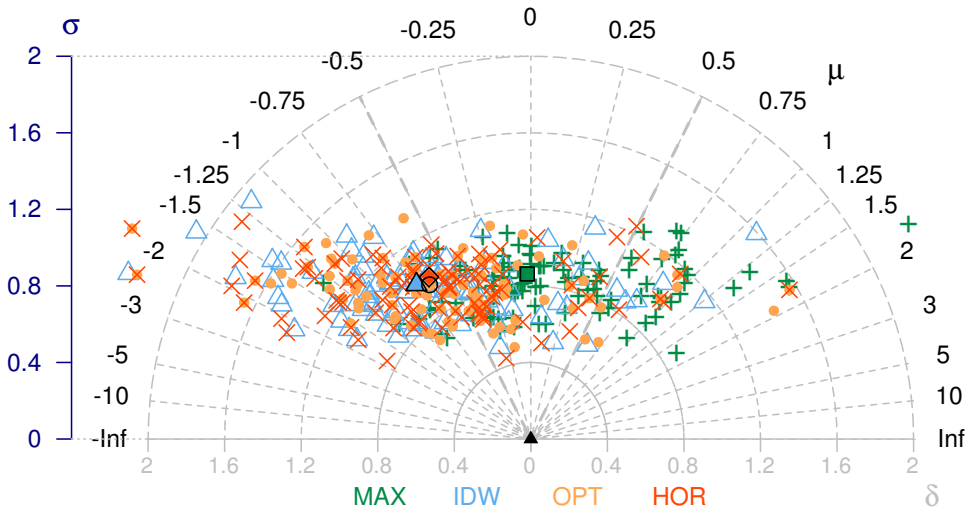

Figure 4.13: Error decomposition diagram showing the normalised RMSE δ, the normlised bias μ and the normalised pattern error σ of the maxima of all events that have SWGs of ***all weather situations*** *between all COSMO-2 data sets and the measurements. Each point shows the result of one station and each colour represents a different data set. Several points are outside the shown range; see Fig. A.34 to A.41 for all μ and δ values. The points with the black edges are the medians of the equally coloured point clouds. For more explanations about the diagram and median, please read chapter 3.5.4.*

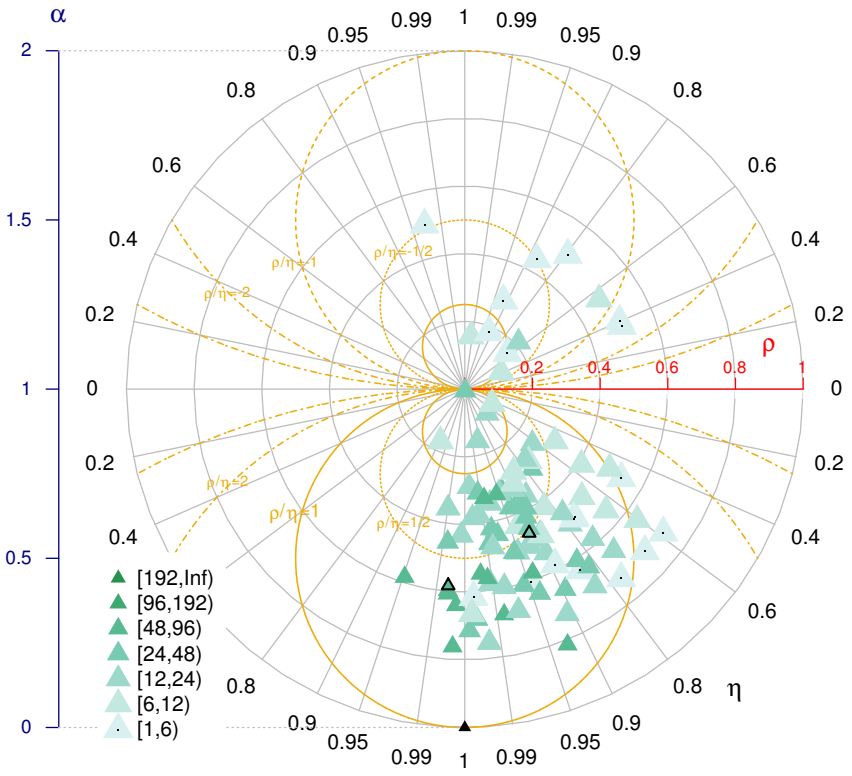

*Figure 4.14: Same as Fig. 4.12 but showing only the data set **MAX** and calculated for **winter storm** situations. The coloured triangles show the numbers of value pairs that were used to calculate the accuracy measures for each station divided into classes as shown in the legend. The two black triangles show the medians of ρ and η of the stations that have 6 or more value pairs (all points within the two bottom quarters of the diagram except the triangles that have a black dot).*

4.4.2 Spatial patterns

In chapter 4.4.1 the main focus was to show differences between data sets and weather class. This chapter will mainly illustrate the difference between the maximum gusts and all gusts by investigating how the individual accuracy measures rank correlate with stations criteria and by comparing spatial distributions. Since the total difference between the simulations and measurements (referred to as "total error") is mainly divided into the bias error and the pattern error, the patterns of the normalised bias μ and of the normalised error variance α will be investigated more thoroughly than the other variables. α is chosen in place of the normalised pattern error σ because α is equal to the square of σ and thus different values should be easier to see on the maps.
Including all gusts, the maximum gusts and all six weather classes, 70% of the 5 accuracy measures (α and σ are counted as one) significantly rank correlate either with the altitudes or the (avg) vertical distances or both. Half of these 70% have absolute values above 0.4 with at least one of both stations criteria. The sign of the rank correlations depends on the variable and if the calculation is done with all or with the maximum wind gusts. With the maximum gusts, the "better" values generally appear at stations in high altitudes and for stations with little (avg) vertical distances. With all gusts, the results indicate "better" values at stations in low altitudes.

All gusts

The normalised error variance α rank correlates the strongest with the (avg) vertical distances in *convective* (0.58** to 0.64**; Fig. 4.15) and *all* and *front* situations (0.5** to 0.6**). For *mixed* situations, the rank correlation is slightly weaker and in *winter storm* situations only around 0.3**. In *foehn* situations, α of MAX, IDW and OPT weakly but negatively rank correlate with the vertical distances by -0.3**. For *foehn* situations, the rank correlation with the altitudes is stronger (values between 0.4** and 0.5**). In *winter storm* situations, α rank correlates as much with the altitudes (0.3**) as with the (avg) vertical dist. The patterns of α and their rank correlations can easily be recognised in the maps of *all*, *front* and *mixed* situations: The northern stations have clearly lower α than the alpine stations (see for example Fig. 4.16).
As maybe hinted by the error decomposition diagrams, the rank correlations between the normalised bias μ and the stations criteria are different for MAX than for IDW, OPT and HOR. For every weather class, the μ of MAX rank correlate by values around 0.5** (0.4** for *foehn*) with the avg vert dist. Involving *all* weather situations, the μ of IDW, OPT and HOR rank correlate more strongly with the altitudes (between -0.4** and -0.5**) than with the (avg) vert dist (less than 0.35**). The μ of IDW weakly positively rank correlate with CIMO and Davenport. In *foehn* situations, μ of IDW and OPT rank correlate weakly with the altitudes. In *convective* situations, IDW, OPT and HOR rank correlate equally weakly with the altitudes as with the (avg) vert dist (absolute values around 0.3*). The more important rank correlations are with CIMO, Davenport and ERL: In *convective* situations, μ rank correlates positively with these

criteria. Similar rank correlations exist also with the normalised RMSE (δ). The μ of *fronts* have the same rank correlations as the *convective* situations, except that the rank correlation values of IDW, OPT and HOR with the altitudes and the vertical distance (CIMO/Davenport/ERL) are higher (lower) by about 0.1. The μ of *winter storms* do not significantly rank correlate with the altitudes and for IDW, OPT and HOR the rank correlation values with the (avg) vert dist are lower than for MAX.

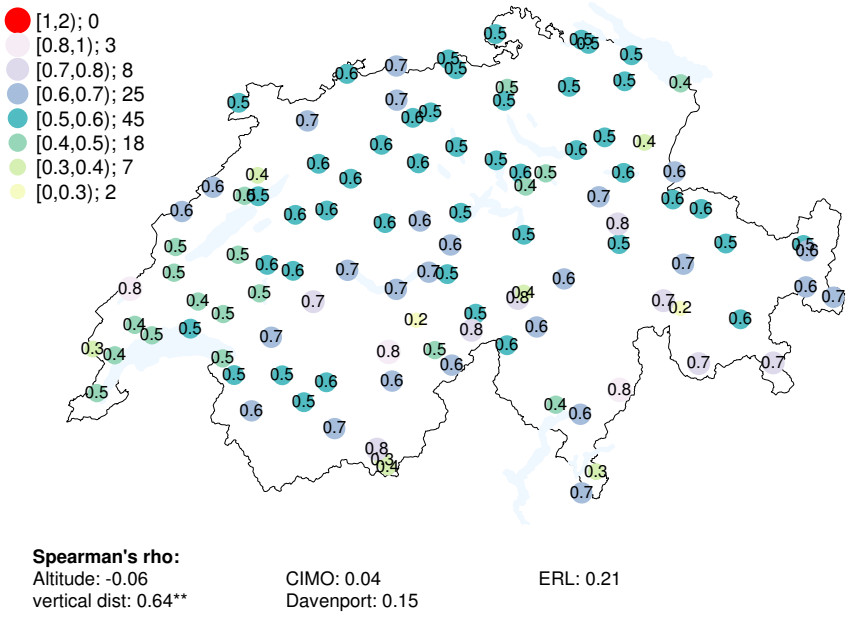

Figure 4.15: Map of Switzerland with values of the normalised error variance (α) of all wind gust speeds of all ***convective*** *events between the data set OPT and the measurements, as numbers and divided into classes as shown in the legend. The legend shows the ranges of each class and the number of stations that are within each class. The legend at the bottom lists the Spearman's rank correlation coefficients. They were calculated between the shown data set and the stations criteria described in chapter 2.1. If a correlation coefficient has one (two) asterisks, the correlation coefficient has a p-value <0.05 (0.01) and is thus considered to be significant.*

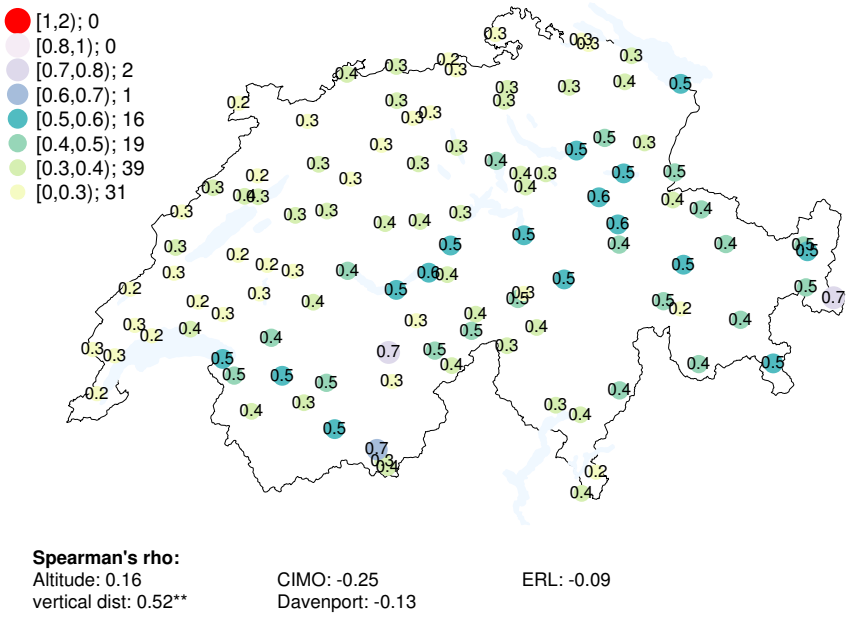

Figure 4.16: Same as Fig. 4.15 but showing the α of OPT of front situations.

Maximum gusts

With the maximum gusts method, almost all normalised biases (μ) and normalised RMSE (δ) do not significantly rank correlate with any stations criterion except in two cases. In *convective* situations, the μ of IDW rank correlate by 0.45* with CIMO and in *mixed* situations, with the same data sets by 0.59*. When comparing the normalised error variances (α), the variability at each station stands out: The α values at the individual stations are not constantly low or high in the different weather situations. Here are two examples showing the contrary: With OPT, the station ARH (Altenrhein; the easternmost station along the Lake Constance) has an α of 0.1 in *convective*, 0.2 in *mixed*, 0.6 in *foehn* and *all*, 0.8 in *winter storm* and 1.1 in *front* situations. Another station, GRE (Grenchen) has α values of 1.2 in *convective*, 0.6 in *mixed*, 0.9 in *all*, 0.7 in *winter storm* and 0.4 in *front* situations. However, although more weakly than the all gusts, the α still rank correlate with the altitudes and the (avg) vert dist. In *front* an *all* weather situations, the rank correlations are weakly negative with the altitudes and (for all situations only with OPT) above 0.4* with the vertical dist. With OPT, HOR and IDW, the α (and ρ with the opposite sign) of *fronts* rank correlates by values around -0.5* with Davenport and ERL. With IDW and OPT, the normalised RMSE δ rank correlates negatively with CIMO, Davenport and ERL (values between -0.41* and -0.52*). In *convective* situations, the rank correlations of any accuracy measure never exceeds absolute values of 0.31 (except the one mentioned above), which is a strong contrast to the all gusts results. In *foehn* situations, no significant rank correlations exist. However, Fig. 4.18 shows that the α tend to have lower values at the stations south of Lake Lucerne than in other regions. In w*inter storm* situations, no absolute rank correlation above 0.4 exists; MAX, however, has visibly smaller α values than the other data sets (Fig. 4.17). Weak rank correlations exist between α, ρ and δ and CIMO and Davenport. The *mixed* situations α rank correlate negatively with the altitudes too (-0.49** (HOR and IDW) and -0.48** (OPT)) and with OPT also with the vertical distances. In *mixed* situations, the normalised variances (α; with ρ as well but negatively) positively rank correlate by values between 0.5* and 0.6* with CIMO.

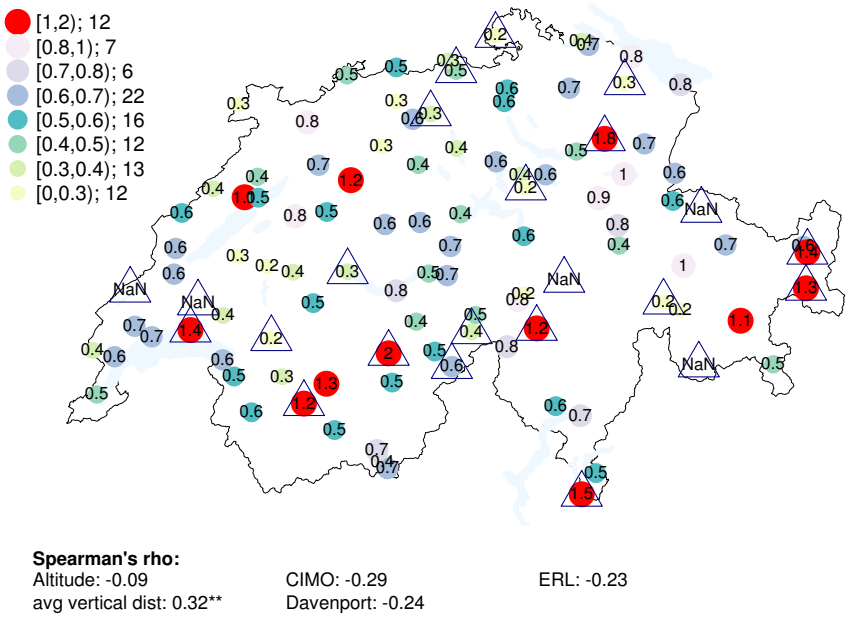

Figure 4.17: Same as Fig. 4.15 but showing the α of MAX, calculated for the maximum wind gusts in strong wind gust events of ***winter storm*** *situations. The triangles indicate stations with less than 6 strong wind gust events in this weather situation. The Spearman's rho were calculated excluding these stations.*

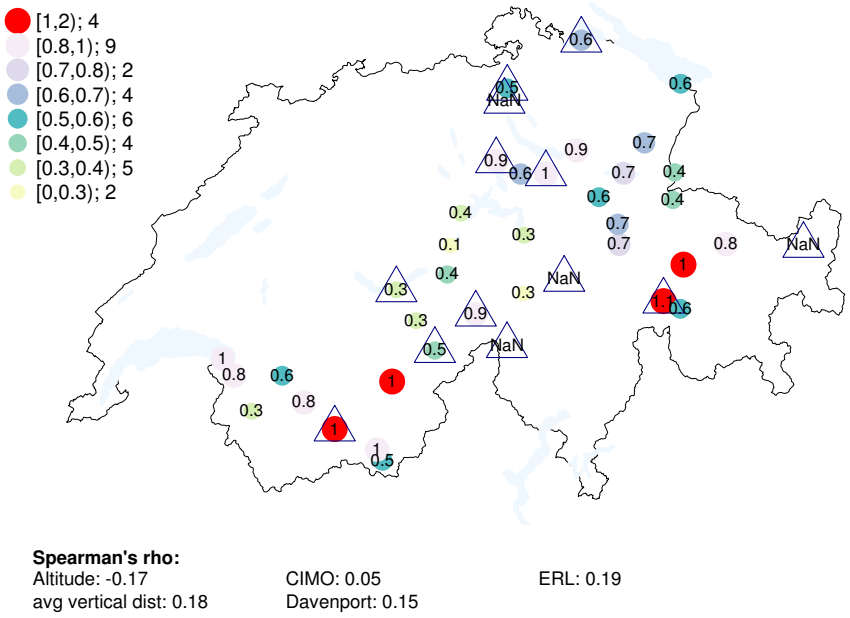

Figure 4.18: Same as Fig. 4.17 but showing the α of MAX calculated with the maximum wind gusts in strong wind gust events of ***foehn*** *situations.*

4.5 Summary

- The model overestimates the maximum wind gust speeds at the locations of stations that have low maximum wind gust speeds (maxima between 20 and 26 ms^{-1} in measurements; model values rather approach 26 to 32 ms^{-1}; see Fig. 4.1).
- The number of hours with measured strong wind gusts varies between stations.
- Data set MAX (details on data sets in chapter 3.3) overestimates the number of hours with wind gusts >20 ms^{-1} (also called strong wind gusts) at most stations; for OPT, HOR and IDW the differences in number of hours are balanced around zero. With OPT, HOR and IDW, the largest differences in number of hours exceed 3000 hours, with MAX they exceed 6000 hours.
- Skill measures (chapter 4.3):
  - According to the hit rates (HR) and false alarm ratios (FAR), the best scores in *convective*, *front*, *foehn* and *mixed* situations are attained by the model data set OPT and in *winter storm* situations by MAX.
  - The Critical Success Index (CSI) agrees with the HR and FAR, except in *foehn* situations. In *foehn* situations, the median CSI of HOR is larger than the median CSI of OPT, however, the lower quartile of the CSI of OPT is higher than the one from HOR.
  - According to the medians of the box plots, the simulations during *winter storms* have the highest skill. The highest rank is followed by the *foehn* and *mixed* situations, then *fronts* and the worst skill scores are with *convective* situations.
  - The skill in *winter storms* is probably artificially improved by the way *winter storm* events were defined (see chapter 3.2.4). Especially the FAR provide a strong indication of that.
  - the simple scores of *convective*, *winter storm*, *front* and *all* situations strongly rank correlate with the altitudes (better skill at high altitudes) and the (average) vertical distances between the grid-point altitudes and the stations altitudes (better skill at stations with low vert dist)
  - While the HR of *front* and *mixed* situations rank correlate positively with CIMO, they rank correlate negatively with CIMO, Davenport and ERL in *foehn* situations.
- Accuracy measures (chapter 4.4): general
  - The largest differences between accuracy values are between stations.
  - The differences between data sets are smaller than the differences between weather situations.

  - The error in correlation is always more important than the error in variance.

- Results from accuracy measures: all gusts
  - The highest correlation coefficients (ρ) are found for *front* and *all* situations; followed by *mixed*, *winter storms*, *foehn* and the lowest in *convective* situations.
  - With IDW, OPT and HOR all median normalised biases (μ) are at 0.5, except in *winter storm* situations where they are between 0 and 0.1 (depending on the data set). For *convective*, *foehn*, *front*, *mixed* and *all* situations, approximately half the stations have biases that significantly contribute to the total error.
  - With MAX the median normalised biases are between 0.8 and 1.1. In all but the *winter storm* situations, more than 80% of the stations have significant biases.
  - The significant biases are all always positive (the model simulates stronger wind gusts than measured by the stations), except at three stations (1 station in *winter storms*, 2 in *foehn* situations) and they weakly tend to increase with the classes of CIMO and Davenport.
  - The median normalised RMSE (δ) are larger with MAX than with OPT, HOR and IDW, except in *winter storm* situations where they are equal.
  - The lowest median normalised RMSE δ occur in *all* and *front* situations; followed by *winter storm* and *mixed* situations. The largest median normalised RMSE δ appear in *foehn* and *convective* situations.
  - Spatial patterns (rank correlations): The better values occur at low altitudes and at stations with small vertical distances.

- Results from accuracy measures: maximum gusts
  - the results from accuracy calculations are more extreme than with all gusts
  - with MAX the median normalised bias μ is positive in *storm* and *foehn* situations, neutral in *front* and *all* situations and negative in *convective* and *mixed* situations.
  - With OPT, HOR and IDW, all median biases are negative. They are the most negative in *front* and *mixed* situations and the least in *foehn* and *all* situations. Most significant biases are negative.
  - For the majority of stations the variances of the simulations are still larger than the variances of the measurements.
  - *Winter storms* have a slightly larger median variance similarity (η) than the other situations.
  - The accuracy is the worst at stations with a low number of strong wind gust events.

- The median normalised RMSE (δ) is larger with OPT, HOR and IDW than with MAX.
- With OPT, HOR and IDW, the lowest median normalised RMSE δ occur in *winter storm* situations; followed by *foehn*, *mixed* and *all* situations. The largest median normalised RMSE δ appear in *front* and *convective* situations.
- With MAX the lowest median normalised RMSE δ occur in *mixed* situations; followed by *winter storm* and *front* situations. At the fourth rank are all situations. The largest median normalised RMSE δ appear in *foehn* and *convective* situations.
- Spatial patterns (rank correlations): The better values occur at high altitudes and at stations with small vertical distances. Some accuracy values from *front* and *mixed* situations also rank correlate with CIMO, Davenport and ERL: The normalised pattern error (α) and the correlation coefficients (ρ; with the opposite sign) of *front* situations rank correlate negatively with ERL and Davenport. In *mixed* situations, however, the rank correlation exists with CIMO and is positive (for ρ negative) by the same strength.

Chapter 5

Discussion

In this verification, the performance of the COSMO-2 model analysis for simulating wind gusts and strong wind gusts (SWG) in different weather situations was assessed. The following chapters will discuss the main results of each weather situation. Overall, the best accuracies and skill appeared when using data set OPT. This confirms the importance of small vertical distances between grid-points and stations. The average vertical distances used for data set IDW and the vertical distances of the closest grid-points (for HOR) are 20 and 12 times greater than 600m, compared to only 4 times with the OPT grid-cells. The choice of data set is however not that crucial; the other data sets did not simulate the wind gusts much worse than OPT. In the results, rank correlations have often been mentioned to show connections between results and stations criteria. Although interesting and important, understanding the reasons behind these connections would require further case study analyses.

5.1 Convective situations

The wind gusts during convective processes are often missed, because they are typical meso-size phenomena. At high altitudes, orographic forcing increases the predictability. However, most valleys are not well resolved and thus so are the convective processes. In the mid-lands, additional to the absence of orographic forcing, the volatility of convective events is increased by the heterogeneous land surface cover. This heterogeneity plays indeed an important role for better and not as good accuracies during *convective* situations. The accuracy of all gusts in *convective* situations tends to be better at higher stations, that have small (avg) vertical distances between the altitudes of the grid-points and the altitudes of the stations (vert dist; methods chapter 3.6) and low CIMO, Davenport and ERL classes or values. The simple scores in *convective* situations are low; 3/4 of all stations have hit rates below 0.5 and false alarm ratios above 0.5. However, considering that a typical thunderstorm cell measures about 10 km in all three directions (Mittermaier, 2014), not allowing a misplacement of more than 3.14 km to a station is quite strict and the results therefore understandable.

5.2 Winter storm situations

A high accuracy is found for *winter storm* wind gusts and SWG. The largest percentages in classified SWG hours fall into this weather class. Although the simple scores give a probably inaccurately high impression on the ability to capture SWG events (see chapter 4.3), the accuracy measures still agree. Compared to the other weather classes, the least stations have significant biases. Furthermore, the maximum gusts are simulated with only a weakly positive (MAX; at about 0.2) and, after *foehn*, the least negative (OPT, HOR, IDW; at 0.75) median normalised biases (μ). *Winter storms* have slightly larger median variance similarities (η; between 0.95 and 0.99) for the maximum gusts than all the other weather classes (between 0.9 and 0.95). Compared to other weather classes, the variances of the simulated SWG are not as often larger than the variances of the measurements. This shows a greater overall accordance between *winter storm* gust speed simulations and measurements.

5.3 Front situations

In *front* situations the accuracies of all gusts rank better compared to the other weather classes, than the maximum gusts. All wind gusts in front situations have median normalised error variances (α) about 0.15 larger than in *winter storm* and *mixed* situations and about 0.25 larger than *foehn* and *convective* situations. Only the median α in *all* situations surpass the median of *fronts* by about 0.05. By contrast, with maximum gusts the median α in *front* situations are only larger than in *convective* situations and about equal to the median α in *foehn*, *winter storm*, *mixed* and *all* situations.

The reason for the small number of hits and the large number of misses could be related to the strongly negative biases in the maximum gusts of OPT, HOR and IDW. The Hit Rate of OPT rank correlates positively with CIMO and α, calculated with the maximum gusts, negatively rank correlates with Davenport and ERL. These two rank correlations indicate a higher skill and accuracy in pattern for stations with high CIMO/Davenport/ERL classes or values. These tendencies might be related to how the boundary layer processes are parametrised in the model.

5.4 Foehn situations

The results for *foehn* are particular, because compared to the other weather situations fewer stations are involved. This smaller number of stations affects the reliability of all statistical analyses. The *foehn* situations and the stations criteria CIMO, Davenport and ERL have only 27 stations in common and if the stations with less than 6 SWG events are left out, this number reduces to 15. In consequence, especially for the maximum gusts, the results should be viewed with caution.

Compared to the other weather situations, the SWG in *foehn* situations are detected and simulated with high skill. The Hit Rates increase with a decreasing CIMO, Davenport and ERL, meaning that the wind gusts are better detected at stations which have less obstacles in their vicinity. However, further investigations need to confirm or deny the influence of these location parameters on foehn SWG. Nevertheless, better simulation of foehn is one of the main improvements that are expected in the model COSMO-1, compared to COSMO-2 (MeteoSwiss, 2016d). All gusts are simulated better in pre-alpine regions than in the northern areas of Switzerland. *Foehn* situations always showed largest normalised RMSE (δ). The median normalised RMSE are mostly as high in *foehn* situations as in *convective* situations. The reason for the much larger range in normalised biases of all gusts (μ) compared to those of all other weather classes may be due to the local terrain and the flow characteristics of foehn. With data sets OPT, HOR and IDW, the maximum gusts have the least negative median biases (μ) at -0.3 (HOR) and close to -0.5 (OPT, IDW) of all weather classes. The median normalised RMSE δ are around 1, which is smaller than the median δ in *convective* and *front* situations.

5.5 Mixed situations

The *mixed* situations are marked by generally fewer numbers of events per station and by a greater number of events in northern Switzerland than in other regions. The largest fraction of *mixed* events are co-occurring during *foehn* and *winter storm* activity or *front* and *winter storms*. The *foehn* and *winter storm* hybrids are probably mostly periods where one weather situation develops into the other due to changing wind directions. The results of the pattern measures resemble very much the ones from *winter storms* and have nothing in common with the measures from *convective* situations. The influence of other weather phenomena on *convective* situations would need to be determined with the help of case studies.

5.6 Unclassified strong wind gust hours

As shown in Fig. 4.5, the most unclassified SWG occur at high altitude stations. At station VIO (Vicosoprano) about 90% of SWG hours are unclassified. The largest absolute number of unclassified SWG hours is found at station DIA (Les Diablerets). Nonetheless, it is not only the stations at high altitude which have large fractions or numbers of unclassified SWG. Other stations with a larger larger fraction than 45% are for example BIE (Bière; 113 unclassified hours), BRZ (Brienz; 102 hours), GVE (Genève-Cointrin; 82 hours) or PRE (St-Prex; 142 hours). BIE, GVE and PRE are all located along the western parts of Lake Geneva on the Swiss Plateau. Aside from the investigated wind situations (except foehn), the weather in this region is sometimes shaped by the "Joran" or the "Bise" (see also Wanner and Furger, 1990), two local winds that are influenced by topography. The "Joran" is a katabatic north-west wind that is generated along the Jura Mountains and usually follows the passage of a cold front. The "Bise" is a wind that

blows from north-east, over the Swiss Plateau and is channelled in between the Alps and the Jura (Etienne and Beniston, 2012). The wind direction and the time at which the unclassified SWG occur could indicate if these winds should be included to the list of wind classes that produce SWG in Switzerland.

Chapter 6

Conclusions

In this study, the wind gusts and strong wind gusts (SWG) of the COSMO-2 model analysis were verified for different weather situations. Different neighbourhood data sets were compared to measurements from SwissMetNet ground weather stations for the period 18.02.2008 - 31.12.2014. The verification has yielded the following results:

- The performance of the model in all weather classes depends very much on the station location. Particularly high accuracy and skill is found for example at stations PMA (Piz Martegnas), RUE (Rünenberg), BRL (La Brévine), PRE (St-Prex), GEN (Monte Generoso), CIM (Cimetta) and ORO (Oron).
- The best skill and accuracy are found when using the values of the grid-points within 3.14 km that have the least three dimensional distance to the stations (called OPT; except in *winter storm* situations). However, the difference between the four neighbourhood methods is marginal.
- Using the maximum value within a 3.14 km neighbourhood, resulted in a distinct overestimation of the number of SWG hours at most stations. However, for *winter storms*, this data set has the highest skill and accuracy.
- According to the Hit Rates and the False Alarm Ratios, the highest skill in detecting SWG are found in *winter storms*, followed by *foehn*, *mixed* situations, *fronts* and lastly *convective* situations.
- The skill in *winter storm*, *front* and *convective* situations increase with an increasing altitude and with a decreasing vertical distance between the altitudes of the grid-points and the altitudes of the stations.
- The largest differences between accuracies are found between stations, followed by weather situations. Differences in accuracy between the four neighbourhood methods are very small.

For both all gusts and the SWG, the error in correlation is always more important than the error in variance.

- **All wind gusts**
  About 50% of the stations have positive biases (model has higher speeds) in OPT, HOR and IDW that are significant in all wind gusts and for all weather classes except for *winter storms*. These stations are scattered in every region of Switzerland. With data set MAX, about 80% of the stations have positive normalised biases. The remaining stations' biases are insignificant. In *winter storm* situations, more stations have insignificant biases in OPT, HOR and IDW (about 58%) and about twice as many stations have significantly positive biases as opposed to negative. For data set MAX, 40% of all stations have insignificant biases and only 1 station (DOL; La Dôle) has a significantly negative bias. The highest correlation coefficients (ρ) are found for *front* and *all* situations; followed by *mixed*, *winter storms* and *foehn* and the lowest ρ are found in *convective* situations. The lowest median normalised RMSE (δ) occur in *all* and *front* situations; followed by *winter storm* and *mixed* situations and the largest median normalised RMSE (δ) appear in *foehn* and *convective* situations.

- **Strong wind gusts (maximum gusts)**
  The findings for data sets OPT, HOR and IDW agree well with the results from Schubiger et al. (2012) and Stucki et al. (2016). With OPT, HOR and IDW, all median normalised biases (μ) are negative. They are the most negative in *front* and *mixed* situations and the least in *foehn* and *all* situations. At most stations, the significant biases are negative. With MAX, the median normalised bias is positive in *winter storm* and *foehn* situations, neutral in *front* and *all* situations and negative in *convective* and *mixed* situations.
  With OPT, HOR and IDW, the lowest median normalised RMSE δ occur in *winter storm* situations; followed by *foehn*, *mixed* and *all* situations. The largest median normalised RMSE δ are found in *front* and *convective* situations. With MAX the lowest median normalised RMSE δ occur in *mixed* situations, followed by *winter storm* and *front* situations. On the next rank are all situations. The largest median normalised RMSE δ appear in *foehn* and *convective* situations. *Winter storms* have slightly larger median variance similarities (η; between 0.95 and 0.99) than the other classes (between 0.9 and 0.95).

6.1 Outlook

In this study, the wind gusts and strong wind gusts in COSMO-2 have successfully been verified and differences between weather situations have been quantified. There are however a great number of additional steps that could, on the one hand, strengthen and prove the findings and, on the other hand, reveal more fascinating details about the simulation of wind gusts and strong wind gusts:

1. Even though the verification measures have exposed differences between weather situations, their value would be increased by calculating uncertainties as suggested in Jolliffe (2007). The advantage would be the possibility of telling whether differences between skill and accuracies are significant or not. In a similar way as the significance of a Spearman's rank correlation was indicated, the significance or confidence intervals for the other measures could quantify the power of the results.

2. Additional to the uncertainties, case studies could expose reasons for large or small skill and accuracy values. Such a case study could further show how different strong wind gusts (or strong wind gust simulations) behave during different mixed events (events with more than one weather situation simultaneously) as compared to individual weather phenomena. Another investigation could also be done on the unclassified strong wind gust hours or on the seasonality of model accuracy. For example, the correlation between the COSMO-2 wind gust simulations of MAX and the measurements is higher during summer than during winter. This may be related to the distribution of weather phenomena during the year, but it deserves further research.

3. Although the wind directions of wind gusts are not parametrised in COSMO-2, a further verification could involve a comparison of the measured and simulated mean wind directions.

4. Great effort has been put into making a good weather classification but not much time could be devoted to validating it. A validation of the weather classification could be done using radar data. In addition to the validation, one could also find out, which radius fits bets to define convective events using lightning data. There is also great potential in the sector of machine learning, which by pattern recognition could produce an even better weather classification. Liu et al. (2016) for example applied Deep Convolutional Neural Networks to detect extreme weather in climate simulations and reanalysis data sets.

In spring 2016, the model COSMO-1 replaced the model COSMO-2 for operational forecasts at MeteoSwiss (MeteoSwiss, 2016e). Since only a few months of data were available at that time, this analysis could not be done with COSMO-1 simulations. However, the higher resolution of 1.1 km is expected to considerably improve the simulation of ground-level wind, which could be of interest for the reader of this thesis. In particular, convection and foehn, as well as the formation of lifting and fog is expected to be simulated much more accurately by COSMO-1 than by COSMO-2 (MeteoSwiss, 2016d). Once enough data is available, the methods used in this Master's Thesis could very well be applied to this new model.

Appendix

This appendix comprises all lists, tables and figures that were mentioned in the main part. Other correlation-similarity and error-decomposition diagrams showing results from individual data sets like in Fig. 4.14, as well as maps showing the spatial distributions of each accuracy variable of each data set for both all and the maximum gusts are readily available upon request.

A.1 List of SwissMetNet Stations

Table A.1: List of SwissMetNet stations that were used for the verification; including abbreviations, full names, coordinates, altitudes and their wind measurement instruments (adapted from Widmer, 2016)

abbr.	station	lon	lat	alt	measurement instrument
AEG	Oberägeri	8.6080833	47.1335806	724	anem_thies_2D
AIG	Aigle	6.9244306	46.3266472	381	anem_lamb_14512_SMN
ALT	Altdorf	8.6218028	46.8870194	438	anem_lamb_14512_SMN
AND	Andeer	9.4319167	46.6101250	987	anem_lamb_14512_SMN
ANT	Andermatt	8.5805472	46.6309167	1438	anem_thies_2D
ARH	Altenrhein	9.5667972	47.4836750	398	anem_thies_2D
BAS	Basel/Binningen	7.5835583	47.5410389	316	anem_lamb_14512_SMN
BER	Bern/Zollikofen	7.4640083	46.9907444	553	anem_lamb_14512_SMN
BEZ	Beznau	8.2332556	47.5572361	326	anem_lamb_14512_SMN
BIE	Bière	6.3424056	46.5248722	684	anem_lamb_14512_SMN
BIN	Binn	8.1909250	46.3654611	1448	anem_thies_2D
BIZ	Bischofszell	9.2346972	47.4973833	470	NA
BLA	Blatten Lötschental	7.8231972	46.4204528	1538	anem_thies_2D
BOL	Boltigen	7.3842083	46.6235222	820	anem_lamb_14512_SMN
BOU	Bouveret	6.8570111	46.3934444	374	anem_lamb_14512_SMN
BRL	La Brévine	6.6103028	46.9838417	1050	anem_thies_2D
BRZ	Brienz	8.0608583	46.7407222	567	anem_lamb_14512_SMN
BUF	Buffalora	10.2671833	46.6481389	1968	anem_thies_2D

continued ...

... continued

abbr.	station	lon	lat	alt	measurement instrument
BUS	Buchs/Aarau	8.0794500	47.3843361	387	anem_lamb_14512_SMN
CDF	La Chaux-de-Fonds	6.7923167	47.0829417	1018	anem_lamb_14512_SMN
CGI	Nyon/Changins	6.2277528	46.4010500	455	anem_lamb_14512_SMN
CHA	Chasseral	7.0543889	47.1317611	1599	anem_thies_2D
CHB	Les Charbonnières	6.3124333	46.6701444	1045	anem_thies_2D
CHD	Château-d'Oex	7.1396528	46.4798167	1029	anem_lamb_14512_SMN
CHM	Chaumont	6.9788278	47.0491639	1136	anem_thies_2D
CHZ	Cham	8.4646306	47.1882778	443	anem_thies_2D
CIM	Cimetta	8.7916417	46.2004222	1661	anem_lamb_14512_SMN
CMA	Crap Masegn	9.1799889	46.8422944	2480	anem_thies_2D
CRM	Cressier	7.0591111	47.0476000	431	anem_lamb_14512_SMN
DEM	Delémont	7.3495556	47.3517028	439	anem_lamb_14512_SMN
DIA	Les Diablerets	7.2037861	46.3267472	2964	anem_thies_2D
DIS	Disentis/Sedrun	8.8534500	46.7065361	1197	anem_lamb_14512_SMN
DOL	La Dôle	6.0994778	46.4247000	1670	anem_thies_2D
EBK	Ebnat-Kappel	9.1084806	47.2733861	623	anem_lamb_14512_SMN
EGH	Eggishorn	8.0927278	46.4265333	2893	anem_thies_2D
EGO	Egolzwil	8.0047556	47.1794222	521	anem_lamb_14512_SMN
EIN	Einsiedeln	8.7565528	47.1330417	910	anem_lamb_14512_SMN
ELM	Elm	9.1753389	46.9237500	958	anem_lamb_14512_SMN
EVI	Evionnaz	7.0267556	46.1829500	482	anem_thies_2D
EVO	Evolène/Villa	7.5086750	46.1121361	1825	anem_lamb_14512_SMN
FAH	Fahy	6.9411028	47.4238167	596	anem_lamb_14512_SMN
FRE	Bullet/La_Frétaz	6.5763167	46.8406194	1205	anem_lamb_14512_SMN
GEN	Monte Generoso	9.0178722	45.9276056	1600	anem_thies_2D
GIH	Giswil	8.1901861	46.8494833	471	anem_lamb_14512_SMN
GLA	Glarus	9.0669028	47.0345917	517	anem_lamb_14512_SMN
GOE	Gösgen	7.9736611	47.3630361	380	anem_lamb_14512_SMN
GOR	Gornergrat	7.7857500	45.9836361	3129	anem_mete_usa1_CN
GRA	Fribourg/Posieux	7.1137111	46.7713972	646	anem_thies_2D
GRE	Grenchen	7.4151028	47.1790833	430	anem_lamb_14512_SMN
GRH	Grimsel Hospiz	8.3332528	46.5716917	1980	anem_lamb_14512_SMN
GRO	Grono	9.1637500	46.2550833	324	anem_thies_2D
GUE	Gütsch ob Andermatt	8.6150472	46.6524361	2283	anem_thies_2D
GUT	Güttingen	9.2793889	47.6017167	440	anem_youn_WM5103-46
GVE	Genève-Cointrin	6.1277500	46.2475167	412	anem_Metek_usa1_SMN

continued ...

... continued

abbr.	station	lon	lat	alt	measurement instrument
HAI	Salen-Reutenen	9.0238972	47.6512417	718	anem_lamb_14512_SMN
HLL	Hallau	8.4704583	47.6972778	419	anem_lamb_14512_SMN
INT	Interlaken	7.8701389	46.6722444	577	anem_youn_WM5103-46
JUN	Jungfraujoch	7.9853306	46.5474472	3580	anem_rose_1774W
KLO	Zürich/Kloten	8.5359500	47.4796111	426	anem_Metek_usa1_SMN
KOP	Koppigen	7.6054861	47.1188444	484	anem_lamb_14512_SMN
LAG	Langnau i.E.	7.8064361	46.9396250	745	anem_lamb_14512_SMN
LEI	Leibstadt	8.1882556	47.5972667	341	anem_lamb_14512_SMN
MAG	Magadino/Cadenazzo	8.9336667	46.1600306	203	anem_lamb_14512_SMN
MAH	Mathod	6.5679889	46.7369722	437	anem_thies_2D
MAS	Marsens	7.0696722	46.6564861	715	anem_thies_2D
MER	Meiringen	8.1692417	46.7322250	589	anem_lamb_14512_SMN
MOA	Mosen	8.2328194	47.2438417	453	anem_thies_2D
MOE	Möhlin	7.8779000	47.5721944	344	anem_lamb_14512_SMN
MRP	Monte Rosa-Plattje	7.8145861	45.9566306	2885	NA
MUB	Mühleberg	7.2781528	46.9732583	480	anem_lamb_14512_SMN
MVE	Montana	7.4607778	46.2987417	1427	anem_lamb_14512_SMN
NAS	Naluns/Schlivera	10.2613889	46.8171639	2400	anem_thies_2D
ORO	Oron	6.8582444	46.5722611	827	anem_lamb_14512_SMN
PAY	Payerne	6.9424194	46.8115833	490	anem_lamb_14512_SMN
PIL	Pilatus	8.2523278	46.9788667	2106	anem_thies_2D
PIO	Piotta	8.6881361	46.5147806	990	anem_lamb_14512_SMN
PLF	Plaffeien	7.2660000	46.7476556	1042	anem_lamb_14512_SMN
PMA	Piz Martegnas	9.5295333	46.5771861	2670	anem_thies_2D
PRE	St-Prex	6.4430056	46.4836778	425	anem_lamb_14512_SMN
PUY	Pully	6.6674111	46.5123111	456	anem_youn_WM5103-46
QUI	Quinten	9.2160417	47.1287417	419	anem_lamb_14512_SMN
RAG	Bad Ragaz	9.5025778	47.0166306	496	anem_lamb_14512_SMN
REH	Zürich/Affoltern	8.5178861	47.4276750	444	anem_lamb_14512_SMN
ROB	Poschiavo/Robbia	10.0611306	46.3466444	1078	anem_lamb_14512_SMN
ROE	Robièi	8.5133861	46.4430694	1896	anem_lamb_14512_SMN
RUE	Rünenberg	7.8793306	47.4345694	611	anem_lamb_14512_SMN
SAE	Säntis	9.3436278	47.2494417	2502	anem_rose_1774W
SAG	Sattel-Aegeri	8.6369556	47.0810667	790	anem_thies_2D
SAM	Samedan	9.8789444	46.5263944	1709	anem_lamb_14512_SMN
SBO	Stabio	8.9323778	45.8433944	353	anem_lamb_14512_SMN

continued ...

... continued

abbr.	station	lon	lat	alt	measurement instrument
SCM	Schmerikon	8.9402333	47.2246000	408	anem_lamb_14512_SMN
SCU	Scuol	10.2832139	46.7932722	1304	anem_lamb_14512_SMN
SIO	Sion	7.3301667	46.2185694	482	anem_lamb_14512_SMN
SMM	Sta.Maria Val Müstair	10.4262917	46.6022556	1383	anem_lamb_14512_SMN
SPF	Schüpfheim	8.0124361	46.9470361	742	anem_lamb_14512_SMN
SRS	Schiers	9.6680639	46.9755083	626	anem_thies_2D
STK	Steckborn	8.9814250	47.6686306	398	anem_lamb_14512_SMN
TAE	Aadorf/Tänikon	8.9048833	47.4798667	539	anem_lamb_14512_SMN
THU	Thun	7.5852222	46.7498528	570	anem_lamb_14512_SMN
ULR	Ulrichen	8.3081361	46.5048194	1346	anem_lamb_14512_SMN
VAB	Valbella	9.5544222	46.7550361	1569	anem_thies_2D
VAD	Vaduz	9.5175139	47.1274528	457	anem_lamb_14512_SMN
VIO	Vicosoprano	9.6277889	46.3530222	1089	anem_lamb_14512_SMN
VIS	Visp	7.8429389	46.3028639	639	anem_lamb_14512_SMN
VIT	Villars-Tiercelin	6.7100750	46.6217750	859	anem_thies_2D
WFJ	Weissfluhjoch	9.8063833	46.8333278	2691	anem_Metek_usa1_SMN
WYN	Wynau	7.7874028	47.2550306	422	anem_lamb_14512_SMN
ZER	Zermatt	7.7531083	46.0291417	1638	anem_lamb_14512_SMN

A.2 Station criteria

This chapter shortly explains the stations criteria Davenport, CIMO and effective roughness length (ERL). Davenport divides stations into 8 classes (1-8) according to the aerodynamic roughness length (table A.2). The aerodynamic roughness length measures *"how efficiently momentum can be transferred into the ground at a given wind speed"* (Panofsky and Dutton, 1984). The higher the class, the bigger are the obstacles in the surrounding terrain, with 8 being for instance a location in a city centre with high- and low-rise buildings (WMO, 2008). This classification is important, because trends in wind speeds can be explained by changes in roughness length (Wever, 2012). The larger the roughness length, the more turbulent is the wind (Stull, 2012). Thus, a negative gust speed bias between measurements and simulations may correlate to a certain degree with a high Davenport value. CIMO has five classes, Class 1 being a reference site and Class 5 meaning that the additional uncertainty added by the siting is greater than 50 percent (see table A.3; more details in WMO, 2008). The ERL is used to correct the wind speed according to the characteristics of the upstream terrain (also called fetch). Compared to the already mentioned aerodynamic roughness length, the ERL describes the roughness of the upstream terrain and not the terrain of the measurement site (Jung and Schindler, 2016). WMO (2008) and Zhong et al. (2011) mention several ways of calculating the ERL.

Table A.2: Terrain classification from Davenport (1960) adapted by Wieringa (1980b) in terms of aerodynamic roughness length z0 (WMO, 2008)

Class Index	Short terrain description	z_0(m)
1	Open sea, fetch at least 5 km	0.0002
2	Mud flats, snow; no vegetation, no obstacles	0.005
3	Open flat terrain; grass, few isolated obstacles	0.03
4	Low crops; occasional large obstacles, x/H >20	0.10
5	High crops; scattered obstacles, 15 <x/H <20	0.25
6	Parkland, bushes; numerous obstacles, x/H $\approx$ 10	0.5
7	Regular large obstacle coverage (suburb, forest)	1
8	City centre with high- and low-rise buildings	$\geq$2

Note: Here x is a typical upwind obstacle distance and H is the height of the corresponding major obstacles. For more detailed and updated terrain class descriptions see (Davenport et al., 2000, (see also p. II.11–10)).

Table A.3: CIMO Siting Classifications for surface observing stations on land; Environmental Classification (adated from WMO, 2008).

Class Index	Short description
1	Mast distance $\geq$ 30 times the height of surrounding obstacles; Sensors distance $\geq$ 15 times the width of narrow obstacles and over 8 m high; Single obstacles lower than 4 m can be ignored; roughness length $\leq$0.1 m
2	Mast distance $\geq$ 10 times the height of surrounding obstacles; Sensors distance $\geq$ 15 times the width of narrow obstacles and over 8 m high; Single obstacles lower than 4 m can be ignored; roughness length $\leq$0.25 m
3	Mast distance $\geq$ 5 times the height of surrounding obstacles; Sensors distance $\geq$ 10 times the width of narrow obstacles and over 8 m high; Single obstacles lower than 5 m can be ignored
4	Mast distance $\geq$ 2.5 times the height of surrounding obstacles; No obstacle with an angular width larger than 60° and a height >10 m, within a 40 m distance; Single obstacles lower than 6 m can be ignored, only for measurements at 10 m or above
5	Site not meeting the requirements of class 4

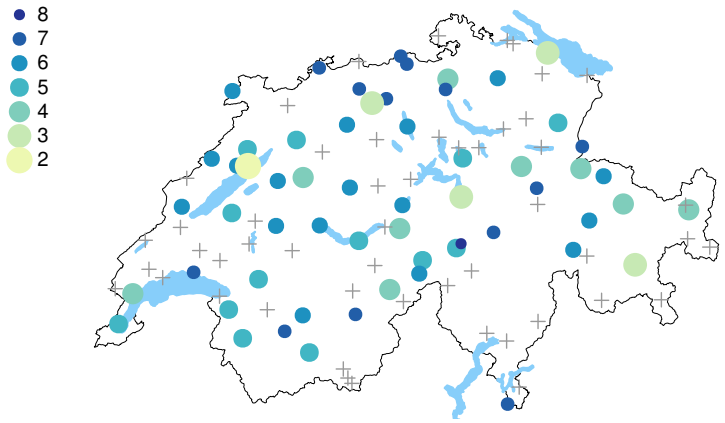

Figure A.1: Wind classes of the stations for which the classification is available according to Davenport. Grey crosses show the stations for which the classification has not yet been undertaken.

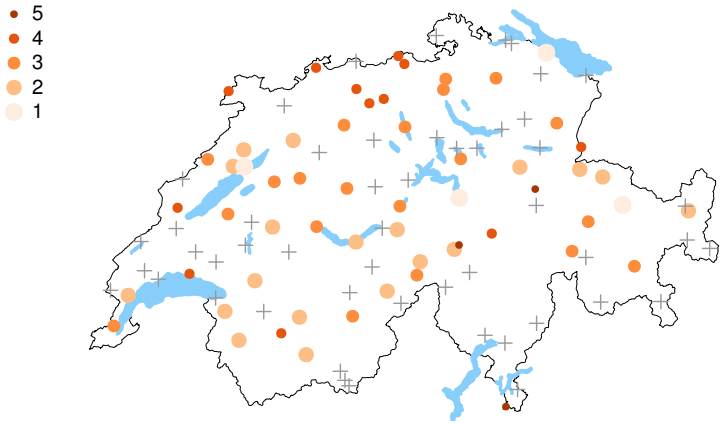

Figure A.2: CIMO Siting Classification for the stations for which the classification is available. Grey crosses show the stations for which the classification has not yet been undertaken.

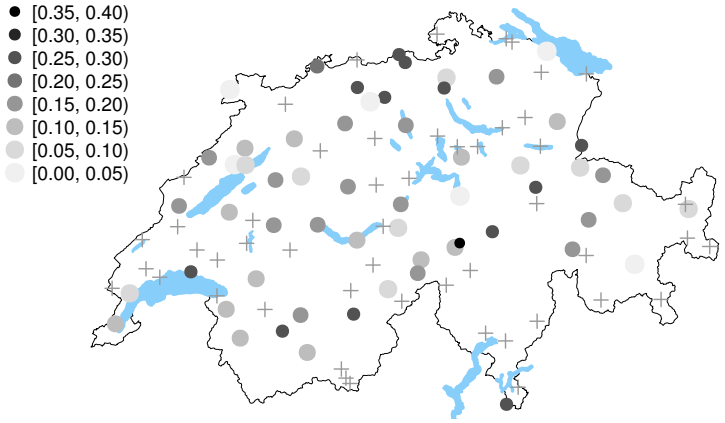

Figure A.3: Effective roughness length divided into 8 classes, for the stations for which the measure exists. Grey crosses show the stations for which the measure has not yet been determined.

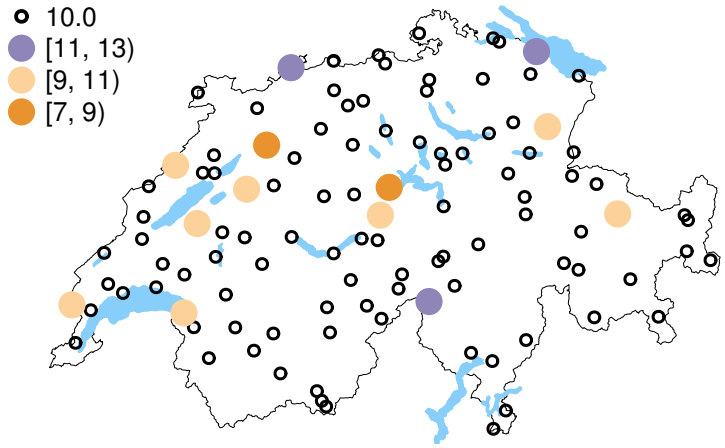

Figure A.4: Measurement heights above ground of the SwissMetNet Stations, divided into 4 classes.

A.3 Number of hours

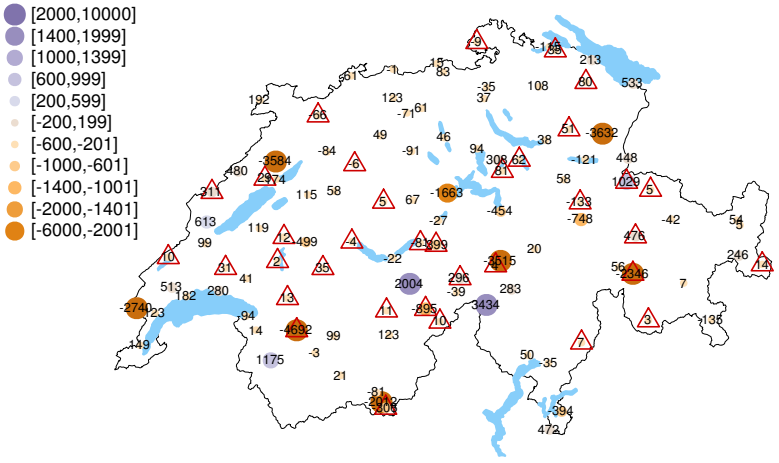

Figure A.5: Map of Switzerland with difference between data sets IDW and measurements for the number of hours with strong wind gusts between 18.02.2008-31.12.2014 at each SwissMetNet station (see absolute Nr of hours in measurements in Fig. 4.2). The red triangles show which stations have data for less than 95 % of the entire research period.

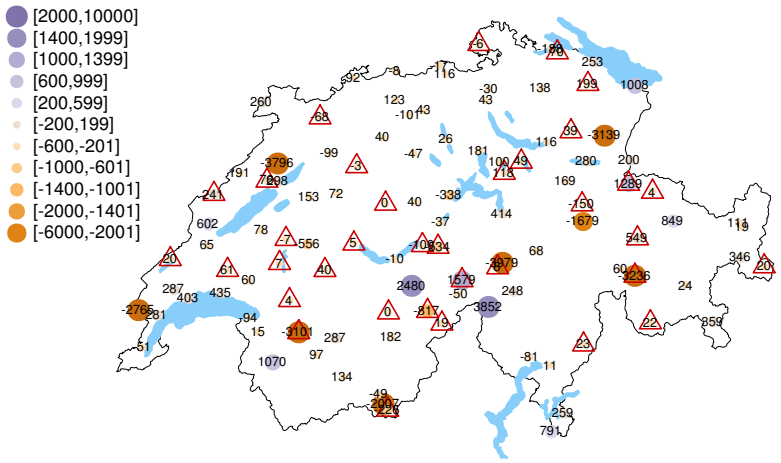

Figure A.6: Same as Fig. A.5 but for data set HOR.

A.4 Weather classification

1	HLL	19	EBK	37	MUB	55	PRE	73	EVI	91	NAS
2	STK	20	WYN	38	SPF	56	CHD	74	ELM	92	GUE
3	HAI	21	MOA	39	LAG	57	CGI	75	SCU	93	BUF
4	GUT	22	SCM	40	ALT	58	BOU	76	VAB	94	PMA
5	LEI	23	CHZ	41	GIH	59	GVE	77	DIS	95	GRH
6	MOE	24	EGO	42	PAY	60	SAE	78	ANT	96	JUN
7	BEZ	25	GRE	43	GRA	61	CHA	79	AND	97	ROE
8	BAS	26	AEG	44	THU	62	CHM	80	SMM	98	EGH
9	BIZ	27	EIN	45	PLF	63	PIL	81	SAM	99	DIA
10	ARH	28	QUI	46	BRZ	64	FRE	82	PIO	100	GOR
11	TAE	29	VAD	47	MAH	65	DOL	83	ULR	101	MRP
12	KLO	30	KOP	48	CHB	66	RAG	84	BLA	102	CIM
13	RUE	31	CDF	49	MAS	67	SRS	85	BIN	103	GEN
14	REH	32	SAG	50	BOL	68	MER	86	MVE	104	VIO
15	FAH	33	CRM	51	VIT	69	INT	87	EVO	105	ROB
16	BUS	34	GLA	52	ORO	70	AIG	88	ZER	106	GRO
17	GOE	35	BER	53	BIE	71	VIS	89	CMA	107	MAG
18	DEM	36	BRL	54	PUY	72	SIO	90	WFJ	108	SBO

Figure A.7: List of stations indicating the order in which the bars in Fig. 4.5 are arranged.

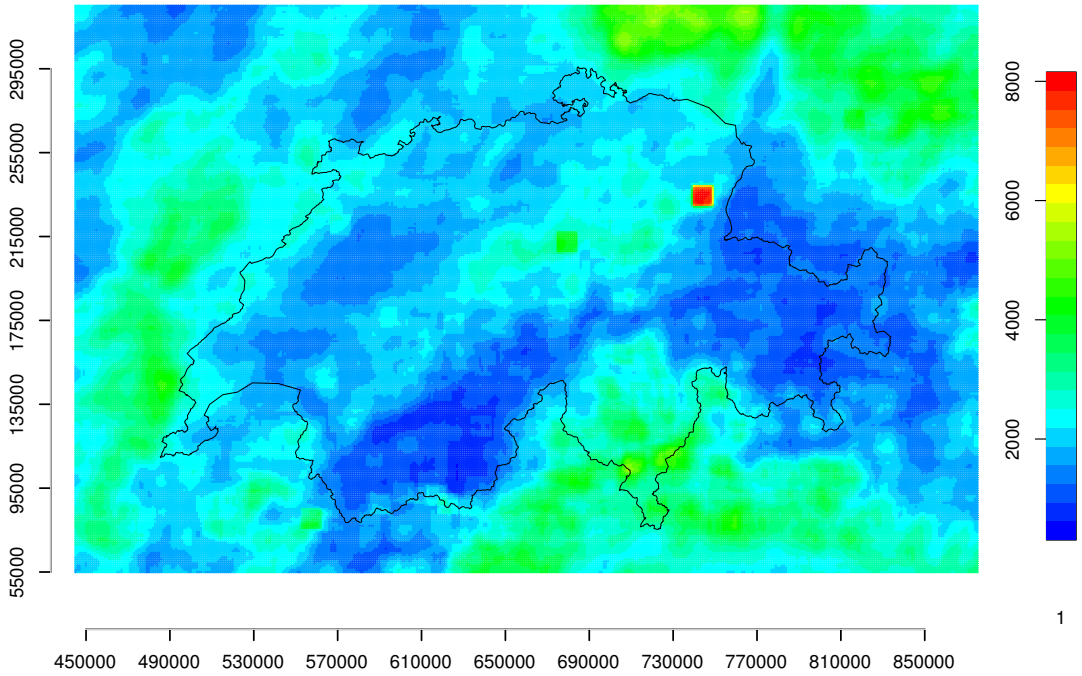

Figure A.8: Map of Switzerland with absolute number of lightning strikes measured within 10x10km squares and within the period 18.02.2008-31.12.2014. A 10x10km square was defined every kilometer in zonal and meridional direction. One coloured pixel shows the centre of one 10x10km square.

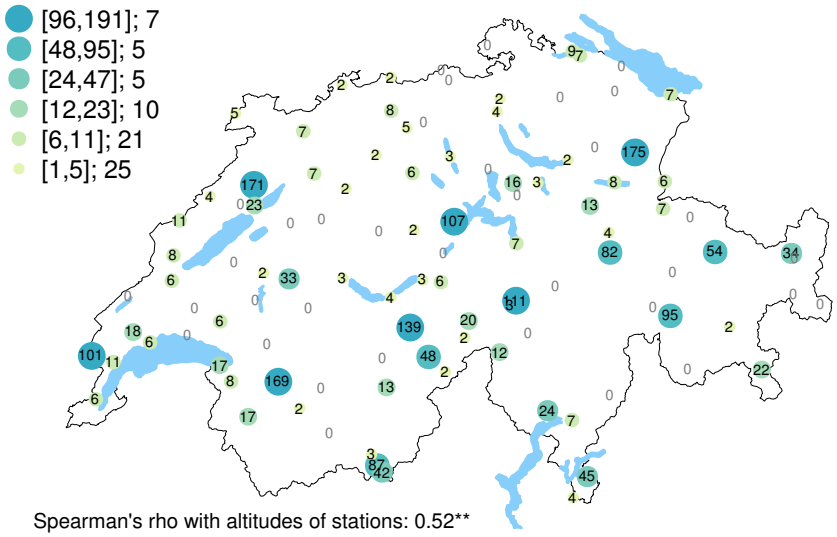

Figure A.9: Number of strong wind gust events in the weather situation "front" at each SwissMetNet Station. Aside from the range of each class, the legend shows the number of stations per class.

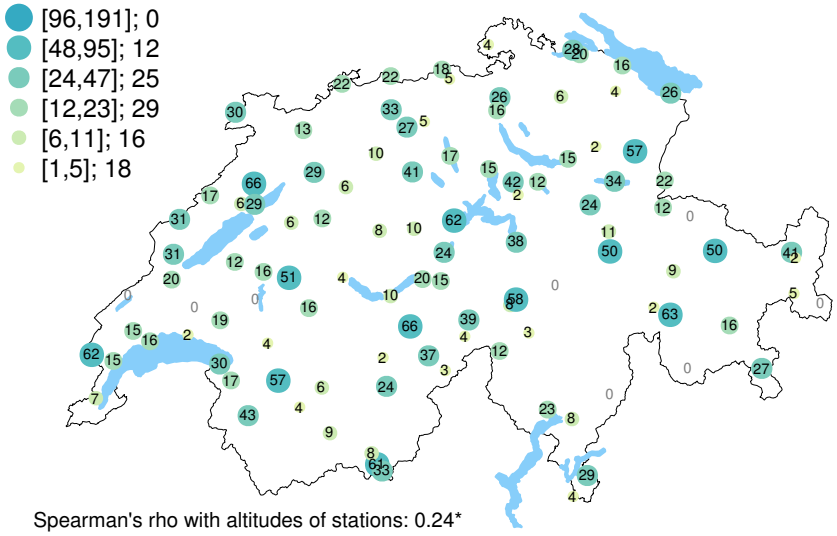

Figure A.10: Number of strong wind gust events in the weather situation "winter storm" at each SwissMetNet Station. Aside from the range of each point class, the legend shows the number of stations per class.

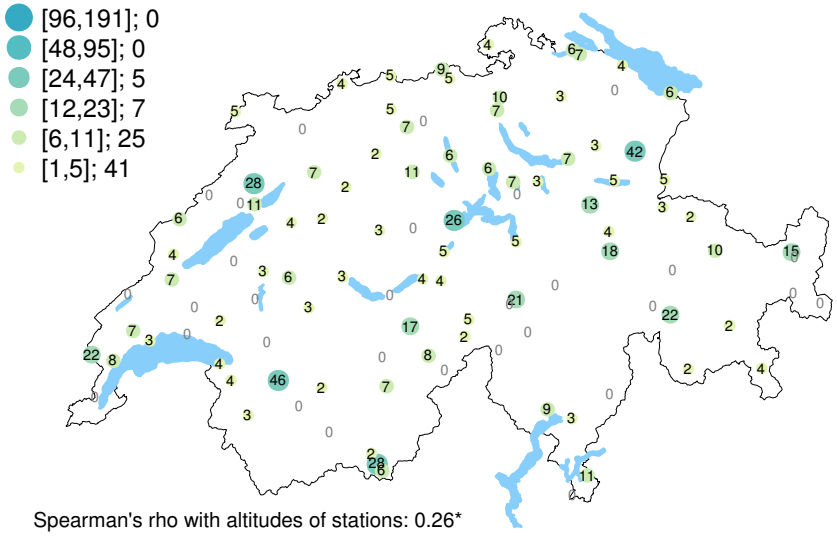

Figure A.11: Number of strong wind gust events with mixed weather situations at each SwissMetNet Station. Aside from the range of each point class, the legend shows the number of stations per class.

A.5 Details on attempts to calculate the number of correct non-events and EDI/SEDI

Many verification measures quantify model quality and are widely used, such as the skill scores presented and used in the main part. Some properties can be attributed to verification measures that indicate their weaknesses and strengths. These are for example base-rate (in)dependence, hedgability, regularity, equitability, boundedness, consistency, propriety, complement symmetry or linearity (Jolliffe and Stephenson, 2012; Ferro and Stephenson, 2011) (they are also well explained in Mason, 2003). The base-rate p is the fraction of observed events to all events (see eq. A.1); it describes the frequency (or rarity) of observed events. If a base-rate independent measure changes, this modification can be attributed entirely to a change in skill and not to a change in base-rate (Ferro and Stephenson, 2011). For this study, such a property is desirable, for it allows a spatial comparison that is not influenced by the number of observed events at each location.

$$p = \frac{a+c}{n} \tag{A.1}$$

A measure that is base-rate independent is the Extreme Dependency Index (EDI; eq. A.3) (Ferro and Stephenson, 2011). It is calculated with the Hit Rate (eq. 3.3) and the False Alarm Rate (eq. A.2).

$$F = \frac{b}{b+d} \tag{A.2}$$

Other properties of the EDI are that it is regular but not complement symmetric, its range goes from -1 to 1 and it is maximized (minimized) whenever the Hit Rate (H) (False Alarm Rate (F)) is equal to 1. The Symmetric Extreme Dependency Index (SEDI) has the same properties except that it is complement symmetric and that it approaches its maximum(minimum) values as H goes to 1(0) and F goes to 0(1). These two indices are expected to give a true impression of skill, regardless of the rarity of events. The EDI and SEDI are determined by using the following equations:

$$EDI = \frac{log(F) - log(HR)}{log(F) + log(HR)} \tag{A.3}$$

and

$$SEDI = \frac{log(F) - log(HR) - log(1-F) + log(1-HR)}{log(F) + log(HR) + log(1-F) + log(1-HR)} \tag{A.4}$$

(Ferro and Stephenson, 2011).
Even though the EDI and SEDI are base-rate independent, they still depend on the size of the number of correct non-events (d in the contingency table 3.2 and eq. A.2). The EDI and SEDI have been calculated for a constant number of hits (a), false alarms (b) and misses (c), but with a changing number of correct non-events (d; Fig. A.12). The EDI and SEDI clearly increase with an increasing d. This emphasizes the importance of correct d values for any subsequent

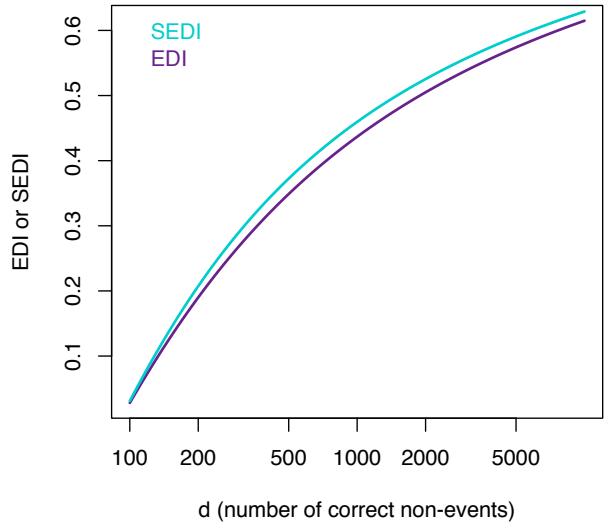

Figure A.12: Values the EDI and SEDI plotted against the number of correct non-events (d). The numbers of hits (a), false alarms (b) and misses (c) are constantly at 15, 30 and 45.

spatial comparison. In this study, reasonable values for a, b and c were successfully deduced from the weather event classifications and wind gust speeds at each location (Fig. A.13, panels 1-3). Although the weather event classification determined convective, foehn, front, winter storm events, long periods with no weather events remained. During these periods, weather situations with weaker wind gusts, such as for example high pressure systems dominate the winds at the ground-level. Determining events for these other weather situations would have been too time consuming. An alternative idea was to count the number of hours without strong wind gusts in either the model nor the measurements and to divide it by the median length of the classified events. The boxplots of these d values are shown on the fourth panel in Fig. A.13. The box plots shows how different the d values for each weather situation are. They differ so much that the EDI or SEDI values are not expected to be comparable between weather situations. The number in front situations is probably high because of the coarse time and spatial resolution of the front data. Because of that, many stations have a lot of correct non-events.

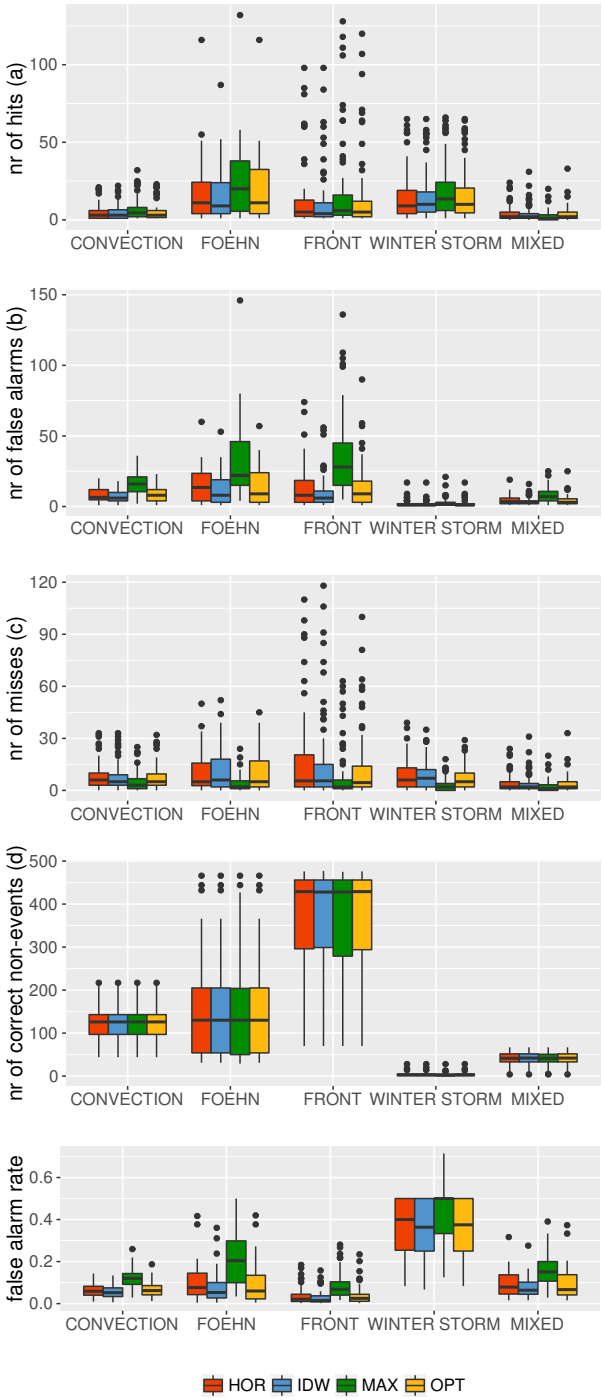

Figure A.13: Values of the contingency tables and false alarm rate for each data set and weather situation.

A.6 Accuracy measures

A.6.1 All gusts

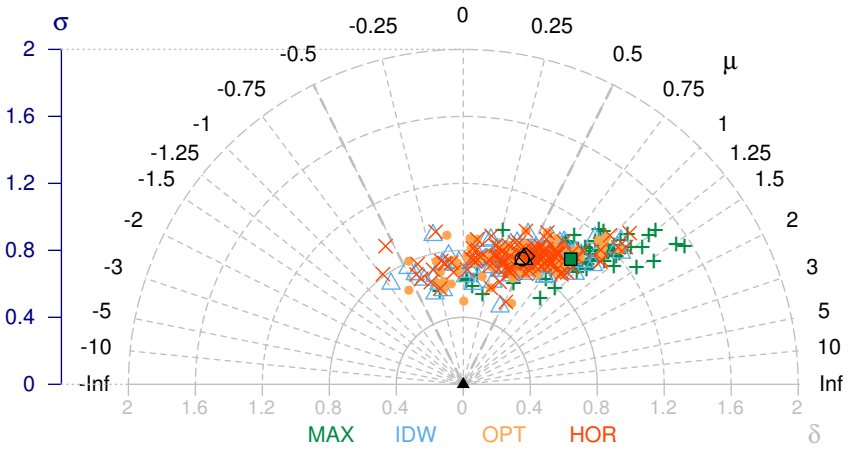

Figure A.14: Error decomposition diagram showing the normalised RMSE δ, normalised bias μ and the normalized pattern error σ of all wind gust speeds of all ***convective*** *events between all COSMO-2 data sets and the measurements (model minus measurements). Each point shows the results of one station and each colour represents a different data set. The points with the black edges are the medians of the equally coloured point clouds. For more explanations about the diagram and median, please read chapter 3.5.4.*

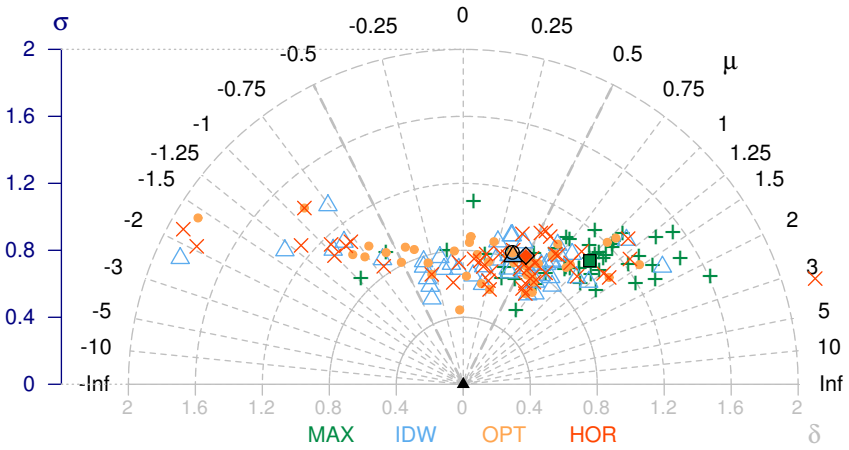

Figure A.15: Same as Fig. A.14 but calculated for all ***foehn*** *events.*

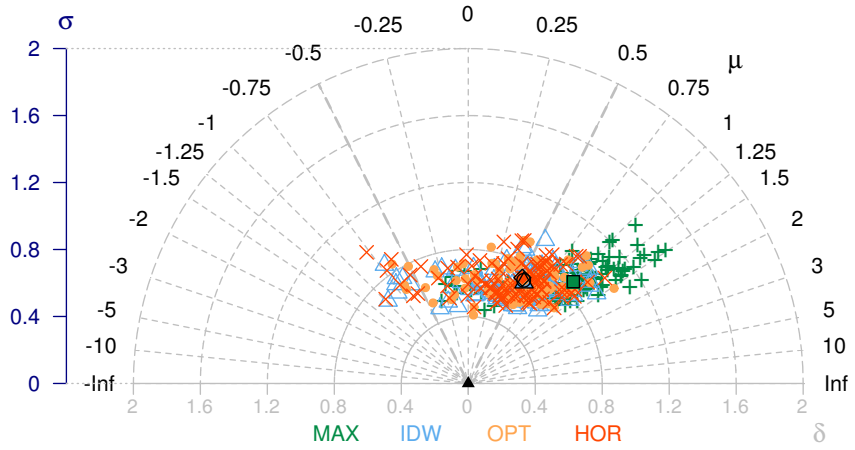

*Figure A.16: Same as Fig. A.14 but calculated for all **front** events.*

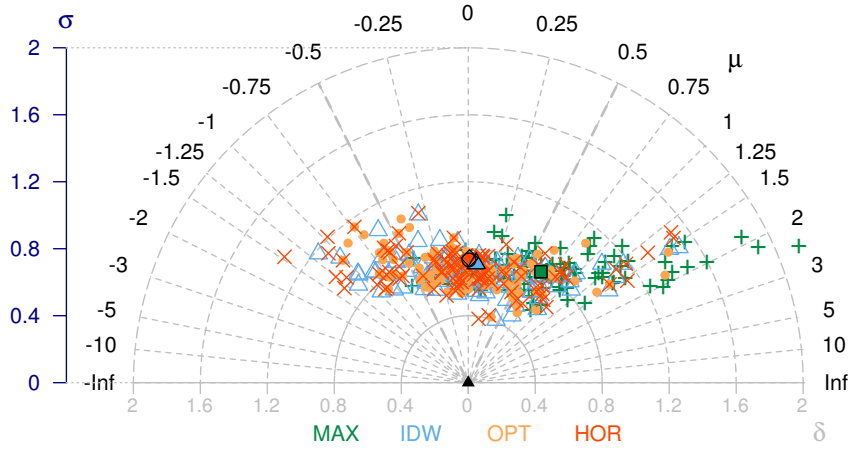

*Figure A.17: Same as Fig. A.14 but calculated for all **winter storm** events.*

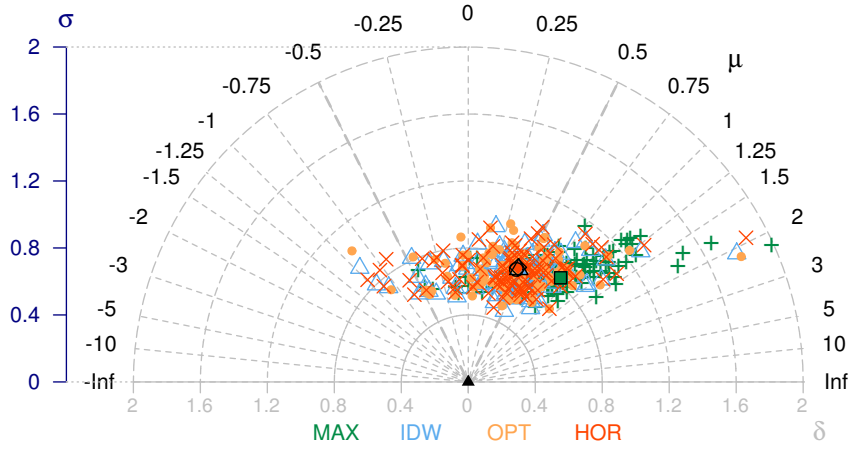

*Figure A.18: Same as Fig. A.14 but calculated for all **mixed** events.*

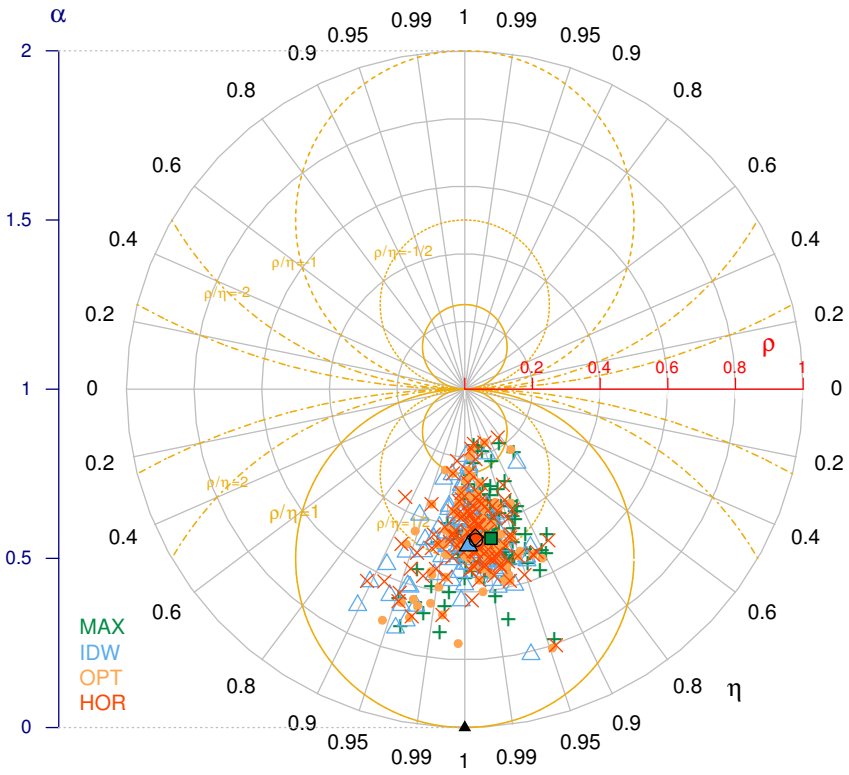

Figure A.19: Correlation similarity diagram showing the natural generalisation of the correlation coefficient ρ, the variance similarity η and the normalised error variance α of all wind gust speeds of all ***convective*** *events between all COSMO-2 data sets and the measurements. Each point shows the result of one station and each colour represents a different data set. The points with the black edges are the medians of the equally coloured point clouds. For more explanations about the diagram and median, please read chapter 3.5.2.*

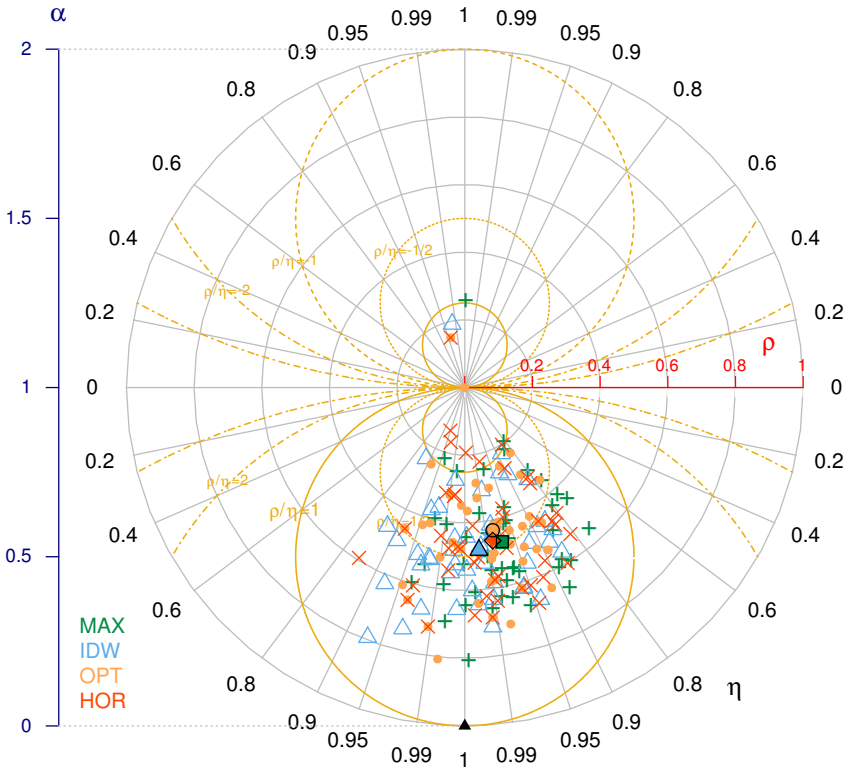

*Figure A.20: Same as Fig. A.19 but calculated for all **foehn** events.*

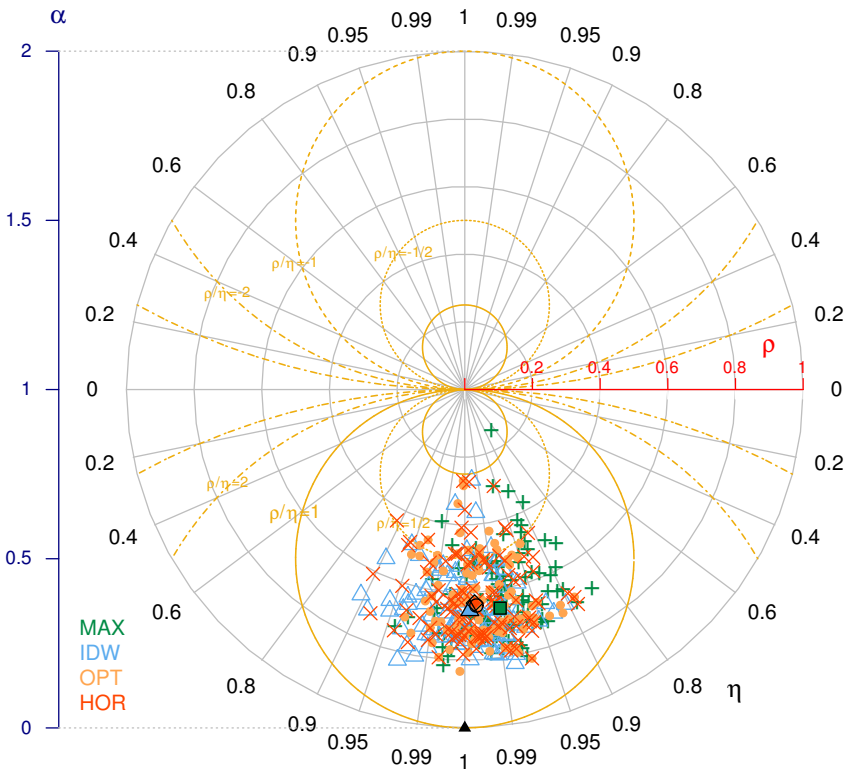

*Figure A.21: Same as Fig. A.19 but calculated for all **front** events.*

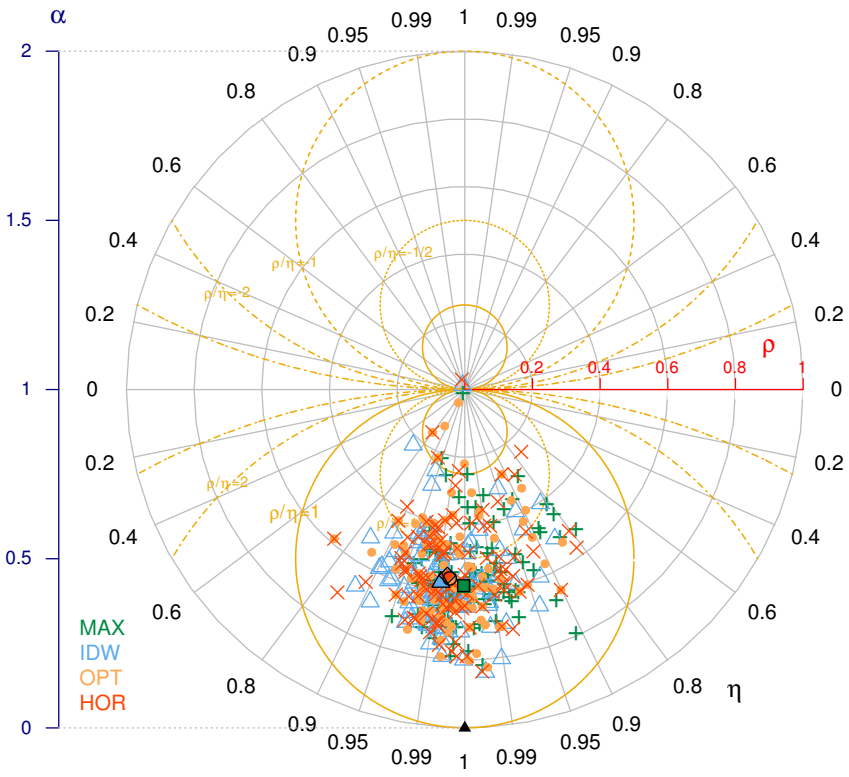

*Figure A.22: Same as Fig. A.19 but calculated for all **winter storm** events.*

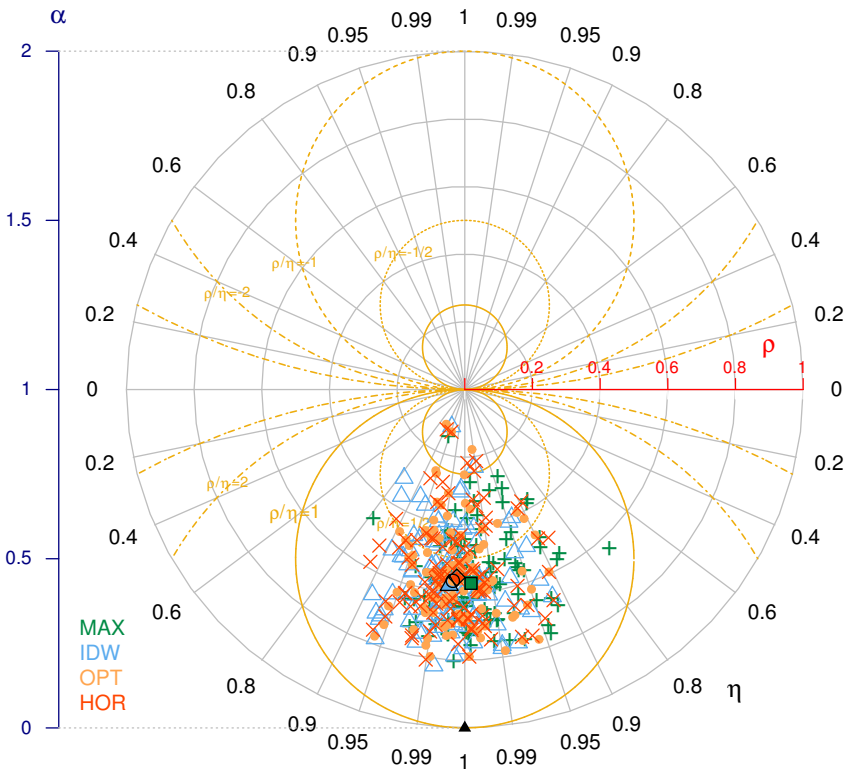

*Figure A.23: Same as Fig. A.19 but calculated for all **mixed** events.*

A.6.2 Maximum gusts

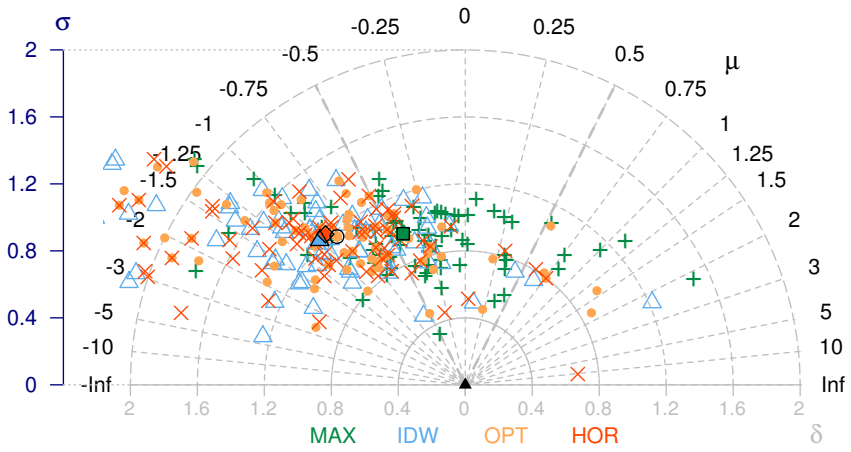

Figure A.24: Error decomposition diagram showing the normalised RMSE δ, normalised bias μ and the normalized pattern error σ of the maximum wind gust speeds of all ***convective*** *events with measured strong wind gusts between all COSMO-2 data sets and the measurements (model minus measurements). Each point shows the results of one station and each colour represents a different data set. A few points for OPT, HOR and IDW are outside the visible range. The points with the black edges are the medians of the equally coloured point clouds. For more explanations about the diagram and median, please read chapter 3.5.4.*

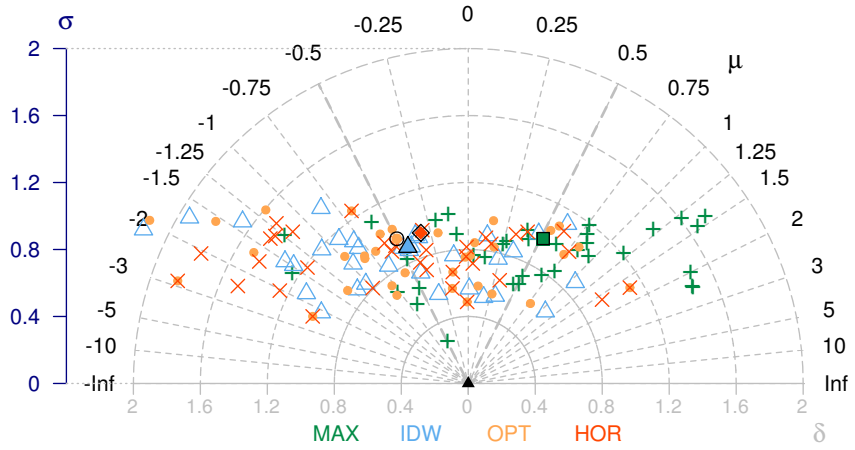

*Figure A.25: Same as Fig. A.24 but calculated for all **foehn** events.*

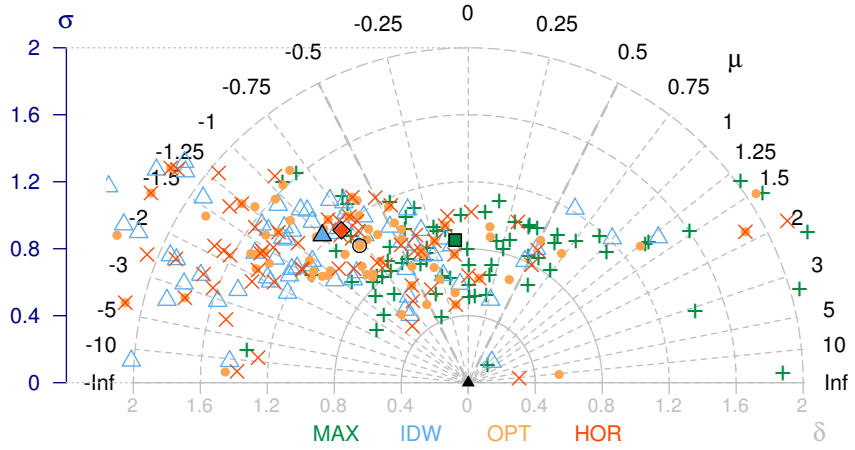

*Figure A.26: Same as Fig. A.24 but calculated for all **front** events.*

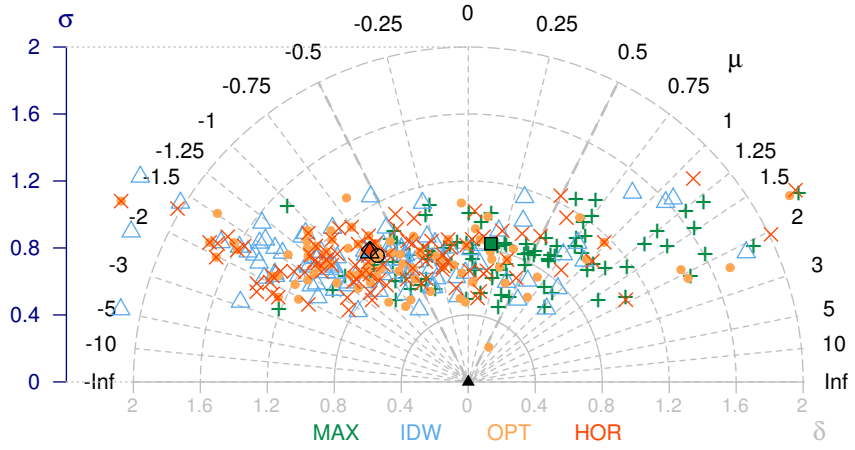

*Figure A.27: Same as Fig. A.24 but calculated for all **winter storm** events.*

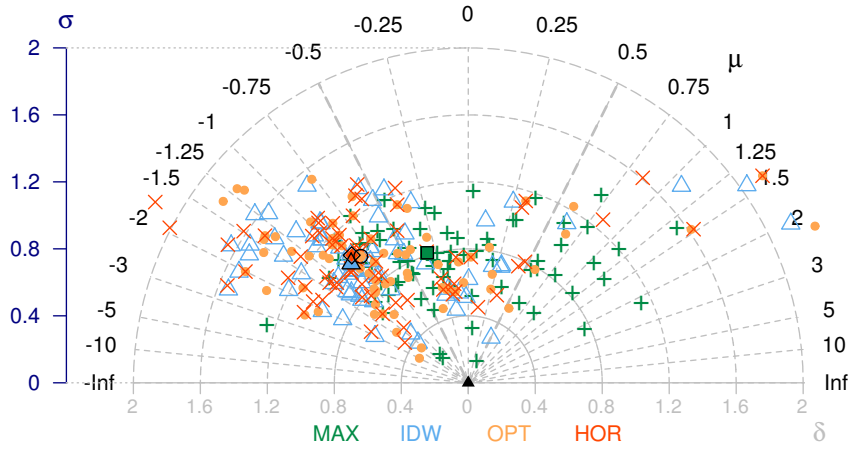

*Figure A.28: Same as Fig. A.24 but calculated for all **mixed** events.*

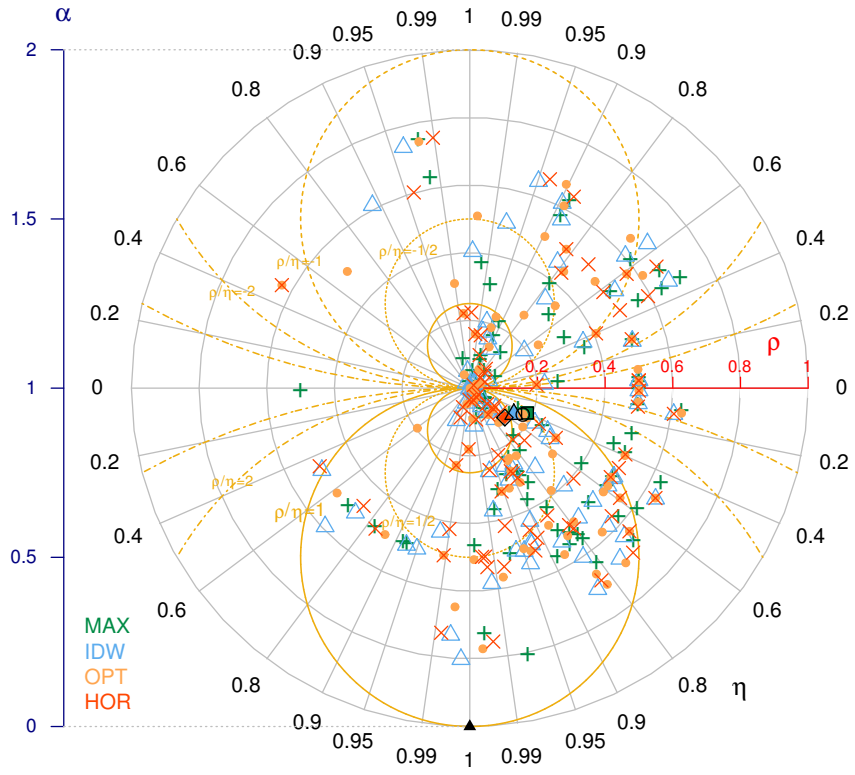

*Figure A.29: Correlation similarity diagram showing the natural generalisation of the correlation coefficient ρ, the variance similarity η and the normalised error variance α of all wind gust speeds of all **convective** events between all COSMO-2 data sets and the measurements. Each point shows the result of one station and each colour represents a different data set. The points with the black edges are the medians of the equally coloured point clouds. For more explanations about the diagram and median, please read chapter 3.5.2.*

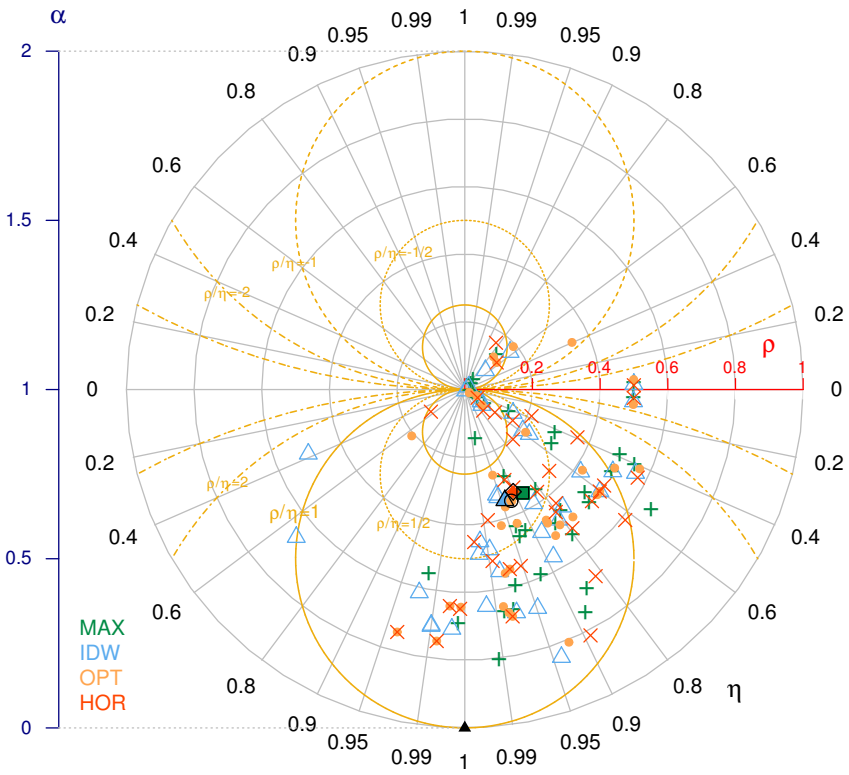

*Figure A.30: Same as Fig. A.29 but calculated for all **foehn** events.*

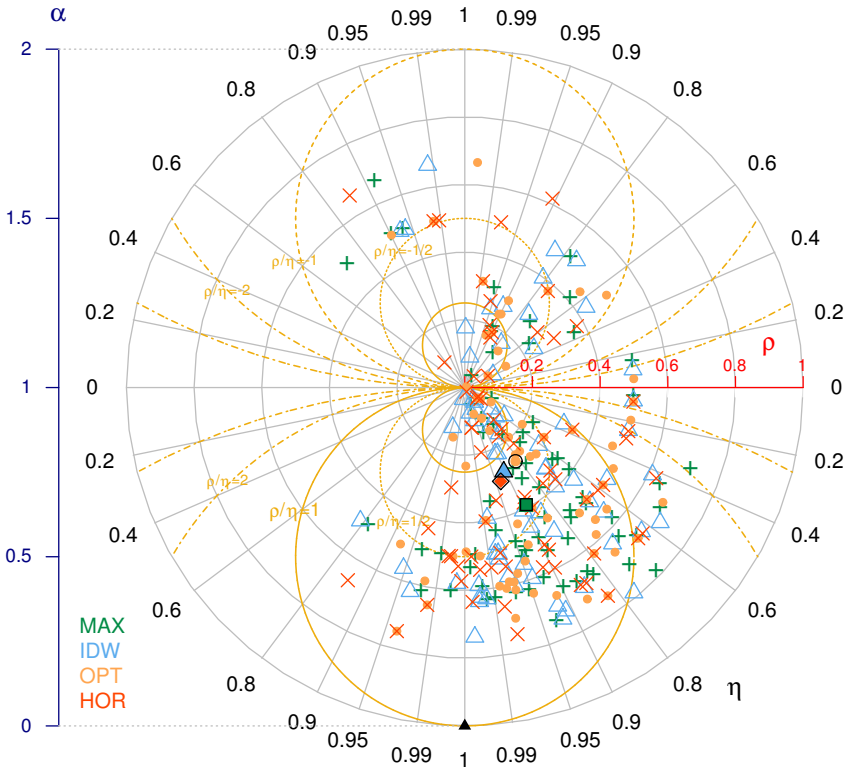

*Figure A.31: Same as Fig. A.29 but calculated for all **front** events.*

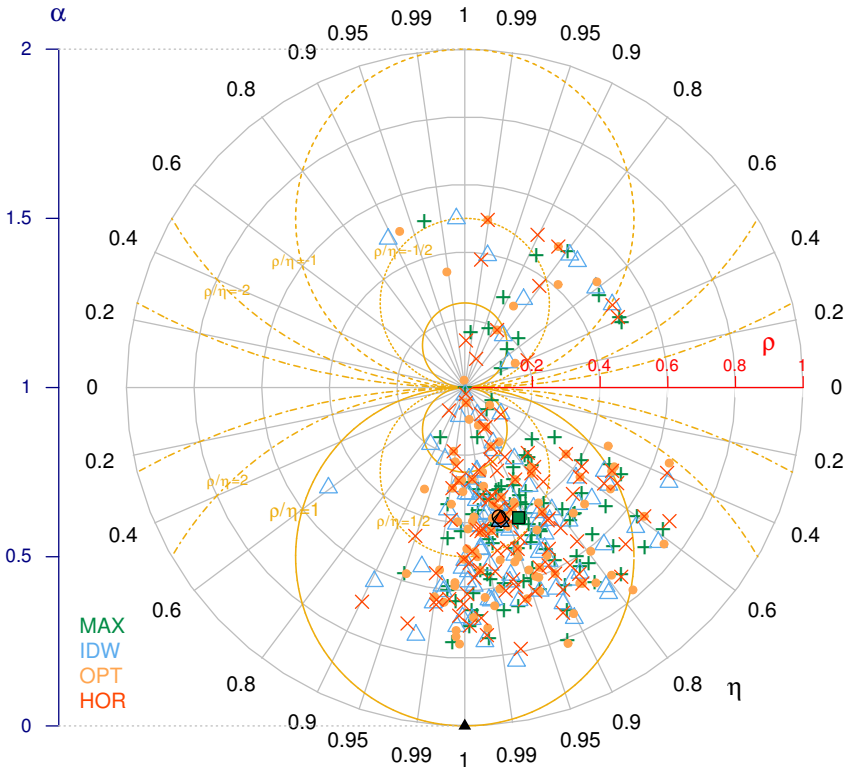

*Figure A.32: Same as Fig. A.29 but calculated for all **winter storm** events.*

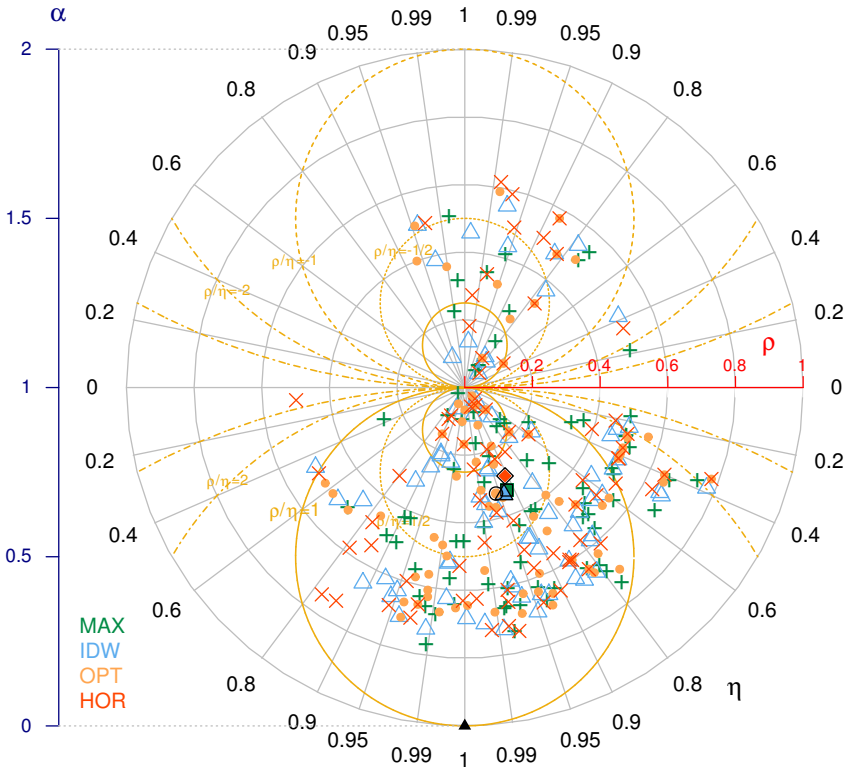

*Figure A.33: Same as Fig. A.29 but calculated for all **mixed** events.*

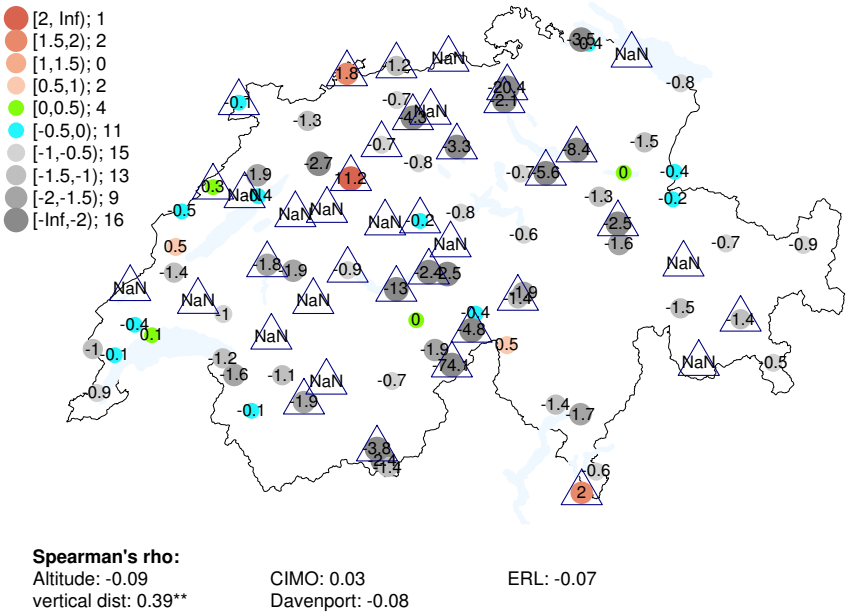

*Figure A.34: Map of Switzerland with values of the normalised bias (μ) of all wind gust speeds of all **front** events between the data set HOR and the measurements, as numbers and divided into classes as shown in the legend. The triangles indicate stations that have less than 6 strong wind gust events in front situations. The legend shows the ranges of each class and the number of stations that are within each class. The legend at the bottom lists the Spearman's rank correlation coefficients. They were calculated between the shown data set (excluding stations with less than 6 strong wind gust events) and the stations criteria described in chapter 2.1. If a correlation coefficient has one (two) asterisks, the correlation coefficient has a p-value <0.05 (0.01) and is thus considered to be significant.*

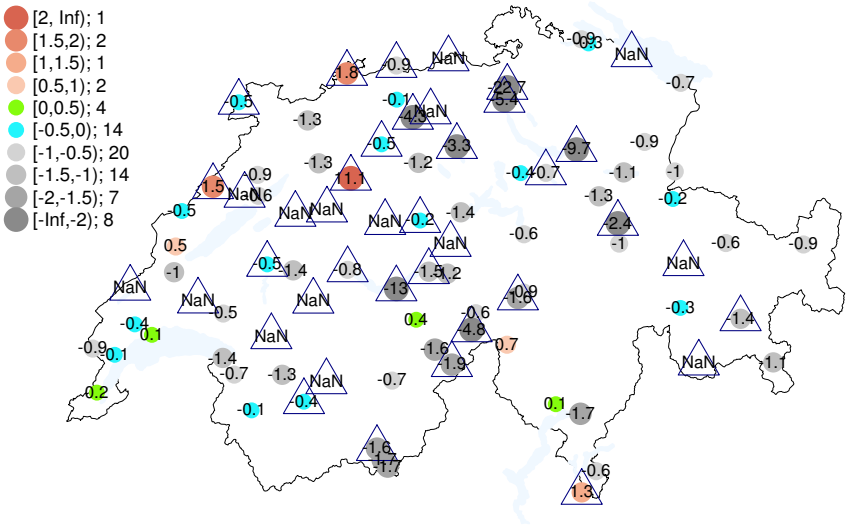

Figure A.35: Same as Fig. A.34 but showing data set OPT (maximum gusts method for front situations).

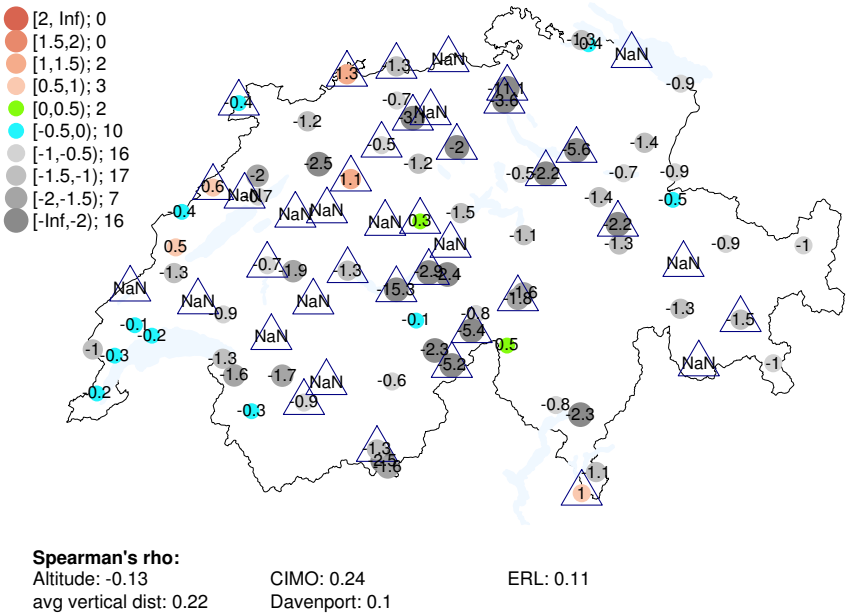

Figure A.36: Same as Fig. A.34 but showing data set IDW (maximum gusts method for front situations).

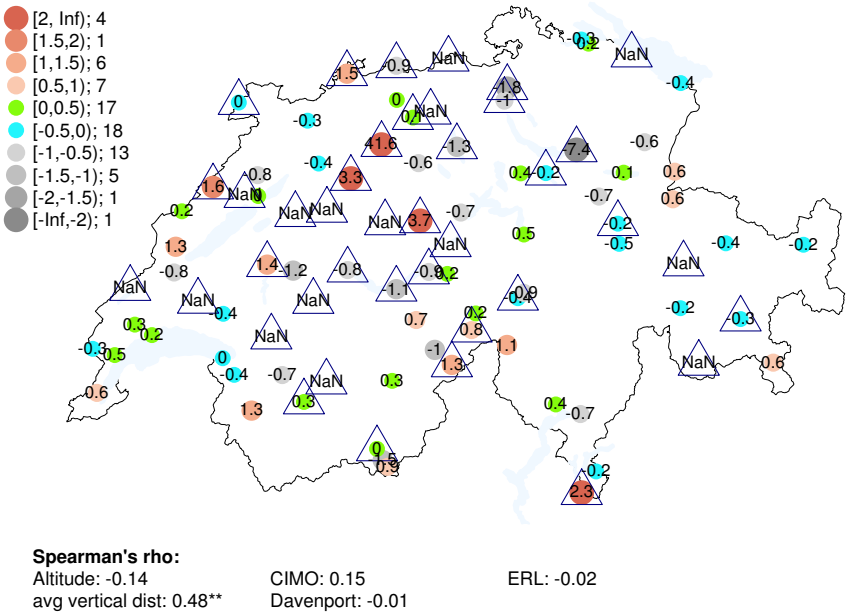

Figure A.37: Same as Fig. A.34 but showing data set MAX (maximum gusts method for front situations).

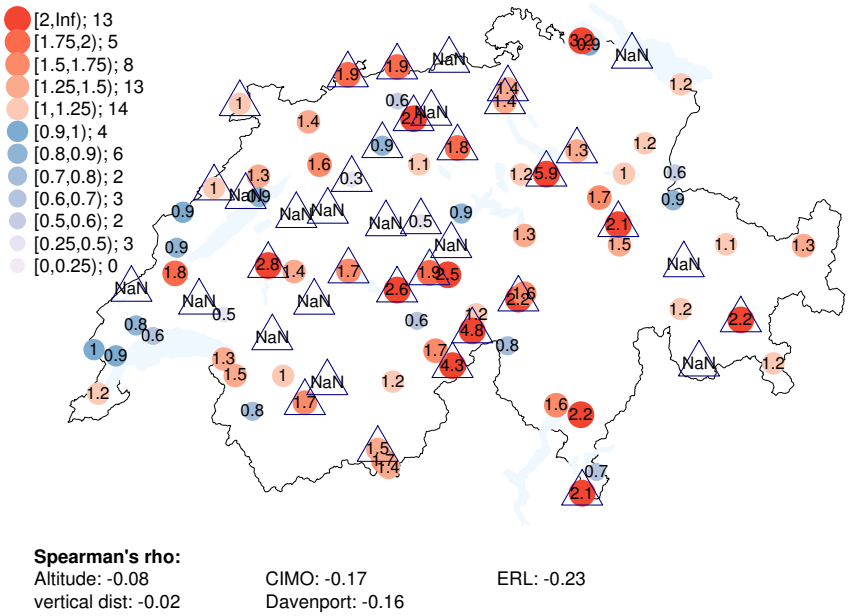

Figure A.38: Same as Fig. A.34 but showing the normalised RMSE (δ) values of data set HOR (maximum gusts method for front situations).

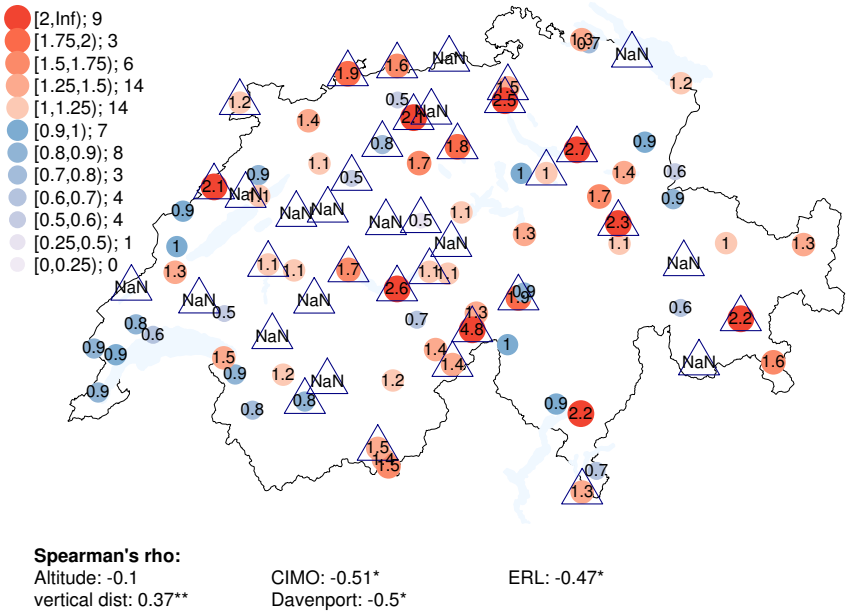

Figure A.39: Same as Fig. A.34 but showing the normalised RMSE (δ) values of data set OPT (maximum gusts method for front situations).

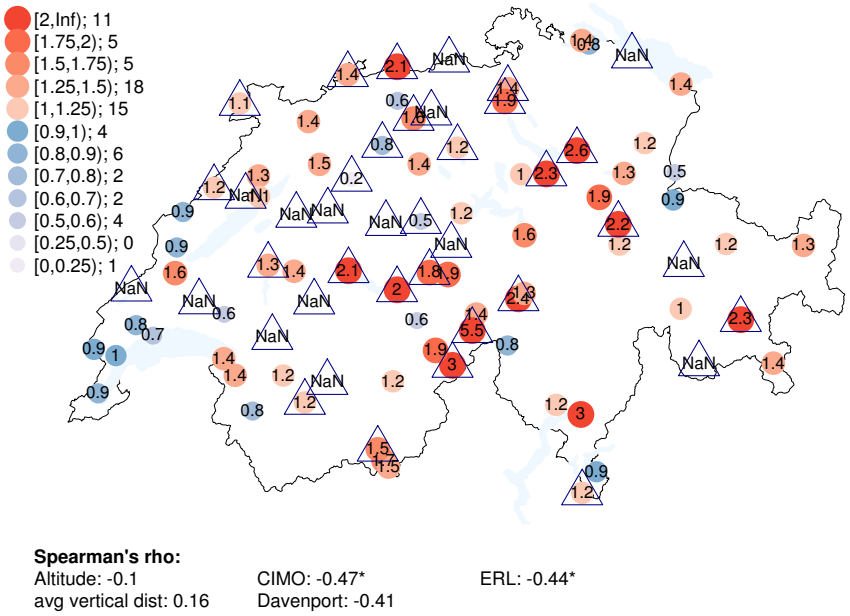

Figure A.40: Same as Fig. A.34 but showing the normalised RMSE (δ) values of data set IDW (maximum gusts method for front situations).

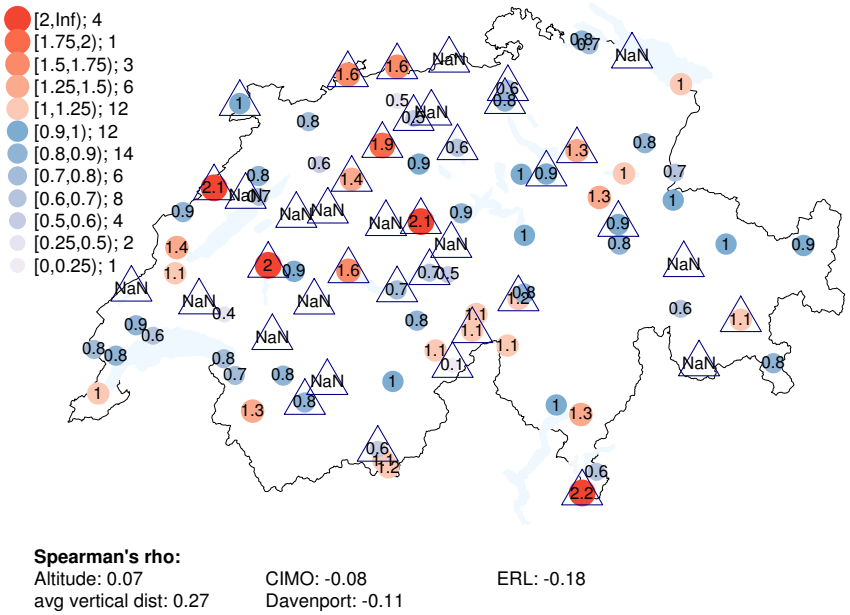

Figure A.41: Same as Fig. A.34 but showing the normalised RMSE (δ) values of data set MAX (maximum gusts method for front situations).

Bibliography

Adolf Thies GmbH & Co. KG (Thies Clima) (2016). Ultrasonic Anemometer 2D; Measurement of Wind direction and Wind velocity. URL: https://thiesclima.com/ultrasonic_anemometer_e.html, Accessed: 07.09.2016.

Aparna, M., Shetye, S., Shankar, D., Shenoi, S., Mehra, P., and Desai, R. (2005). Estimating the seaward extent of sea breeze from quikscat scatterometry. *Geophysical Research Letters*, 32(13).

Barredo, J. I. (2010). No upward trend in normalised windstorm losses in europe: 1970-2008. *Natural Hazards and Earth System Sciences*, 10(1):97–104.

Davenport, A. G., Grimmond, C. S. B., Oke, T. R., and Wieringa, J. (2000). Estimating the roughness of cities and sheltered country. In *Proceedings 12th Conference on Applied Climatology, Asheville, NC, American Meteorological Society, Boston.* 96–99.

Dee, D. P., Uppala, S. M., Simmons, A. J., Berrisford, P., Poli, P., Kobayashi, S., Andrae, U., Balmaseda, M. A., Balsamo, G., Bauer, P., Bechtold, P., Beljaars, A. C. M., van de Berg, L., Bidlot, J., Bormann, N., Delsol, C., Dragani, R., Fuentes, M., Geer, A. J., Haimberger, L., Healy, S. B., Hersbach, H., Holm, E. V., Isaksen, L., Kallberg, P., Koehler, M., Matricardi, M., McNally, A. P., Monge-Sanz, B. M., Morcrette, J. J., Park, B. K., Peubey, C., de Rosnay, P., Tavolato, C., Thepaut, J. N., and Vitart, F. (2011). The ERA-Interim reanalysis: configuration and performance of the data assimilation system. *Quarterly journal of the royal meteorological society*, 137(656, A):553–597.

Della-Marta, P. M., Mathis, H., Frei, C., Liniger, M. A., Kleinn, J., and Appenzeller, C. (2009). The return period of wind storms over Europe. *International journal of climatology*, 29(3, SI):437–459.

Dietzius, R. (1916). Ausdehnung der Korrelationsmethode und der Methode der kleinsten Quadrate auf Vektoren. Hölder. *Sitzungsber. Akad. Wiss. Wien Math. Naturwiss. Kl. Abt 2a*, 125, 3–20.

Doms, G., Förstner, J., Heise, E., Herzog, H.-J., Mironov, D., Raschendorfer, M., Reinhardt, T., Ritter, B., Schrodin, R., Schulz, J.-P., and Vogel, G. (2011). A Description of the Nonhydrostatic Regional COSMO Model, Part II: Physical Parameterization. Deutscher Wetterdienst,

Offenbach, Germany. URL: http://www2.cosmo-model.org/content/model/documentation/core/cosmoPhysParamtr.pdf, Accessed: 14.09.2016.

Dürr, B. (2008). Automatisiertes Verfahren zur Bestimmung von Föhn in Alpentälern. *Arbeitsberichte der MeteoSchweiz*, 223:22pp.

Dürr, B. (2016). personal communications on 16.06.2016 and 02.08.2016.

Ebert, E., Wilson, L., Weigel, A., Mittermaier, M., Nurmi, P., Gill, P., Goeber, M., Joslyn, S., Brown, B., Fowler, T., and Watkins, A. (2013). Progress and challenges in forecast verification. *Meteorological Applications*, 20(2, SI):130–139.

Ebert, E. E. (2008). Fuzzy verification of high-resolution gridded forecasts: a review and proposed framework. *Meteorological Applications*, 15(1):51–64.

Etienne, C. and Beniston, M. (2012). Wind storm loss estimations in the canton of vaud (western switzerland). *Natural Hazards and Earth System Sciences*, 12(12):3789–3798.

EUCLID (2016a). Meteorage network. URL: http://www.euclid.org/meteorage.html; Accessed: 08.09.2016.

EUCLID (2016b). Technology. URL: http://www.euclid.org/technology.html; Accessed: 08.09.2016.

Ferro, C. A. T. and Stephenson, D. B. (2011). Extremal Dependence Indices: Improved Verification Measures for Deterministic Forecasts of Rare Binary Events. *Weather and forecasting*, 26(5):699–713.

Fisler, J. (2016). personal communication on 01.06.2016.

Friederichs, P., Goeber, M., Bentzien, S., Lenz, A., and Krampitz, R. (2009). A probabilistic analysis of wind gusts using extreme value statistics. *Meteorologische Zeitschrift*, 18(6):615–629.

Friederichs, P. and Thorarinsdottir, T. L. (2012). Forecast verification for extreme value distributions with an application to probabilistic peak wind prediction. *Environmentrics*, 23(7):579–594.

Garcia-Diez, M., Fernandez, J., San-Martin, D., Herrera, S., and Gutierrez, J. M. (2015). Assessing and Improving the Local Added Value of WRF for Wind Downscaling. *Journal of applied meteorology and climatology*, 54(7):1556–1568.

Gilleland, E., Ahijevych, D., Brown, B. G., Casati, B., and Ebert, E. E. (2009). Intercomparison of Spatial Forecast Verification Methods. *Weather and forecasting*, 24(5):1416–1430.

Gofa, F., Raspanti, A., and Schubiger, F. (2015). COSMO Science Plan 2015-2020. URL: http://www.cosmo-model.org/content/consortium/reports/sciencePlan_2015-2020.pdf.

Goyette, S., Brasseur, O., and Beniston, M. (2003). Application of a new wind gust parameterization: Multiscale case studies performed with the canadian regional climate model. *Journal of Geophysical Research: Atmospheres*, 108(D13).

Heneka, P. and Ruck, B. (2008). A damage model for the assessment of storm damage to buildings. *Engineering Structures*, 30(12):3603 – 3609.

Hoppmann, U., Koenig, S., Tielkes, T., and Matschke, G. (2002). A short-term strong wind prediction model for railway application: design and verification. *Journal of Wind Engineering and Industrial Aerodynamics*, 90(10):1127 – 1134.

Jolliffe, I. T. (2007). Uncertainty and inference for verification measures. *Weather and forecasting*, 22(3):637–650.

Jolliffe, I. T. and Stephenson, D. B. (2012). Forecast verification: a practitioner's guide in atmospheric science. *John Wiley & Sons, Ltd.*

Jung, C. and Schindler, D. (2016). Modelling monthly near-surface maximum daily gust speed distributions in southwest germany. *International Journal of Climatology*.

Kaufmann, P. (2008). Association of surface stations to NWP model grid points. *COSMO Newsletter*, 9(1):54–55. URL: http://www.cosmo-model.org/content/model/documentation/newsLetters/newsLetter09/cnl9-10.pdf.

Koh, T.-Y., Wang, S., and Bhatt, B. C. (2012). A diagnostic suite to assess NWP performance. *Journal of Geophysical Research: Atmospheres*, 117(D13). D13109.

Lambrecht meteo GMBH (Lambrecht) (2016). Combined Wind Sensor. URL: http://www.lambrecht.net/datasheets/wind/14512_leaflet_en_1.pdf, Accessed: 07.09.2016.

Landberg, L., Myllerup, L., Rathmann, O., Petersen, E. L., Jørgensen, B. H., Badger, J., and Mortensen, N. G. (2003). Wind resource estimation—an overview. *Wind Energy*, 6(3):261–271.

Liu, Y., Racah, E., Correa, J., Khosrowshahi, A., Lavers, D., Kunkel, K., Wehner, M., Collins, W., et al. (2016). Application of deep convolutional neural networks for detecting extreme weather in climate datasets. *arXiv preprint arXiv:1605.01156*.

Markowski, P. and Richardson, Y. (2010). Mesoscale meteorology in midlatitudes. *John Wiley & Sons, Ltd.*, page 118.

Mason, I. (2003). Binary events. In Jolliffe, I. and Stephenson, D., editors, *Forecast verification: a practitioner's guide in atmospheric science*, pages 37–76. John Wiley & Sons, Ltd.

MeteoSwiss (2016a). Data management. Federal Office of Meteorology and Climatology, Zurich, Switzerland. URL: http://www.meteoswiss.admin.ch/home/measurement-and-forecasting-systems/datenmanagement.html, Accessed: 07.09.2016.

MeteoSwiss (2016b). Measurement instruments. Federal Office of Meteorology and Climatology, Zurich, Switzerland. URL: http://www.meteoswiss.admin.ch/home/measurement-and-forecasting-systems/land-based-stations/automatisches-messnetz/measurement-instruments.html, Accessed: 07.09.2016.

MeteoSwiss (2016c). SwissMetNet: Das Referenzmessnetz der MeteoSchweiz. Federal Office of Meteorology and Climatology, Zurich, Switzerland. URL: http://www.meteoschweiz.admin.ch/content/dam/meteoswiss/de/Mess-und-Prognosesysteme/Bodenstationen/Automatisches-Messnetz/doc/SwissMetNet_Das_Referenzmessnetz_der_MeteoSchweiz.pdf, Accessed: 07.09.2016.

MeteoSwiss (2016d). The new forecasting model COSMO-1 – Storm clouds, beware! Federal Office of Meteorology and Climatology, Zurich, Switzerland. URL: http://www.cscs.ch/fileadmin/Highlights/Blog_Operationalisierung-COSMO_Nutzersicht_EN_def.pdf, Accessed: 07.09.2016.

MeteoSwiss (2016e). The new weather forecasting model for the Alpine region. Federal Office of Meteorology and Climatology, Zurich, Switzerland. URL: http://www.meteoswiss.admin.ch/home/latest-news/news.subpage.html/en/data/news/2016/3/the-new-weather-forecasting-model-for-the-alpine-region.html, Accessed: 14.09.2016.

Mittermaier, M. P. (2014). A strategy for verifying near-convection-resolving model forecasts at observing sites. *Weather and forecasting*, 29(2):185–204.

Mohr, Susanna; Piper, D. (2015). personal communications on 18.12.2015.

Panofsky, H. A. and Dutton, J. A. (1984). Atmospheric Turbulence. Models and Methods for Engineering Applications. *John Wiley & Sons, Ltd.*

Pinson, P. and Hagedorn, R. (2012). Verification of the ecmwf ensemble forecasts of wind speed against analyses and observations. *Meteorological Applications*, 19(4):484–500.

Schemm, S., Rudeva, I., and Simmonds, I. (2015). Extratropical fronts in the lower troposphere-global perspectives obtained from two automated methods. *Quarterly journal of the royal meteorological society*, 141(690, A):1686–1698.

Schubiger, F., Stauch, V., and Kaufmann, P. (2012). Verification of different wind gust parametrizations; Overview of verification results at MeteoSwiss in the year 2012. Presentation at the COSMO General Meeting 2012. Federal Office of Meteorology and Climatology, Zurich, Switzerland. URL: http://www2.cosmo-model.org/content/consortium/generalMeetings/general2012/wg5-versus/shubiger_gusts.pdf, Accessed: 07.09.2016.

Schuepp, M., Schiesser, H., Huntrieser, H., Scherrer, H., and Schmidtke, H. (1994). The Winterstorm Vivian of 27 February 1990 - About the meteorological development, wind forces and damage situation in the forests of Switzerland. *Theoretical and applied climatology*, 49(3):183–200.

Schwierz, C., Koellner-Heck, P., Mutter, E. Z., Bresch, D. N., Vidale, P.-L., Wild, M., and Schaer, C. (2010). Modelling European winter wind storm losses in current and future climate. *Climatic Change*, 101(3-4):485–514.

Storm, B., Dudhia, J., Basu, S., Swift, A., and Giammanco, I. (2009). Evaluation of the Weather Research and Forecasting Model on Forecasting Low-level Jets: Implications for Wind Energy. *Wind Energy*, 12(1):81–90.

Stucki, P., Dierer, S., Welker, C., Gómez-Navarro, J. J., Raible, C., Martius, O., and Brönnimann, S. (2016). Evaluation of downscaled wind speeds and parameterised gusts for recent and historical windstorms in switzerland. *Tellus A*, 68(0).

Stull, R. B. (2012). *An introduction to boundary layer meteorology*, volume 13. Springer Science & Business Media.

Wanner, H. and Furger, M. (1990). The bise - Climatology of a regional wind north of the Alps. *Meteorology and Atmospheric Physics*, 43(1-4):105–115.

Weber, R. and Furger, M. (2001). Climatology of near-surface wind patterns over Switzerland. *International Journal of Climatology*, 21(7):809–827.

Weusthoff, T. (2011). Weather Type Classification at MeteoSwiss – Introduction of new automatic classifications schemes. *Arbeitsberichte der MeteoSchweiz*, 235:46pp.

Wever, N. (2012). Quantifying trends in surface roughness and the effect on surface wind speed observations. *Journal of Geophysical Research - Atmospheres*, 117.

Widmer, A. (2016). personal communication on 07.01.2016.

Wilks, D. S. (2011). *Statistical methods in the atmospheric sciences*, volume 100. Academic press.

World Meteorological Organization (WMO) (2008). Guide to Meteorological Instruments and Methods of Observation. updated in 2010; URL: http://library.wmo.int/pmb_ged/wmo_8_en-2012.pdf, Accessed: 07.09.2016.

Zhong, Z., Lu, W., Song, S., and Zhang, Y. (2011). A new scheme for effective roughness length and effective zero-plane displacement in land surface models. *Journal of Hydrometeorology*, 12(6):1610–1620.

Acknowledgements

I would like to express my gratitude to a number of people who supported me in this project. I would like to thank Olivia Romppainen-Martius for giving me the opportunity to write a Master's Thesis on an applied research topic, which was important to me. Olivia has shown excellent leadership and has been very generous with her time, help and encouragement. Special thanks also go to my advisor Simona Trefalt, who gave me great advice and always took time to answer my questions meticulously. Great thanks go to ...

... MeteoSwiss for providing the SwissMetNet, COSMO-2 and foehn index data

... Bruno Dürr for his helpful comments and for complementing the foehn data sets

... Susanna Mohr and David Piper for providing the method to define convective events with lightning data and for their explanations

... Joël Fisler and Alexander Widmer for providing additional data about the SwissMetNet stations

... Sebastian Schemm for making the ERA-Interim front data available

... Andrey Martynov for the IT-Support

... Yannick Barton for his Ferro-and-Segers-R-Script and his motivating words.

Many thanks go to everyone in the climate impact group for providing a pleasant working atmosphere and for the interesting group meetings. I am also grateful to everyone on the GIUB 5th floor for the fun coffee breaks and relaxing lunches. I am indebted in particular to my friends Stéphanie Arcusa and Leonie Bernet for reviewing and proofreading my thesis. I would also like to thank my friends and fellow students Steph, Leonie, David, Simone and Pascal without whom all of this would not have been as fun. Finally, my warmest thanks go to my family for their support, strength and enthusiastic motivation.

Declaration

under Art. 28 Para. 2 RSL 05

Last, first name: Barras, Hélène

Matriculation number: 10-060-739

Programme: M.Sc. in Climate Sciences

Bachelor ☐ Master ☒ Dissertation ☐

Thesis title: Verification of strong wind gusts in COSMO-2

Thesis supervisor: Prof. Dr. Olivia Romppainen-Martius

I hereby declare that this submission is my own work and that, to the best of my knowledge and belief, it contains no material previously published or written by another person, except where due acknowledgement has been made in the text. In accordance with academic rules and ethical conduct, I have fully cited and referenced all material and results that are not original to this work. I am well aware of the fact that, on the basis of Article 36 Paragraph 1 Letter o of the University Law of 5 September 1996, the Senate is entitled to deny the title awarded on the basis of this work if proven otherwise. I grant inspection of my thesis.

Bern, 20.09.2016

Hélène Barras